Nitrogen and Phosphorus Budgets in the Northwestern Mediterranean Deep Convection Region

Fayçal Kessouri, Caroline Ulses, Claude Estournel, Patrick Marsaleix, Tatiana Séverin, Mireille Pujo-Pay, Jocelyne Caparros, Patrick Raimbault, Orens Pasqueron de Fommervault, Fabrizio d'Ortenzio, et al.

Nitrogen and phosphorus budgets in the Northwestern Mediterranean deep convection region

Faycal Kessouri[1,†], Caroline Ulses[1], Claude Estournel[1], Patrick Marsaleix[1], Tatiana Severin[2], Mireille Pujo-Pay[3], Jocelyne Caparros[3], Patrick Raimbault[4], Orens Pasqueron de Fommervault[5], Fabrizio D'Ortenzio[5], Vincent Taillandier[5], Pierre Testor[6], Pascal Conan[3]

(1) Laboratoire d'Aérologie, CNRS, Toulouse University

(†) Atmospheric and oceanic sciences department, University of California Los Angeles

(2) Marine Science Institute, The University of Texas at Austin

(3) Laboratoire d'Oceanographie Microbienne

(4) Institut Méditerranéen d'Océanologie

(5) Sorbonne Universités, UPMC Univ. Paris 06, and CNRS UMR 7093, LOV, Observatoire océanologique

(6) CNRS/LOCEAN

Key points up to three (<140 characters)

- Modeling of annual nitrogen and phosphorus cycles in the northwestern Mediterranean deep convection region for the period 2012-2013.

- The deep convection area was a sink of inorganic matter and a source of organic matter for the surrounding area over the period 2012-2013.

- The N:P ratio in the surface layer is submitted to drastic variations during deep convection and bloom transition periods.

Abstract

The aim of this study is to understand the biogeochemical cycles of the northwestern Mediterranean Sea (NW Med), where a recurrent spring bloom related to dense water formation occurs. We used a coupled physical-biogeochemical model at high resolution to simulate realistic one-year period and analyze the nitrogen (N) and phosphorus (P) cycles. First, the model was evaluated using cruises carried out in winter, spring and summer and a Bio-Argo float deployed in spring. Then, the annual cycle of meteorological and hydrodynamical forcing and nutrients stocks in the upper layer were analyzed. Third, the effect of biogeochemical and physical processes on N and P was quantified. Fourth, we quantified the effects of the physical and biological processes on the seasonal changes of the molar NO_3:PO_4 ratio, particularly high compared to the global ocean. The deep convection reduced the NO_3:PO_4 ratio of upper waters, but consumption by phytoplankton increased it. Finally, N and P budgets were estimated. At the annual scale, this area constituted a sink of inorganic and a source of organic N and P for the peripheral area. NO_3 and PO_4 were horizontally advected from the peripheral regions into the intermediate waters (130-800 m) of the deep convection area, while organic matter was exported throughout the whole water column toward the surrounding areas. The annual budget suggests that the NW Med deep convection constitutes a major source of nutrients for the photic zone of the Mediterranean Sea.

Index Terms and Keywords

Mediterranean Sea, physical-biogeochemical modeling, nutrient seasonal dynamics, nitrate and phosphate budget, N:P stoichiometry

1. Introduction

The Mediterranean Sea, often considered as an oligotrophic region [*Antoine et al.,* 1995], exhibits nutrient-depleted surface waters most of the year and low nutrient concentrations in

deep waters [*Krom et al., 1991*]. With respect to the global ocean Redfield nitrate (NO_3) to phosphate (PO_4) ratio of 16:1 [*Redfield,* 1964], the Mediterranean Sea is characterized by particularly high values [*Ribera d'Alcalà et al.*, 2003]. Moreover, these oligotrophic conditions and high NO_3:PO_4 (hereafter N:P) ratios show a pronounced east-west gradient [*Pujo-Pay et al.*, 2011], with the eastern basin presenting ultra-oligotrophic conditions. The N:P ratios in deep layers were estimated at 20-22 in the western sub-basin [*Béthoux et al.*1998] and at 27-30 in the eastern sub-basin [*Ribera d'Alcala et al.*, 2003] of the Mediterranean.

The distribution of nutrients in the semi-enclosed Mediterranean Sea results from internal physical and biogeochemical dynamics, from atmospheric and terrestrial inputs, and from exchanges with the Atlantic Ocean and the Black Sea. Physical dynamics are partly controlled by the formation of intermediate and deep waters as the winter climate of the Mediterranean Sea is characterized by cold, dry local winds blowing from the north [*Hauser et al.*, 2003], which induce an increase of the surface layer density by strong evaporation and cooling, and then trigger the deep convection mixing. This process is responsible for the formation of intermediate and deep water masses in the northwestern basin (hereafter NW Med) [*Medoc Group*, 1970], the south Adriatic [*Pollak et al.*, 1951], the Aegean [*Nittis et al.*, 2003] and the Rhodes Gyre [*Ovchinnikov et al.*, 1984]. The high nitrate and phosphate surface concentrations (values close to deep concentrations) observed during convective episodes in these regions [*Yilmaz and Tugrul*, 1998; *Gacic et al.*, 2002; *Santinelli et al.*, 2012; *Severin et al., 2014*] demonstrate that the deep convection process is also responsible for large nutrient enrichments of the upper layers. In addition, a study based on satellite-derived chlorophyll a data [*D'Ortenzio and Ribera d'Alcalà*, 2009] has shown that the deep convection regions are characterized by intense to moderate spring blooms, while phytoplankton development in the rest of the open Mediterranean Sea is of low magnitude. This feature of phytoplankton dynamics in convection regions may be explained by the large amounts of nutrient supplied during the intense vertical mixing events [*Lavigne et al.*, 2015].

Among the deep convection regions of the Mediterranean Sea, the NW Med (Fig. 1A) has been identified as the region where the vertical mixing and the associated phytoplankton spring bloom are the most intense and recurrent [*Houpert et al.*, 2015; *D'Ortenzio and Ribera d'Alcalà*, 2009; *Lavigne et al.*, 2013; *Mayot et al.*, 2016]. The NW Med convection has been shown to largely influence the regional biogeochemical cycles and marine ecosystems, mostly by importing nutrient-enriched deep waters to the surface [*Severin et al.*, 2014; *Ulses et al.*, 2016]. This enrichment changes the biogeochemical characteristics of the surface layers [*Durrieu de Madron et al.*, 2011; *Herrmann et al., 2013*; *Auger et al.*, 2014], induces a large phytoplankton spring bloom [*D'Ortenzio et al.*, 2009; *Lavigne et al.*, 2013; *Estrada et al.*, 2014], favors high particulate carbon export [*Gogou et al.*, 2014; *Ulses et al.*, 2016] and shifts the zooplankton community toward larger sized organisms [*Auger et al.*, 2014]. Moreover, deep convection in the NW Med has also been shown to promote a change of the surface nutrient ratios [*Severin et al.*, 2014; *Pasqueron de Fommervault et al.*, 2015a]. However, the impact of nutrient replenishments on the seasonal cycles of nitrogen and phosphorus has been poorly explored. The few quantifications of the upward flux of nitrate and phosphate that have been performed [*Severin et al.*, 2014; *Ulses et al.*, 2016] remain limited in space and/or time. A thorough quantification of the processes linked to the seasonal variations of nitrogen and phosphorus cycles during one complete year has not yet been proposed in this region.

The objectives of the DeWEX project (Deep Water formation EXperiment) are (i) to better understand the impact of dense water formation on the marine biogeochemical cycles and (ii) to provide a consistent dataset of hydrological and biogeochemical parameters to improve the numerical modeling of the convection hydrology and coupled biogeochemical processes. To fulfill these objectives, oceanographic research vessels covered the deep convection area during each season from summer 2012 to summer 2013. Once calibrated and validated, numerical modeling is expected to achieve goals at different time scales. In the short term, the model is

97 expected to interpolate between the DeWEX cruises to calculate the nutrient and organic matter
98 budgets over an annual cycle. In the long term, and after complementary validations with multi-
99 year datasets, modeling will be used as an integrative tool to investigate the question of how
100 climate change and anthropogenic activities could impact the cycle of biogenic elements and
101 marine ecosystems.

102 The present study aims to quantify the dynamics of nutrients at the seasonal scale and to estimate
103 an annual budget of nitrogen and phosphorus, in the NW Med dense water formation area. After
104 a brief description of the observation network, the modeling strategy is described (section 2), and
105 then evaluated through comparisons with observations (section 3). The seasonal variabilities of
106 the atmospheric forcing and hydrography are presented (section 4.1.1), together with the annual
107 cycles of nutrient stocks in the upper layer (4.1.2). In section 4.1.3, we discuss the impact of
108 physical and biogeochemical processes on the N:P ratio in the upper layer. Finally, an annual
109 nitrogen and phosphorus budget of the region is proposed (section 4.2).

110 ## 2. Method

111 ### 2.1.Observations

112 During the period from September 2012 to September 2013, a large number of hydrological and
113 biogeochemical observations (>178 profiles) were made in the NW Med in the framework of the
114 MERMEX (Marine Ecosystems Response in the Mediterranean Experiment) and HyMeX
115 (Hydrological cycle in the Mediterranean Experiment) programs. The objective was to better
116 understand the interactions between horizontal and vertical physical processes during a
117 convection event [*Estournel et al.*, 2016a] and their impact on nutrient budgets and marine
118 ecosystems.

119 In this study, we used the observations collected during three cruises that covered the NW Med
120 in winter, spring and summer of 2013. During DeWEX Leg 1, conducted from 1 to 21 February

2013 on board the R/V Le Suroît, 75 hydrological and 45 biogeochemical profiles were obtained (Fig. 1B) [*Testor*, 2013; *Severin et al.*, 2017], with the objective of globally mapping the convection area, the distribution of the newly formed deep waters and the distribution of inorganic and organic matter. DeWEX Leg 2 sampled the spring bloom from 5 to 24 April 2013 [*Conan*, 2013; *Mayot et al.*, 2017]. It followed the same sampling network as the winter cruise, with 99 hydrological profiles and 59 biogeochemical profiles (Fig. 1C) [*Severin et al.*, 2017]. The third cruise was carried out during the oligotrophic period, between 24 July and 7 August 2013, in the framework of the integrated observation network MOOSE (Mediterranean Ocean Observing System for the Environment) [*Testor et al.*, 2013]. 100 biogeochemical profiles were measured (Fig. 1D).

Then, data provided by the Bio-Argo float LovBio17b between April and September 2013 [*Pasqueron de Fommervault et al.*, 2015b] were used to assess the modeled vertical evolution of the nitrate concentration. LovBio17b provided 73 vertical profiles at a daily frequency during the first 55 days of spring, and then at 5-day frequency for the next summer weeks. Calibration was performed at the deployment using *in situ* observations from 0 to 1000 m depth (about 10 m resolution in the 0-250 m layer, and 30 m below).

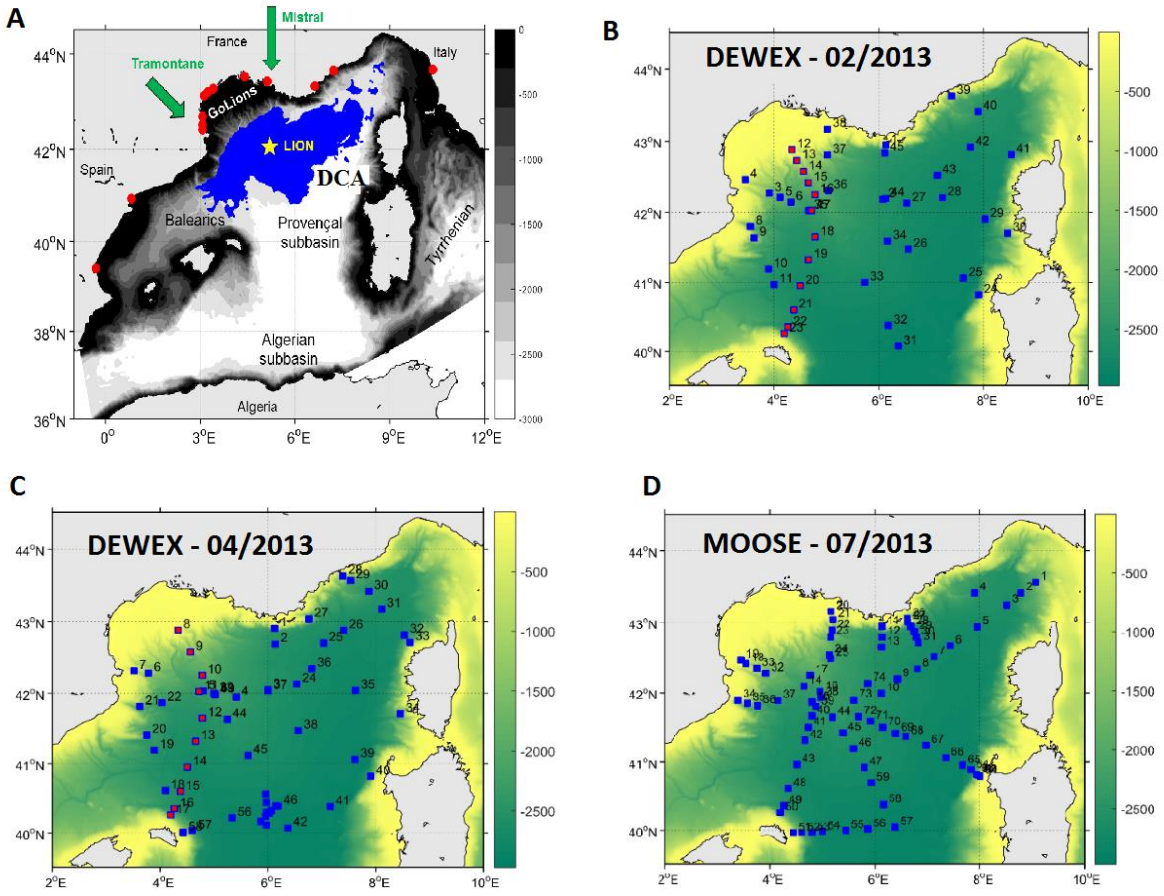

Figure 1. A/ Bathymetry (m) of the coupled physical-biogeochemical model domain. The red dots represent the modeled river locations. The blue area DCA (Deep Convection Area) corresponds to the simulation analysis area. The yellow star corresponds to the LION station where the heat flux plotted on Fig. 6 was modeled. Maps B, C and D represent the biogeochemical measurement stations of the DeWEX Leg 1 (February 2013), DeWEX Leg 2 (April 2013) and MOOSE-GE 2013 (July 2013) cruises respectively. Stations in red on Fig. B and C are located on the transect presented in Fig. 3 and Fig. 4.

2.2.Modeling

2.2.1. Hydrodynamics

The SYMPHONIE model used in this study is a 3D primitive equation, with free surface and generalized sigma vertical coordinate, described by *Marsaleix et al.* [2008, 2009, 2011 and 2012]. It was previously used for the Mediterranean Sea to simulate convection in the deep sea [*Herrmann et al*., 2008; *Estournel et al.*, 2016b], coastal dense water formation [*Estournel et al.*, 2005; *Ulses et al.*, 2008] and circulation on the continental shelf of the Gulf of Lions [*Petrenko et al.*, 2008]. The numerical domain (Fig. 1A) covers most of the western Mediterranean basin, using a curvilinear grid with variable horizontal resolution [*Bentsen et al.*, 1999]. The resolution is 1.4 km to the south and about 0.8 km to the north. The southward decrease of the resolution is intended to cover the W Med basin at a more reasonable cost while considering the northward decrease of the Rossby radius, in particular the need for increased resolution in the winter dense water formation area [*Estournel et al.*, 2016b].

Forty vertical levels were used with closer spacing near the surface (15 levels in the first 100 meters in the center of the convection zone characterized by depths of ~2500 m). The model was initialized and forced at its lateral boundaries with daily analyses provided by the Mercator-Ocean operational system based on the NEMO ocean model [*Maraldi et al.*, 2013]. The configuration of this model was the PSY2V2R4 prototype based on the NEMO Ocean modeling platform and the SAM data assimilation system [*Lellouche et al.*, 2013] at a resolution of 1/12° over the Atlantic and the Mediterranean from 20° S to 80° N. As in *Estournel et al.* [2016b], the initial field and open boundary conditions were corrected for stratification biases deduced from comparisons between analysis and observations taken during the MOOSE cruise of August 2012. The atmospheric forcing (turbulent fluxes) was calculated using the bulk formulae of *Large and*

Yeager [2004]. Meteorological parameters, including radiative fluxes, were given by the ECMWF operational forecasts at 1/8° horizontal resolution and 3-hour temporal resolution based on daily analysis at 00.00 UTC. Since the underestimation of strong winds is a source of uncertainty in atmospheric forcing [*Herrmann et al.*, 2010], *Estournel et al.* [2016b] performed sensitivity tests to the wind speed. According to those tests, the wind velocity was increased by 13% in order to increase the accuracy of the model results in reproducing the convection event [*Estournel et al.*, 2016b] in our hydrodynamic simulation. River runoffs were considered using measured daily values for French rivers (data provided by Banque Hydro, www.hydro.eaufrance.fr) and the Ebro (data provided by SAIH Ebro, www.saihebro.com) and mean annual values for the others.

2.2.2. Biogeochemistry

The Eco3M-S model [*Ulses et al.*, 2016] is a multi-nutrient and multi-plankton functional type model that simulates the dynamics of the biogeochemical decoupled cycles of several biogenic elements (carbon, nitrogen, phosphorus, silicon and oxygen) and of non-Redfieldian plankton groups. The model comprises seven compartments. A first compartment of phytoplankton classified by size is described by the mechanistic formulations of the model Eco3M [*Baklouti et al.*, 2006], where pico-phytoplankton [0.7–2 μm] and nanophytoplankton [2–20 μm] are composed of dinoflagellates, and micro-phytoplankton [20–200 μm] is composed of diatoms. A second compartment of zooplankton is composed of nano-zooplankton [5–20 μm] (small flagellates), micro-zooplankton [20–200 μm] (ciliates and large flagellates) and meso-zooplankton [>200 μm] (copepods and amphipods). A third compartment, bacteria, is also considered. The behavior of heterotrophic organisms is derived from the model by *Anderson and Pondaven* [2003]. The other compartments are dissolved organic matter, particulate organic matter (small and large, differentiated by the settling speed and origin), inorganic nutrients (nitrate, ammonium, phosphate and silicate) and dissolved oxygen. A total of 34 state variables

are calculated. The model structure (Fig. 2) used in this study is based on the same pelagic plankton ecosystem model as the one fully described and used by *Auger et al.* [2011] and *Ulses et al.* [2016]. Here we recall the equations of the rates of change of the nitrate and phosphate, since we will discuss the time evolution of their stock and of their ratios in section 4.1:

$$\frac{\partial[NO_3]}{\partial t} = Nitrification - PhytoplanktonUptake \qquad (1)$$

$$\frac{\partial[PO_4]}{\partial t} = ZooplanktonExcretion + BacteriaExcretion - PhytoplanktonUptake \qquad (2)$$

where *Nitrification* is the nitrification rate, *PhytoplanktonUptake* is the nutrient uptake by phytoplankton, and *ZooplanktonExcretion* and *BacteriaExcretion* are the nutrient excretions by zooplankton and bacteria, respectively. The formulas of these fluxes are given in *Auger et al.* [2011] (their Table A4). The uptake of nutrients by phytoplankton (*PhytoplanktonUptake*) depends on the gross primary production rate and on the nutrient concentrations (A19 to A22 in Table A.4 of *Auger et al*., 2011). Excretions (*ZooplanktonExcretion* and *BacteriaExcretion*) are the processes enabling heterotrophs to keep their internal composition constant by releasing the excess elements in the form of dissolved inorganic matter (A38 to A42 in Table A.4 of *Auger et al*., 2011). *Nitrification* is the production of nitrate by bacteria, represented here in an implicit way by a first order function of the ammonium concentration (A55 in Table A.4 of *Auger et al*., 2011). *Nitrification* is regulated by light intensity and temperature. For the present study of the NW Med, where winter convection favors strong vertical transport of nutrients in the photic zone, we neglected the process of nitrogen fixation. This process has been shown to have only a small effect on stoichiometry in the W Med [*Ribera d'Alcala et al.*, 2003]. Most of the values of biogeochemical model parameters were based on the previous modeling study by *Ulses et al.* [*2016*], but some parameters were re-calibrated using several datasets (MODIS, BOUM, MOOSE-GE and DeWEX cruises).

In this study, we used the "Source Splitting" coupling method [*Butenschön al.*, 2012]. It consists

in an offline forcing of the biogeochemical model by the daily averaged outputs of the physical model. A time step of a few minutes was used for the advection and diffusion of biogeochemical variables, while Eco3M-S computed the biogeochemical fluxes with a time step of about one hour. It was then assumed that biogeochemical properties do not significantly impact the hydrodynamics.

The biogeochemical model was downscaled from the Mediterranean basin scale to the regional scale as described hereafter. First, the biogeochemical basin scale model was forced by the daily fields from the NEMO model (PSY2V2R4 analyses), also used for the boundary conditions of the hydrodynamic model as indicated in section 2.2.1. This basin configuration was initialized in June 2010 with climatological nutrient fields from the Medar/MedAtlas database [*Manca et al.*, 2004] corresponding to oligotrophic conditions. Daily values of all state variables were extracted from the basin run for the initial and lateral boundary conditions of the regional model. This nesting protocol ensures coherence of the physical and biogeochemical fields at the open boundaries. The regional model was initialized in August 2012.

At the mouth of the Rhone river, nitrate, ammonium, phosphate, silicate and dissolved organic carbon concentrations were prescribed using *in situ* daily data [*P. Raimbault*, personal communication, 2015]. Concentrations of dissolved organic phosphorus and nitrogen and also of particulate organic matter were estimated from these data and the relations deduced from the literature [*Moutin et al.*, 1998; *Sempéré et al.*, 2000] as described in *Auger et al.* [2011]. At the other river mouths, climatological values were prescribed according to *Ludwig et al.* [2010]. The deposition of organic and inorganic matter from the atmosphere was neglected in this study. The benthic fluxes of inorganic nutrients were considered by coupling the pelagic model with a simplified version of the meta-model described by *Soetaert et al.* [2001]. The parameters of this model were set according to the modeling study on the Gulf of Lions shelf performed by *Pastor et al.* [2011].

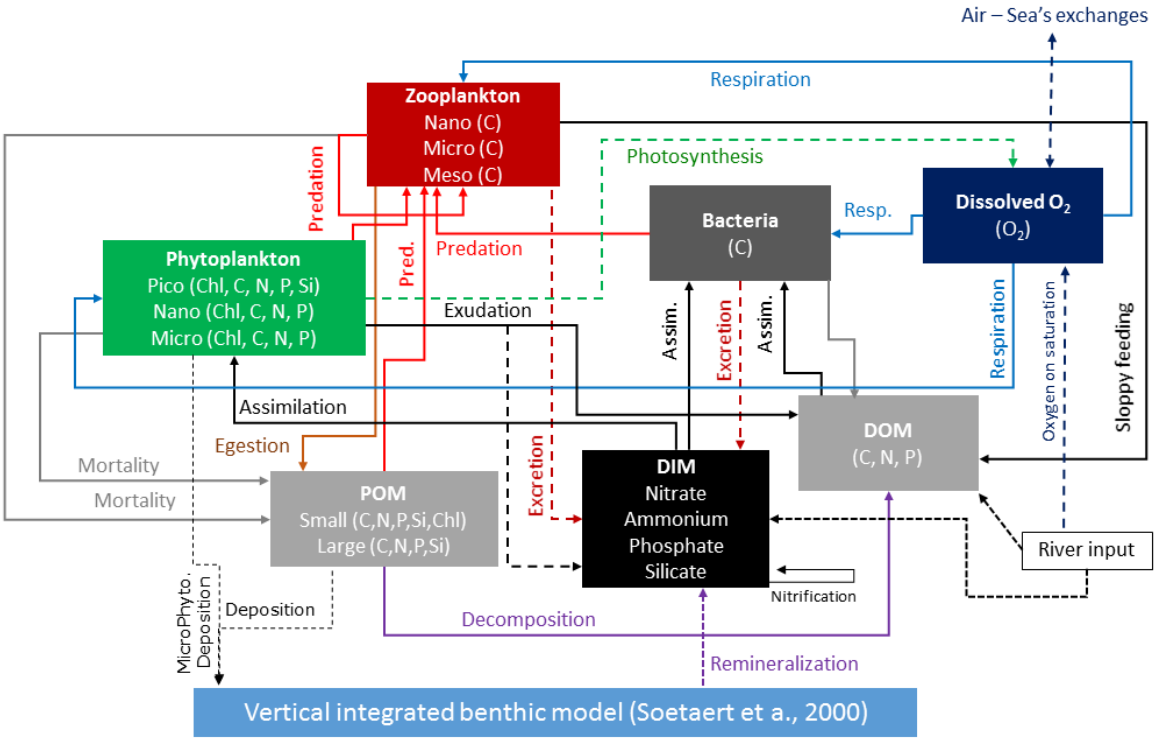

Figure 2. Eco3m-S biogeochemical model scheme.

2.3. Area of study

The analysis of the nitrogen and phosphorus seasonal cycles, and annual budgets, was performed for the deep convection area of the NW Med, defined here using a mixed layer criterion. This region (indicated in blue on Fig. 1A), named Deep Convection Area (DCA) hereafter, represents the area where the mixed layer depth (MLD), defined in section 2.4, exceeded 1000 m for at least one day during the study period. According to the model, it covered more than 61 700 km^2 in 2013.

For the analysis and budget estimates, we divided the water column into two layers: an upper layer corresponding to the layer where primary production takes place, and a deep layer corresponding to the reservoir of inorganic nutrients. We chose to delimit these two layers with a nutricline criterion. The depth of the nutricline varies over time. As a variable depth would not allow a simple analysis of stock variations and annual budget of processes, we took a constant value corresponding to the maximum depth of the nutricline in the model domain, equal to 130 m, as our criterion. As the gradient of nutrient concentration is strong at the nutricline depth, the model estimate of nutrient stock in the upper layer is highly sensitivity to the depth criterion. For instance, an overestimation of the nutricline depth in the model would lead to an underestimation of the modeled nutrient stock. In this study, we focus then on the variation of the nutrient inventory rather than on the value of this inventory. Moreover, we consider the temporal variation of nutricline depth when analyzing that of upper layer nutrient stock.

Besides, previous studies [Martin and Pondaven, 2006; Kortzinger et al., 2008] demonstrated that material exported below the productive layer could be resuspended within this zone during mixing periods. Then the maximum yearly mixed layer depth was recommended as a threshold to calculate the export flux or new primary production [Martin and Pondaven, 2006; Palevsky et al., 2016]. The computation of the modeled export of organic and inorganic matter as the sum of sedimentation (for particulate matter) and net flux induced by turbulent mixing and vertical advection in the present study avoids counting the export of organic and inorganic matter that is then reinjected into the upper layer during mixing periods. However, we are aware that if new primary production is considered as the algal growth fueled by nitrate coming in the upper layer for the first time of the studied year, then it could be overestimated due to the recycling of exported organic material in the deep layer whose products would be upwelled back in the upper layer during the mixing period. The estimate of nitrification in the upper layer will be used to estimate this overestimation.

2.4. Derived variables

Variables used for the analysis of the annual cycles and budgets were derived from the coupled model. The modeled MLD is defined as the depth where the potential density exceeds its value at 10 m below the surface by 0.01 kg m^{-3}. We calculated the depths of the 1 mmolN m^{-3} and 0.05 mmolP m^{-3} iso-concentrations of nitrate and phosphate, as a proxy of the depths of the nitracline and phosphacline, respectively, according to *Lavigne et al*. [2013] and *Lazzari et al.* [2012] studies. Both depths are significantly correlated in time in this region ($R=0.84$, $p<0.01$) and the maximum difference between the depths of the nutriclines is 10 m. For this reason, the nutricline refers to both the nitracline and the phosphacline hereafter. The stock of nutrients in the surface layer [0-130 m] was calculated in the simulation. Moreover, we computed a second estimate of the nutrient stock in the Deep Convection Area using the observations from the three cruises described in section 2.1. The nutrient concentrations measured during the cruises were interpolated over the model grid and then integrated in the 0-130 m layer as in the model. The interpolation method considers the notion of distance in space but also the deviation from selected physical fields (temperature, salinity). In practice, the nitrate and phosphate fields are interpolated from the cruise data (74 vertical nutrient profiles for MOOSE, 104 nutrient profiles for DEWEX cruises). It is therefore possible to estimate the deviation of temperature and salinity between all points of the numerical grid and the points corresponding to the position of the nutrient profiles to be interpolated. Since the bathymetry of a region such as the Mediterranean has a great influence on the organization of the circulation, the bathymetry deviation was also considered in a similar way. Finally, the concentration of the nutrients C at grid point (x, y, z) was obtained in the following way:

$$C(x,y,z) = \frac{\sum_q W_q C(q,z)}{\sum_q W_q} \quad (3)$$

where q is the nutrient profile number, $C(q,z)$ the concentration of nutrients at the point

corresponding to the position of the nutrient profile q and depth z, and W_q the weight depending on the tracers and bathymetry deviations according to:

$$w_q = e^{-\left(\frac{S_{x,y,z}-S_{q,z}}{\delta S_0}\right)^2} \times e^{-\left(\frac{T_{x,y,z}-T_{q,z}}{\delta T_0}\right)^2} \times e^{-\left(\frac{H_{x,y}-H_q}{\delta H_0}\right)^2} \times e^{-\left(\frac{D_q}{D_0}\right)^2} \quad (4)$$

where S is the salinity, and δS_0 is an empirically determined scale of salinity variation (the terms related to temperature (T) and bathymetry (H) are obtained in a similar manner), Dq is the horizontal distance between the considered grid point and the nutrient profile q, $D0$ is an empirically determined scale of distance.

Finally, we deduced a value of the N:P ratio from the ratio of nitrate to phosphate stocks in the upper layer, INO_3 *and* IPO_4(in mmol m^{-2}), respectively. The contribution of biogeochemical or physical processes to the change of N:P ratio, was computed with Eq. 5:

$$\frac{\partial(N:P)}{\partial t} = \frac{IPO_4 \frac{\partial INO_3}{\partial t} - INO_3 \frac{\partial IPO_4}{\partial t}}{(IPO_4)^2}$$

where $\frac{\partial INO_3}{\partial t}$ and $\frac{\partial IPO_4}{\partial t}$ (in mmol m^{-2} d^{-1}) are the rates of change of upper layer nitrate and phosphate stocks, respectively:

$$\frac{\partial INO_3}{\partial t} = VertNO_3 + HorAdvNO_3 + I\left(\frac{\partial [NO_3]}{\partial t}\right)_{bio} \quad (6)$$

$$\frac{\partial IPO_4}{\partial t} = VertPO_4 + HorAdvPO_4 + I\left(\frac{\partial [PO_4]}{\partial t}\right)_{bio} \quad (7)$$

where $VertNO_3$ and $VertPO_4$ are the net upward fluxes of nitrate and phosphate, respectively, at 130 m depth, due to vertical advection and turbulent mixing, $HorAdvNO_3$ and $HorAdvPO_4$ are the net horizontally advected inputs of nitrate and phosphate, respectively, in the upper layer from surrounding regions, $I\left(\frac{\partial [NO_3]}{\partial t}\right)_{bio}$ and $I\left(\frac{\partial [PO_4]}{\partial t}\right)_{bio}$ are the upper layer integrated

biogeochemical processes (see Eq. 1 and Eq. 2).

2.5 Statistical analysis of the model results

A point-to-point approach was used to quantify the performance of the model in its ability to represent the dynamics of inorganic nutrients and chlorophyll over the study period. The model results were compared with the observations at the same dates and positions. Following the recommendations of *Allen et al.* [2007] we calculated four metrics: the standard deviation ratio ($r_\sigma = \frac{\sigma_m}{\sigma_o}$ where σ_m and σ_o are the standard deviation of model outputs and observations, respectively); the Pearson correlation coefficient ($R = \frac{\frac{1}{k}\sum_{n=1}^{N}(m_n-\bar{m})-(o_n-\bar{o})}{\sigma_m \times \sigma_O}$), where K is the number of observations, m_n is the model output that corresponds to the observation n, o_n, $\bar{m}$ and $\bar{o}$ are the mean of model outputs and observations respectively); the Nash-Sutcliffe efficiency ($NS = 1 - \frac{\frac{1}{N}\sum_{n=1}^{N}(o_n-m_n)^2}{\sum_{n=1}^{N}(o_n-\bar{o})^2}$) and the percentage bias ($PB = \frac{\bar{m}-\bar{o}}{\bar{o}}$). The calculation of these four-complementary metrics enabled different aspects of the model results to be assessed. The standard deviation ratio assessed the variability in the model results compared to that in observations, a value of $r_\sigma > 1$ indicating that the variability was stronger in the model outputs than in observations. The correlation coefficient assessed the similarity between model and observations and significative correlations ($p<0.01$) were obtained for all R calculations presented in section 3. The Nash-Sutcliffe efficiency assessed the difference between model and observations compared to the variability in the observations. According to *Allen et al.* [2007] a value > 0.65 indicates excellent performance, [0.65,0.5] is very good, [0.5,0.2] is good, and <0.2 indicates poor performance. Finally, the percentage bias indicated a general overestimation in the model results when it was positive and conversely. According to *Allen et al.* [2007] the performance of the model can be considered as excellent if the percentage bias is < 10%.

3. Comparison of model results with observations

An evaluation of the hydrodynamic simulation is described in *Estournel et al.* [2016b] where modeled temperature and salinity were compared with different available sets of observations.. The present study focuses on evaluating the model's ability to reproduce the spatial and temporal variability of inorganic nutrients.

3.1 Comparison with winter, spring and summer cruise observations

To evaluate the model's performance to reproduce the horizontal and vertical biogeochemical patterns in relation with the hydrology, the simulation was compared to the observations from cruises that took place during three key periods for the ecosystem (winter, spring and summer). For winter and spring periods, first, we compared the surface concentrations of nutrients. Then the model/observations comparison was made over the water column along a transect across the deep convection area, from the Balearic Islands to the Gulf of Lions shelf (measurement locations are indicated by the red dots on Fig. 1B for winter and 1C for spring). For both comparisons, the modeled concentrations of nutrients were averaged over the period of sampling: 21 and 20 days for the surface observations, and 2 and 3 days for the transect observations, for the winter and spring cruises, respectively.

3.1.1 **Winter**

In winter, during the winter cruise, modeled and observed surface concentrations of nitrate and phosphate (Fig. 3A and 3B) show some heterogeneity. The model indicates that the patch of high surface nutrient concentrations (> 7.5 mmol m^{-3} for nitrate and > 0.3 mmol m^{-3} for phosphate) was located between 40.5°N and 43°N and between 3°E and 8°E. These characteristics and values match the observations, which show surface concentrations >7.64 mmol m^{-3} for nitrate and >0.35 mmol m^{-3} for phosphate [*Severin et al.*, 2017]. The highest values corresponded to the center of the Deep Convection region where intense convection brought nutrients to the surface

layer [*Severin et al.*, 2017]. Outside the convective mixed patch, the surface nutrient concentrations were very low (<1 mmol m^{-3} for nitrate and <0.05 mmol m^{-3} for phosphate) as detected in the observations south of latitude 41°N. Between these two regions, a strong gradient was observed and modeled on a narrow band. Around the convective patch, in the Balearic Sea and in the Gulf of Lions, the observations show values close to 2.95 mmol m^{-3} for nitrate and 0.11 mmol m^{-3} for phosphate, while the model overestimates these values by 1 mmol m^{-3} for nitrate and by 0.4 mmol m^{-3} for phosphate. The strong gradient between the deep convection patch and the surrounding areas was a location of complex frontal dynamics. The greatest biases could originate from vertical motions at very fine scale on these fronts. Nevertheless, it is interesting to note the fine scale structures in the model, which could be explained by the enrichment of deep nutrients induced by the small-scale dynamics.

Figures 3C-E give complementary information on the vertical distribution of chlorophyll and nutrient concentrations in the model compared with the observations. Between latitudes 41.5°N and 42.5°N, the modeled and observed water column was homogeneous in biogeochemical variables. Both model and observations show that the surface chlorophyll a concentration was minimum in the deep convection area (lower than 0.10 mg m-3 in the model, lower than 0.16 mg m-3 in the observations). This feature was previously highlighted using satellite data and 3D coupled modeling [*Auger et al.*, 2014; Houpert et al., 2016; Herrmann et al. 2017]) and was explained by a low phytoplankton growth and/or the vertical dilution of phytoplankton cells throughout the whole mixed layer that can reach the ocean bottom (~2500 m). The maximum vertical gradient of nutrients corresponded to the 29.05 kg m^{-3} isopycnal (superimposed on vertical sections; Fig. 3C-E) at the northern and southern limits of the Deep Convection Area. The isopycnal depth varies between 200 m to the south and 400 m to the north. Beyond this threshold, modeled nitrate concentration increased from 6 to 8 mmol m^{-3} and phosphate concentration from 0.2 to 0.35 mmol m^{-3}.

Vertical homogeneity, at least over several hundred meters in the center of the Deep Convection Area, in temperature, salinity [*Estournel et al.*, 2016b] and nutrient concentrations, was also observed during winter 2011 as reported by *Severin et al.* [2014] and *D'Ortenzio et al.* [2014]. Other authors [*Yilmaz and Tugrul*, 1998; *Gacic et al.*, 2002; *Dilek et al.*, 2005; *Santinelli et al.*, 2012] have reported some homogeneous biogeochemical profiles and high surface inorganic matter enrichment by convective mixing in the eastern Mediterranean basin as mentioned before.

When comparing modeled nitrate and phosphate concentrations (mean values and standard deviations: 6.35 ± 1.92, 0.26 ± 0.09 mmol m^{-3}), respectively with the whole winter cruise observations (mean values and standard deviations: 6.45 ± 2.66, 0.28 ± 0.13 mmol m^{-3}), we find a Pearson correlation coefficient of 0.87 and 0.89 (p-value<0.01), respectively, and a Nash-Sutcliffe efficiency of 0.73 and 0.75, respectively, both indicating excellent performance of the coupled simulation. The standard deviation ratio of 0.72 and 0.73, for nitrate and phosphate concentrations respectively, indicates a lower variability in model results than in observations, and the percentage biases of -1.5% and -5.5%, respectively, an underestimation of nutrient concentrations, visible around the convective region on Figure 3. Regarding the modeled chlorophyll concentrations (mean value and standard deviation: 0.12 ± 0.16 mg m^{-3}) compared to that observed on the cruise period (mean value and standard deviation: 0.18 ± 0.19 mg m^{-3}), the Pearson coefficient correlation of 0.81 and the Nash-Sutcliffe efficiency of 0.56 show that the model reproduces very well the spatial phytoplankton distribution. However, the percentage bias shows that the model underestimates the observations by 32% in average.

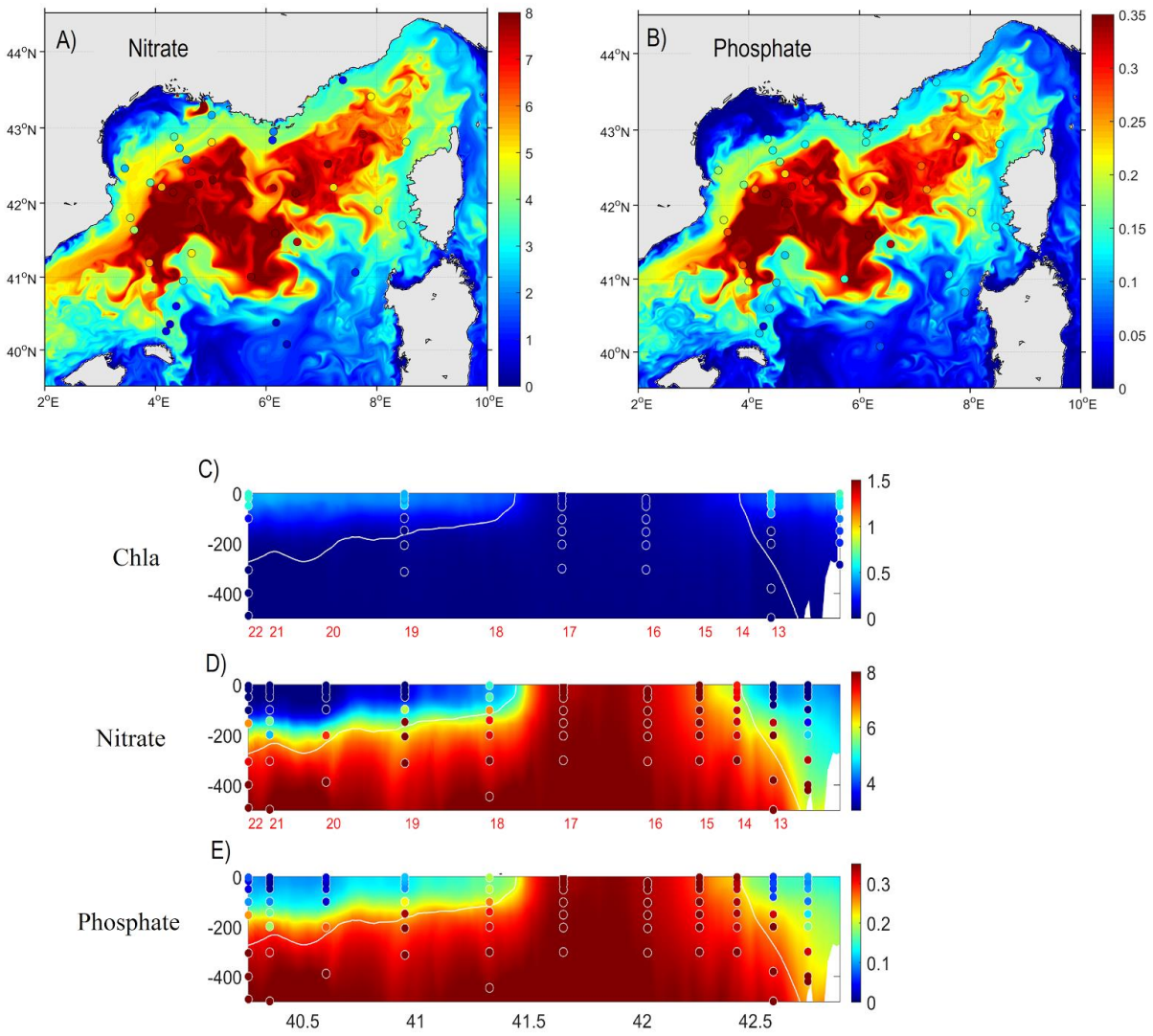

Figure 3. Comparison of modeled and observed surface (A) nitrate and (B) phosphate concentrations (mmol m^{-3}) during the winter cruise. Vertical section of (C) chlorophyll (mg m^{-3}), (D) nitrate (mmol m^{-3}) and (E) phosphate (mmol m^{-3}) concentrations across the Deep Convection Area, indicated by red dots on Fig. 1B. The model is represented by background colors and observations are indicated in colored circles (DeWEX Leg1, February 2013). White lines in the

vertical sections (C to E) represent the 29.05 kg m^{-3} isopycnal potential density anomaly. The maps (A and B) correspond to an average modeled concentration over the period of the cruise (1 to 21 February) while the vertical cross section represents a model average over the transect observation period (12 to 13 February). The numbers of the measurement stations along the vertical section are indicated on the x-axis of panels. C and D. Latitudes are indicated on the x-axis of panel. E.

3.1.2 Spring

In spring, nutrient and chlorophyll patterns (Fig. 4) changed drastically compared to February 2013. *Severin al.* [2017] attributed these changes to a strong phytoplankton development, that was considered as a bloom by *Mayot et al.* [2017]. In this study, the onset of the bloom was considered as the day when the net accumulation rate of the carbon biomass integrated through the water column [*Behrenfeld*, 2010] exceeded 50% of its maximum yearly value. Surface nutrient concentrations were low (Fig. 4A and 4B) but remained higher in the Deep Convection Area than outside. In the observations, as in the model, surface values of 2 to 3 mmol m^{-3} of nitrate and 0.08 to 0.12 mmol m^{-3} of phosphate were observed in the center of the basin, while oligotrophic conditions were becoming established outside the Deep Convection Area, with surface nutrient concentrations down to 0 mmol m^{-3} in some areas away from the convection zone. In general, the model appears to underestimate the surface nutrient concentrations.

Figures 4D and 4E give an estimation of the nutricline depth, located at 60 m in average (standard deviation: 20 m) in the model, and following the density gradient. A surface chlorophyll development was observed and modeled (Figure 4C) in conjunction with the nutrient depletion (Fig. 4D and 4E), with a concentration exceeding 1.5 mg m^{-3} in the first 30 m, then 0.4 ± 0.2 $mg.m^{-3}$ from 30 to 60 m and zero below 60 m. A homogeneous physical, biogeochemical profile was observed at the station 42°N 5°E in April 8. Although the model reproduces this

445 homogeneous feature, the modeled nutrient concentrations are underestimated and the
446 chlorophyll concentration is overestimated in the surface layer at this station (not shown on the
447 three-days average in Fig. 4C, 4D and 4E). The model simulates during April, several short wind
448 gust events that interrupted the bloom development and mixed the upper layer. The strong gusts
449 of wind associated with negative heat flux that occurred on April 6 and 19 are examples, visible
450 on Figure 7. These events resulted in a temporary decrease of the chlorophyll surface
451 concentrations, and an increase of nutrients in mesoscale structures. Restratification followed the
452 wind events, and reconstructed the bloom conditions. The comparisons of model results with
453 observations suggest that the location of these mesoscale structures is not correctly reproduced in
454 the model.

455 The calculation of metrics indicates that the model reproduces very well the spatial distribution
456 of the whole nitrate and phosphate concentrations observed during the spring cruise (mean
457 values and standard deviations in the model: 5.07 ± 2.92, 0.21 ± 0.13 mmol m^{-3}, respectively,
458 mean values and standard deviations in observations: 5.44 ± 3.09, 0.23 ± 0.14 mmol m^{-3},
459 respectively): the correlation coefficients are 0.91 and 0.90 (p-value<0.01), respectively, the
460 Nash-Sutcliffe efficiencies are 0.80 and 0.77, respectively. The model presents lower variability
461 by 5 and 6% and underestimates by 6 and 8 % the nitrate and phosphate concentrations,
462 respectively. Regarding the chlorophyll concentrations (mean value and standard deviation in the
463 model: 0.38 ± 0.45 mg m^{-3}, mean value and standard deviation in observations: 0.56 ± 0.79 mg
464 m^{-3}), a good correlation (0.77) and a good Nash-Sutcliffe efficiency (0.50) between model and
465 observations are found. The percentage bias indicates that the model underestimates observed
466 chlorophyll concentration by 32%.

467

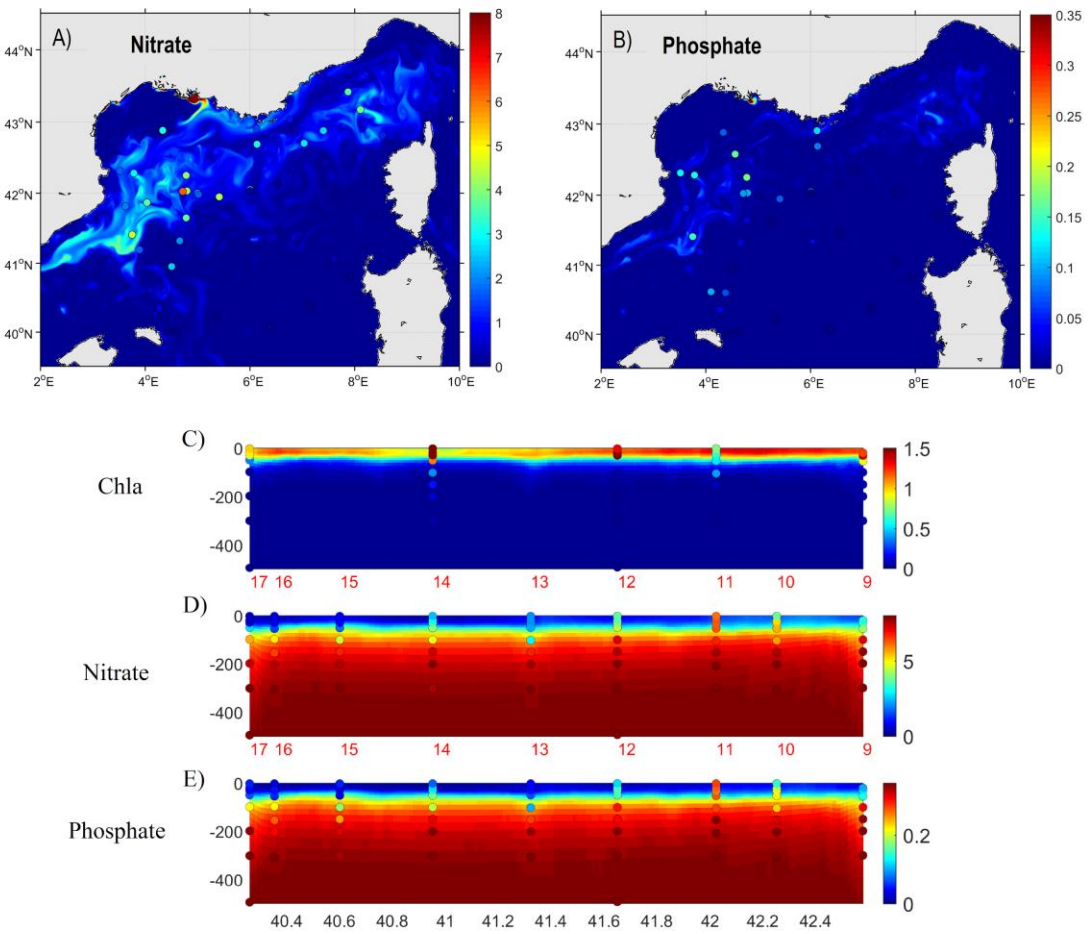

Figure 4. Same as Figure 3 but for spring cruise (DeWEX Leg 2) in April 2013. Model outputs are averaged over the period 5-24 April for panel. A and B, and over the period 8-10 April for panels C, D, and E. The numbers of the measurement stations along the vertical section are indicated on the x-axis of panels C and D. Latitudes are indicated on the x-axis of panel E.

3.1.3 Summer

Comparisons of modeled nitrate and phosphate concentrations in summer conditions (mean

values and standard deviations: 6.24 ± 3.10, 0.15 ± 0.25 mmol m^{-3}, respectively) with the whole summer cruise observations (mean values and standard deviations: 5.02 ± 3.28, 0.15 ± 0.19 mmol m^{-3}, respectively), at the same dates and locations, are shown in Fig. 5. From the bottom to 300 m depth, the modeled nutrient concentrations fall in the observed range. However, one can notice that most of the modeled nutrient concentrations in deep layers are in the upper range of the observed profiles. The nutrient gradient at 100 m depth is well reproduced by the model. However, higher values of modeled phosphate are visible at 50, 150 and 200 m depth. The model reproduces then correctly the depletion of nutrients in the 0-50 m surface layer.

We find a Pearson correlation coefficient of 0.82 and 0.82 (p-value<0.01), and a Nash-Sutcliffe efficiency of 0.52 and 0.46, for nitrate and phosphate concentrations respectively, both metrics indicating excellent performance of the coupled simulation. The standard deviation ratio of 0.94 and 1.04, for nitrate and phosphate concentrations respectively, indicates small differences in the variability in model results compared to observations, and the percentage bias of 24% and 32%, respectively, an overestimation of nutrient concentrations in the model.

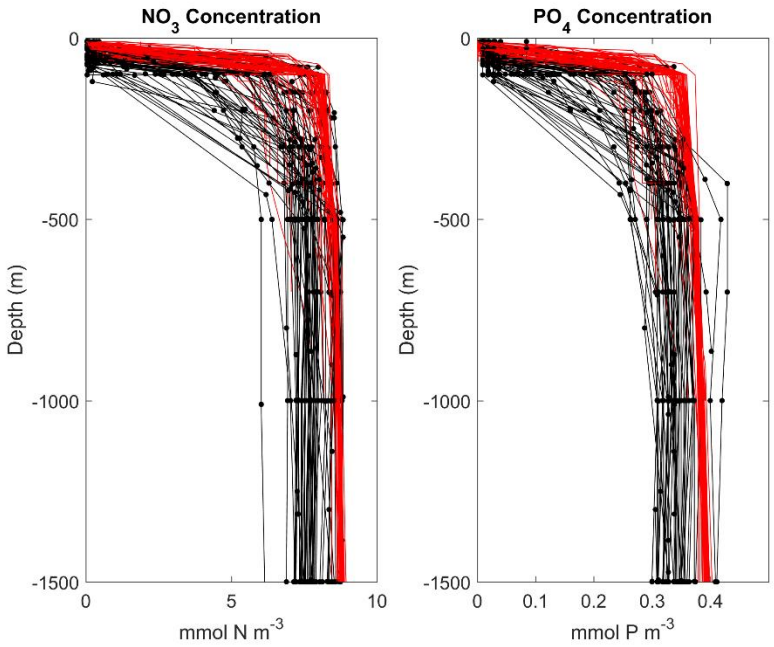

Figure 5: Comparison of modeled (red) and observed (black) nitrate and phosphate concentration (mmol m^{-3}) profiles during MOOSE cruise in July 2013.

3.2 Variability between April and September 2013

The objective of this section is to evaluate the ability of the model to reproduce the variability of the biogeochemistry during a transitional phase. The Bio-Argo float Lovbio17B deployed in the NW Med in April 2013 during the bloom presents a time-series of the nitrate concentration that describes the transition in the surface layer from the bloom to the oligotrophic phase.

Figure 6 shows an evolution of nitrate concentration measured by the float and simulated by the model at the same points. The deepening of the nitracline occurs earlier in the model than in the observations. The nitrate concentration measured by the float in April is 1 mmol m^{-3} higher than in the model but measured and modeled concentrations are identical in May, with a nutricline

503 located at the same depth (~ 50 m). Variations of nitrate concentrations from 0 to 7 mmol m^{-3} in
504 less than 30 m were observed in the surface layer and were correlated to high frequency motions
505 distinctly detected in both observations and model in April and May. These motions seem to
506 supply nutrients into the mixed layer (the depth of which is indicated by the green dashed line on
507 Fig. 6) more efficiently in the observations. This could be explained by an underestimation of the
508 vertical gradient at 100 m in the model, as shown also in Fig. 4D and 4E. However, in the model
509 results and observations, after each pulse of nutrient injection, the nitrate depletion in the surface
510 layer was fast and the nutricline deepened with time from 50 m at the beginning of June to 70 m
511 during the whole summer. At the same time, a shallow mixed layer was observed around 10-15
512 m.

513 The calculated metrics show that the model can correctly reproduce the transitional phase
514 observed by the float. The Pearson correlation coefficient (R=0.94) and the Nash-Sutcliffe
515 efficiency (NS=0.82) indicate excellent performance of the model. However, slightly higher
516 variability in the observation is indicated by the standard deviation ratio of 0.95. The float
517 measured concentrations higher than 1 mmol m^{-3} in the upper layer from May to October, when
518 the model's concentrations were very low above the nitracline. A general underestimation by the
519 model is indicated by the percentage bias of -16%.

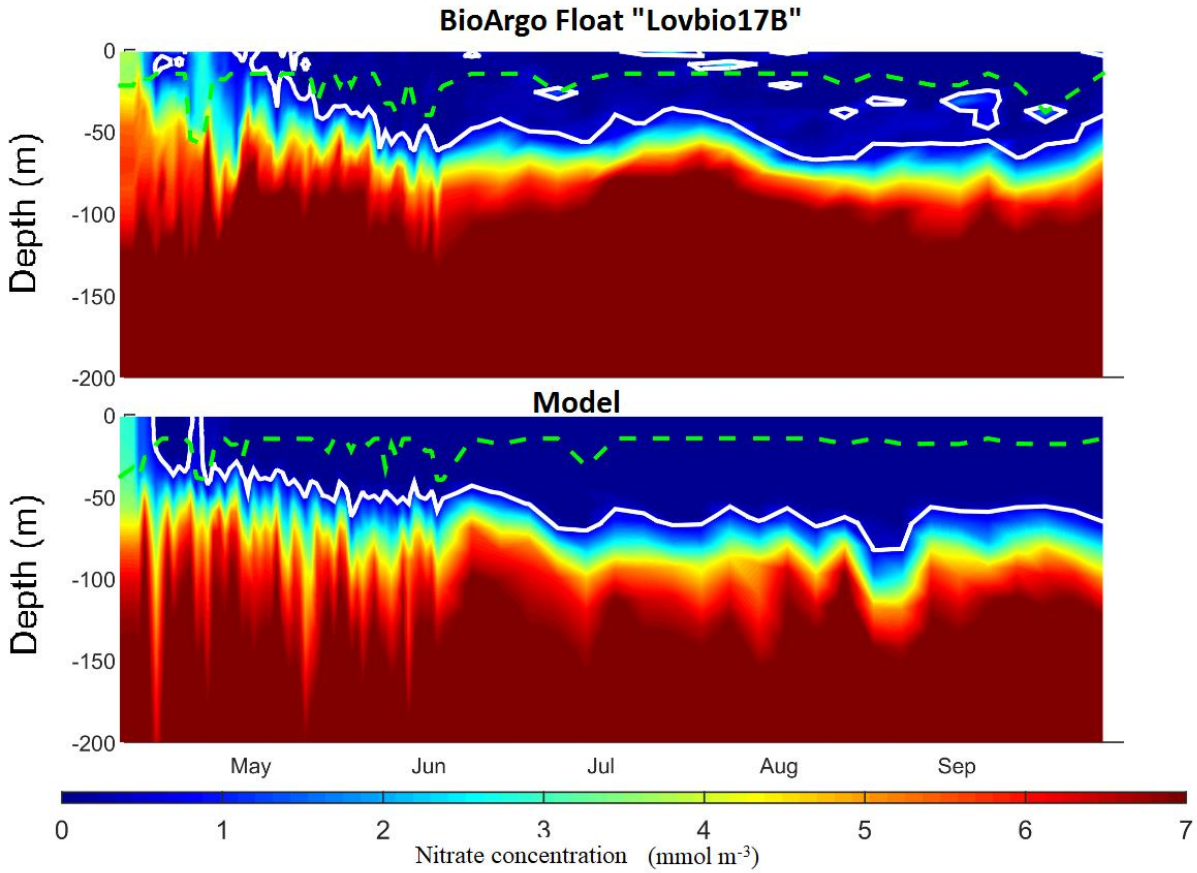

Figure 6. Hovemöller diagram of the nitrate concentration (mmol m^{-3}) along the float track from April to September 2013. Data are extracted from the float Lovbio17B (upper panel) and from the model (lower panel). White line represents the depth of the nitracline (position of the 1 mmol m^{-3} concentration) and the green dashed line represents the MLD.

4. Results and Discussion

The comparison exercise reveals that the coupled model is able to reproduce the general seasonal

dynamics of inorganic nutrients and phytoplankton growth deduced from the cruise observations. The spatial extension of the convection area, where deep inorganic nutrients were upwelled and phytoplankton were diluted over the whole water column, appears to be in good agreement with cruise observations. The model reproduces the strong inorganic nutrient decrease between winter and spring cruises. Finally, the modeled depletion of nutrients of the upper layer in summer agrees with MOOSE and Lovbio17B observations. However, the model appears to generally underestimates the observed surface nutrient concentrations in spring and to anticipate the deepening of the nutricline observed by the Bio-Argo float.

Aware of the weaknesses and the strengths of the present coupled simulation, in the following sections, we use the model outputs to disentangle the impact of the physical and biogeochemical processes on the seasonal variations of the nutrient stock and stoichiometry in the upper layer of the Deep Convection Area, from September 2012 to September 2013. Finally, the model is also used to estimate a budget of nitrogen and phosphorus in the upper and deeper layers over the one-year study period.

4.1.Annual cycle of nutrients

4.1.1 Atmospheric forcing and ocean vertical mixing

Figure 7 presents the time series of the modeled heat flux at the LION station (42°N, 5°E), located in the center of the Deep Convection Area, and Fig. 8 presents the time series of the modeled MLD averaged over the Deep Convection Area, from September 2012 to September 2013. Seasonal variability of the atmospheric forcing is clearly visible. In September and October 2012, positive heat fluxes were regularly interrupted by short, strong heat loss events corresponding to wind gusts from the north. In late October, an extreme heat loss event (-1300 W m^{-2}) severely weakened the stratification of the upper layer and the spatially-averaged MLD deepened by 20 m (Fig.8). In late November/early December, a strong wind episode lasted three

552 weeks. Then a succession of heat loss events followed from mid-January to the end of February.
553 From December, each event produced a pronounced increase of the MLD. At the beginning of
554 February, the ML reached the seafloor in the deep convection center (not shown), when the
555 spatially averaged MLD reached 1500 m (maximum deepening not shown in Fig. 8). A final
556 short, strong wind episode occurred between the second and the third weeks of March. This
557 event caused a breakdown of the weak restratification established during the calm second week
558 of March. Winter 2013 was thus characterized by a first and main convection event, from mid-
559 January to early March, and a secondary convection event occurring during the third week of
560 March. During the last week of March, the heat flux became durably positive in general. The
561 frequency of the short, intense wind events decreased from three per month in April to one per
562 month in summer. After March, the heat gain was a component of the progressive surface layer
563 restratification, the development of instabilities around the mixed patch being the other
564 component [*Estournel et al*, 2016b]. In spring, large variations (40 m) of the MLD (Fig. 8) can
565 be noted because of the wind effect on a weak stratified surface layer, as during the third week of
566 April.

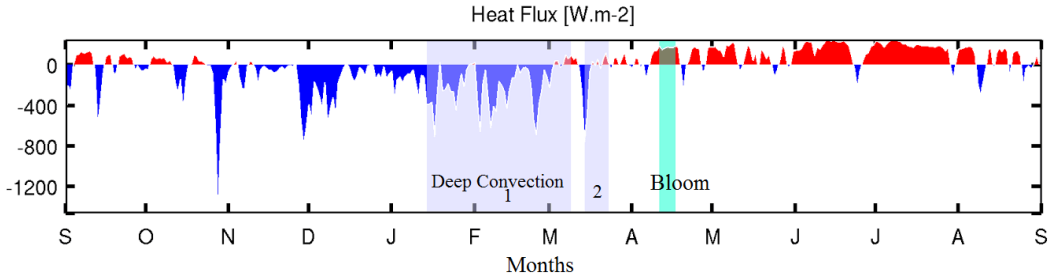

567

568 **Figure 7.** Time series of modeled total heat flux (W m^{-2}) at LION (indicated on Fig. 1A) from
569 September 2012 to September 2013. Blue bars represent the period when the MLD was higher
570 than 1000 m (convective mixing), while the green bar represents the restratification period
571 coinciding with the phytoplankton development maximum.

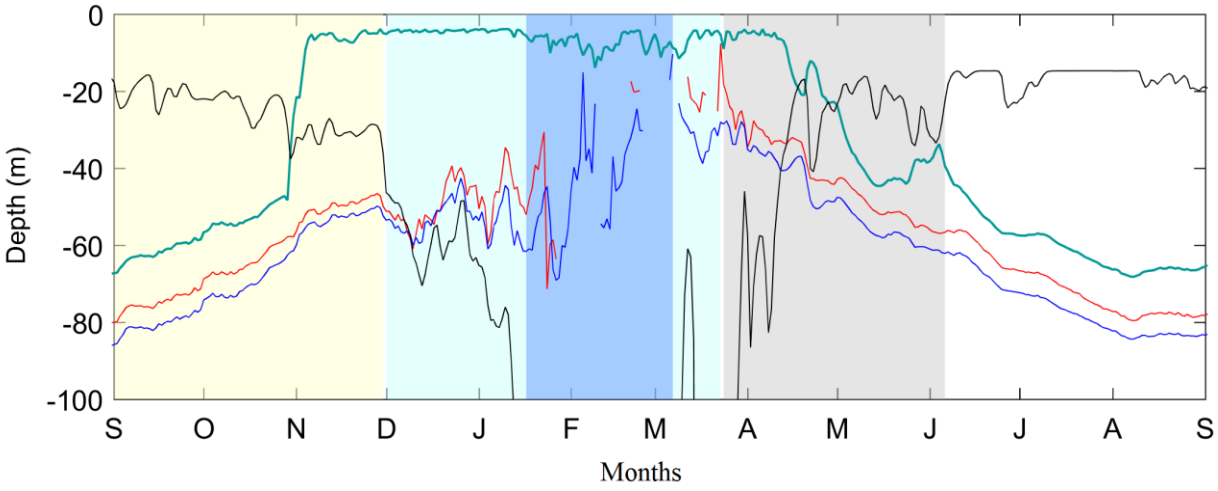

572

573 **Figure 8.** Time series of the depth (m) of the modeled mixed layer (in black), nitracline (in red),
574 phosphacline (in blue) and deep chlorophyll maximum (in green) averaged over the deep
575 convection region from September 2012 to September 2013. The background color stands for the
576 season: yellow for autumn, blue for winter, with the dark blue representing the period when the
577 MLD was higher than 1000 m (convective mixing), gray for spring and white for summer.

578 **4.1.2 Stock of nutrients in the upper layer**

579 Figure 9 presents the annual cycle of the simulated nitrate and phosphate stocks in the upper 130
580 m of the Deep Convection Area. Stocks deduced from the cruise observations (see section 2.4 for
581 details) are shown as horizontal bars overlaying the model output. The model reproduces the
582 trend and orders of magnitude of the nutrient stock as estimated from the observations made
583 during the three cruises, in winter (800 mmolN m^{-2} and 35 mmolP m^{-2}), spring (<450 mmolN m^{-2}
584 and 20 mmolP m^{-2}) and summer (<200 mmolN m^{-2} and 10 mmolP m^{-2}). An underestimation of
585 10 mmolN m^{-2} (7% of the stock) for the stock of nitrate and 4 mmolP m^{-2} for the stock of
586 phosphate (16% of the stock) is, however, visible in the model estimates for February 2013 when
587 they are compared with the observations. In this section, we use the model outputs to analyze the

588 impact of the physical and biogeochemical processes on the seasonal variations of the nutrient
589 stock. The biogeochemical interfaces (nitracline, phosphacline and deep chlorophyll maximum –
590 DCM) are plotted in Fig. 8. The year is divided into four periods corresponding to the seasons
591 analyzed individually (they are indicated by colored vertical bars in Figs. 8, 9, 10 and 11). The
592 first season is autumn, from 1 September to 1 December 2012. Winter was chosen to start when
593 both strong negative heat fluxes (from 1 December 2012 to 23 March 2013) (Fig. 7) and
594 relatively deep mixed layer (> 50 m, Fig. 8) conditions co-occurred. Spring, which begins on 24
595 March here, corresponds to the period where the mixed layer became shallower than the
596 epipelagic layer, which was at 120 m in average (standard deviation: 30 m). It ends on 6 June
597 when the mixed layer stabilized at very shallow depth (< 20 m) and the DCM became established
598 below 40 m. Summer is the last stage, which starts on 6 June and lasts until 1 September 2013,
599 the end of the time series.

600

601

602

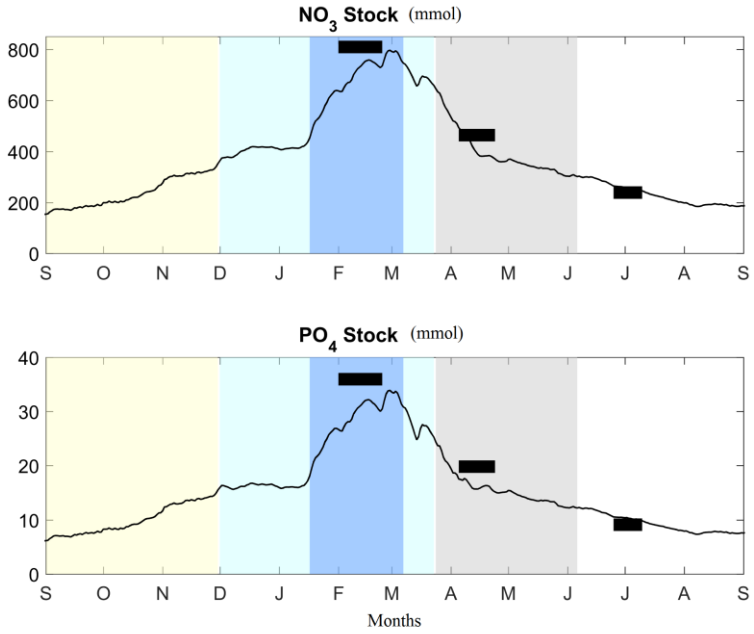

Figure 9. Time evolution of modeled nitrate (upper panel) and phosphate (lower panel) stocks (in mmol m^{-2}) in the upper layer [0-130 m] of the Deep Convection Area from September 2012 to September 2013. Stock estimates derived from observations are shown as horizontal bars overlaying the model outputs. The four seasons identified in section 4.1.2 are indicated with background colors: yellow represents autumn, blue is for winter - with the dark blue representing the period when the MLD was higher than 1000 m (deep convective mixing), gray is for spring and white is for summer.

Figure 10 presents the annual cycle of the biogeochemical sink and source terms of nitrate and phosphate as well as the trends induced by vertical hydrodynamics, for the period 2012-2013. From early September to the end of October 2012, a shallowing of the nutricline from 80 to 60 m was modeled (standard deviation of 20 m). This upward displacement of the nutricline (Fig. 8) could be induced by the isopycnal doming during the preconditioning phase of the deep convection process in the NW Med [*Marshall and Schott*, 1999] and/or by the variation of light

617 intensity [*Mignot et al.*, 2014]. This led to a low but continuous increase of the nutrient stock in
618 the upper layer (Fig. 9). At the same time, the uptake of nutrients decreased continuously (Fig.
619 10B). From October to November 2012, uptake of nitrate (respectively phosphate) became lower
620 than nitrification (respectively excretion of phosphate). Therefore, the net effects of both
621 physical and biogeochemical processes led to an increase of the nutrient stock in the upper layer
622 (Fig. 9).

623 The sudden northern wind event occurring at the end of November - beginning of December
624 (Fig. 7), thickening the ML to 50-60 m depth on average, close to the depth of the nutricline (Fig.
625 8), led to an abrupt import of nutrients into the surface layer (Fig. 10A), which were rapidly
626 assimilated by phytoplankton (Fig. 10B). This was followed by a progressive increase of
627 phosphate excretion (Fig. 10C), reflecting the triggering of the development of heterotrophs.
628 Regarding the surface nutrients stock, after the wind gust of early December, the balance of
629 source (vertical import and nitrification/phosphate excretion) and sink (mainly uptake) terms
630 explains the nearly constant stocks (Fig. 9).

631 The deep convection mixing, beginning in mid-January when the MLD exceeded 100 m (Fig. 8),
632 led to a large upwelling of inorganic nutrients to the surface layer (Fig. 10A). The deep
633 convection event also caused a sudden reduction of nitrate and phosphate uptake which,
634 nevertheless, remained non-negligible (Fig 10B). The phytoplankton biomass was vertically
635 mixed, and preys and predators were then decoupled as shown by *Auger et al.* [2014]. This
636 resulted in an increase of the zooplankton mortality as shown by the intense drop of excretion
637 rates during this period (Fig 10C). The decrease of ammonium and phosphate excretion rates was
638 higher than the decrease of nitrate and phosphate uptake rates. It is noteworthy that the uptake of
639 nitrate (mean value: 6.4 mmolN m^{-2} d^{-1}) was higher than the uptake of ammonium (mean value:
640 1.9 mmolN m^{-2} d^{-1}) during deep convection (Fig. 10B and 10D). Also, nitrification rate in the
641 upper layer (mean value: 1.2 mmolN m^{-2} d^{-1}) was low during this intense mixing period (Fig.

642 10C). Thus, during deep convection, nitrate and phosphate stock in the surface layer increased in
643 the model (Fig. 9) because of the nutrient convective supply and the reduced nutrient uptake.
644 They reached their maximum in early March (Fig. 9), when the main deep convection mixing
645 stopped (Fig. 8).

646 An intense phytoplankton development began during the second week of March, favored by the
647 weakening of vertical mixing (not shown). This bloom was characterized by a sudden, strong
648 consumption of nutrients (Fig. 10B) that provoked a first sharp decrease of their surface stocks
649 (Fig. 9).

650 From the end of March to mid-April, nitrate and phosphate uptake remained strong (Fig. 10B)
651 (phytoplankton biomass reached its maximum in mid-April, not shown). In parallel, excretion
652 increased rapidly (Fig. 10C and 10D). In mid-April, the reduction of vertical mixing (Fig. 10A)
653 led to a clear decrease of the vertical enrichment of the upper layer in nutrients. At this period, a
654 strong decrease of nutrient uptake occurred. At the end of April, a new wind gust induced a brief
655 deepening of the mixed layer (Fig. 8) that enriched the surface layer in nutrients. A last strong,
656 short pulse of nutrient uptake (Fig. 10B) was then observed. Afterwards, the nitrate and
657 phosphate stock continuously decreased (Fig. 9), and the nutricline and DCM depth increased
658 (Fig. 8). It is important to note that, after this last strong wind event, ammonium uptake
659 dominated the total nitrogen uptake (Fig. 10B and 10D). Regarding the nutrient stock, it can be
660 concluded that, during the spring period, the strong rate of uptake (higher than the excretion and
661 nitrification rate) explains the strong decreasing trend (Fig. 9).

662 From June to August, the surface layer was depleted in nutrients (Fig. 8 and 9). The model
663 indicates an increase of the phosphate and ammonium excretion as well as of the nitrification
664 rate (Fig. 10C and 10D). The vertical physical flux was very weak (Fig. 10A) and the net
665 biogeochemical flux resulted in a low, continuous decrease of the nitrate and phosphate surface
666 layer stock until the beginning of August, when it reached the value of November 2012 (Fig. 8).

667 In August, as the DCM and nutricline depths, the nutrient stock stabilized.

668 The trend of the contribution of nitrate and ammonium uptake in the total nitrogen uptake, shown
669 in late spring, remained throughout the summer as the trophic regime was dominated by
670 regenerated production, ammonium being continuously produced (Fig. 10D), while nitrate was
671 weakly imported from intermediate layers (Fig. 10A). During summer, nitrification increased
672 slightly but continuously (from 3 to 4 mmol m^{-2} d^{-1}, Fig. 10C). It constituted from ~60 to 100%
673 of nitrate uptake. The simulated nitrification rate presents the same order of magnitude as the
674 measurements of *Bianchi et al.* [1999] who reported a rate of 1.4 mmol m^{-2} d^{-1} within the DCM
675 in the NW deep sea. In the model results, we found a value of 1.8 mmol m^{-2} d^{-1} (25% higher than
676 in the observations of *Bianchi et al.* [1999]) by integrating nitrification only within the DCM in
677 the Deep Convection Area.

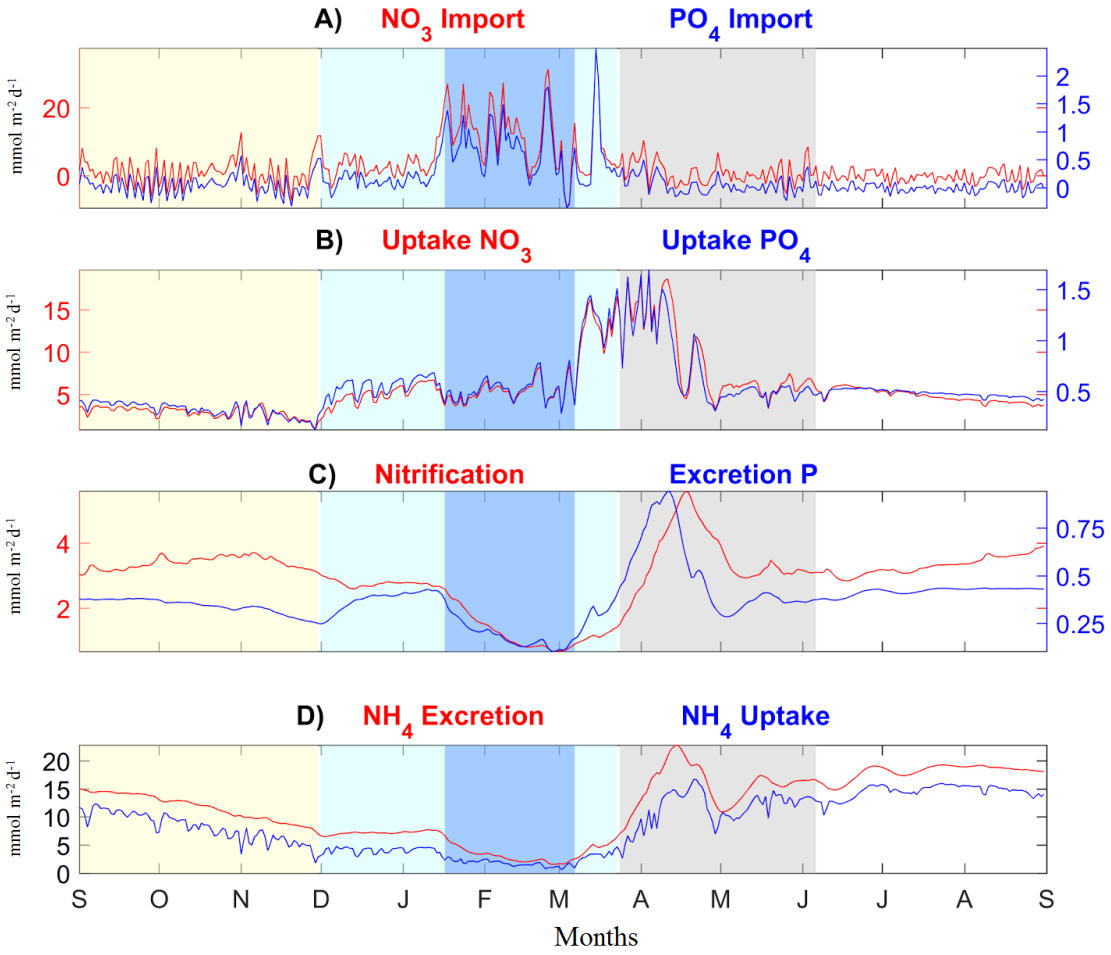

Figure 10. Time series of physical and biogeochemical fluxes that impact the stock of the inorganic nitrogen and phosphorus in the surface layer (0-130 m) from September 2012 to September 2013. These fluxes are inferred from the model and averaged over the open Deep Convection Area. (A) Net import due to vertical advection and turbulent mixing of nitrate (red) and of phosphate (blue) into the surface layer, (B) uptake of nitrate (red) and phosphate (blue), (C) nitrification (red) and inorganic phosphorus excretion rates (blue), (D) ammonia excretion (red) and uptake (blue). Units: mmol m^{-2} d^{-1}.

4.1.3 N:P ratio in the upper layer

In marine ecology, the nitrate to phosphate ratio was determined to be universally 16:1 because of the phytoplankton requirements which control the marine biogeochemistry [*Redfield et al.*, 1963]. Even if this averaged ratio has been reappraised several times [*Banse*, 1994; *Geider and La Roche*, 2002], its dynamics can still be used to understand the nitrogen and the phosphorus reactivity [*Arrigo*, 2005]. Indeed, the N:P stoichiometry reflects relations between several processes: nutrients uptake by phytoplankton and small heterotrophs, rate of mineralization of organic matter, inorganic matter excretion by heterotrophs and finally the effects of physical processes (mixing and advection).

In the Mediterranean Sea, the ratio N:P is higher than the canonical value of 16:1. It was estimated on average at 24 [*Pujo-Pay et al.*, 2011] with a pronounced horizontal gradient from west to east. To the west, the ratio is 22 in the Levantine Intermediate Water and the Western Mediterranean Deep Water while in the Levantine Basin, the ratio reaches 27±3:1 below 200 m [*Ribera d'Alcalà et al.*, 2003]. The N:P ratio can be much higher above the thermocline [*Raimbault and Coste*, 1990] because of the preference of phytoplankton for phosphate compared to nitrate. These ratios confirm that the Mediterranean waters are limited by phosphate, especially in the eastern basin.

In this section, we use our simulation to characterize the time evolution of the stoichiometry in the upper layer of the Deep Convection Area, playing a key role in the water mass biogeochemical characteristics in the Mediterranean Sea, and to quantify the impact of the physical and biogeochemical processes responsible for their seasonal variations, over the period September 2012 to September 2013. The N:P ratio generally presents a negative gradient in the water column as observed in previous observational studies [*Pujo-Pay et al.*, 2011; *Huertas et al.*, 2012; *Severin et al.*, 2014; *Pasqueron de Fommervault et al.*, 2015a]. The deep value (averaged between 130 m and the seafloor in the Deep Convection Area, not shown) is 22.4 on

711 average (standard deviation: 0.5) in the model results (it is 21.7 on average, standard deviation:
712 0.6 according to the interpolation of Dewex cruise observations). The maximum N:P vertical
713 gradient is located below the nutricline (not shown). The N:P ratio presents higher variability in
714 the surface layer than in deep layers [*Pasqueron de Fommervault et al.*, 2015].

715 Figure 11A shows the time series of the spatially averaged N:P ratio in the upper layer of the
716 Deep Convection Area. N:P ratio deduced from the three cruise observations are also indicated
717 by horizontal bars. Since the underestimation of phosphate stock is more pronounced than that of
718 nitrate stock in the model during the winter cruise (Figure 9), the model overestimates the N:P
719 ratio during this period. Besides, the overestimation of phosphate stock during MOOSE cruise
720 period lead to an underestimation of N:P ratio during the summer period.

721 A first general remark about the effect of physical and biogeochemical processes on N:P is that
722 uptake increases seawater N:P ratio while release of nitrate and phosphate decreases N:P (Fig.
723 11B). The N:P ratio of uptake is lower than the ratio in seawater, which presents an excess of
724 nitrate compared to phosphate. The effect of uptake is then to increase the water N:P ratio. For
725 the same reason, the release of nutrients by the ecosystem produces a decrease of water N:P. A
726 second remark is that convective mixing events characterized by depths > 200 m produce a
727 decrease of surface N:P ratio because of the general negative gradient of N:P.

728

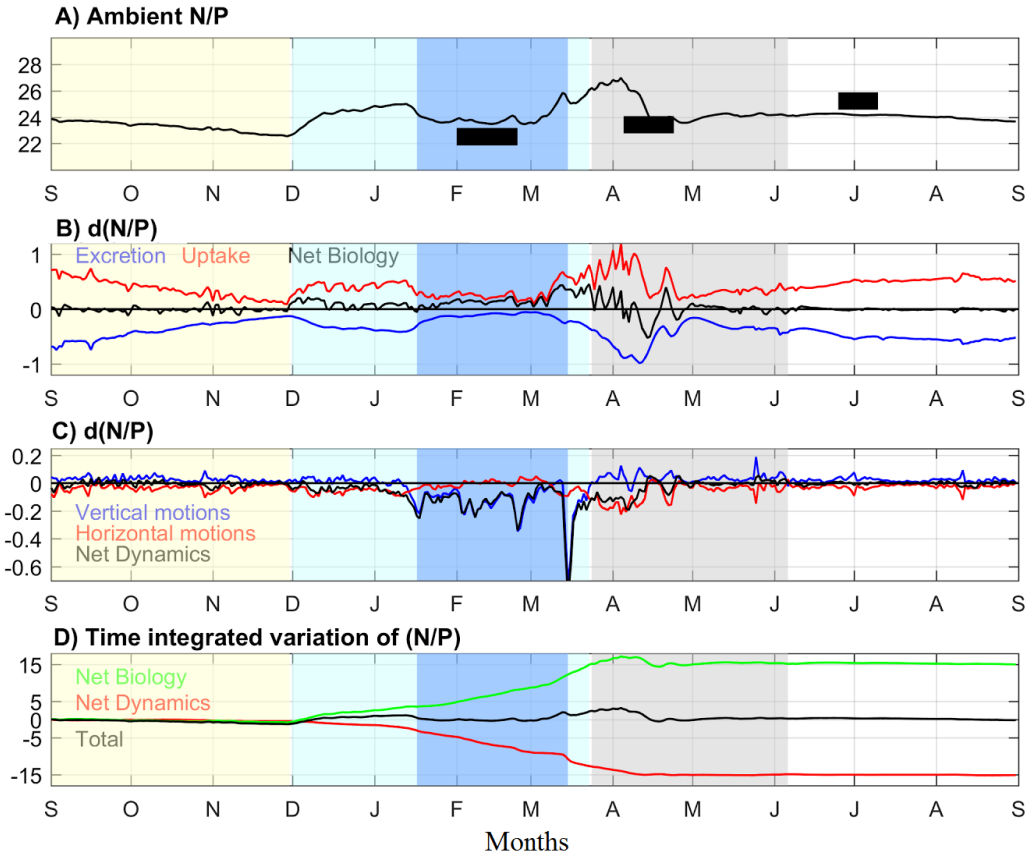

729

730 **Figure 11.** (A) Time series of the modeled N:P ratio (molN $molP^{-1}$) averaged in the upper layer
731 [0-130 m] of the Deep Convection Area from September 2012 to September 2013. Estimates
732 from observations are shown as horizontal bars overlaying the model output. (B)
733 Biogeochemical and (C) physical processes (molN $molP^{-1}$ d^{-1}) influencing the N:P dynamics and
734 (D) their net time integrated resultant.

735

736 At the beginning of September 2012, the spatial mean N:P ratio was 24.1 (standard deviation:
737 0.5) according to the model (Fig. 11A). From September to December 2012, the influence of
738 each physical process on the N:P ratio was lower than the effect of the biogeochemical processes
739 (Fig. 11C and 11D). Yet, both physical and biogeochemical processes had a negative impact on
740 N:P (-0.7 for the net effect of the biogeochemical processes and -0.5 for the net effect of physical
741 processes), explaining its slow and regular decrease.

742 From December 2012 to mid-January 2013, when nitrate and phosphate uptake rates were higher
743 than the nitrification and phosphate excretion, respectively, the biogeochemical processes tended
744 to strongly increase the N:P ratio (Fig. 11B and 11D). In parallel, the horizontal dynamics tended
745 to slightly decrease the N:P ratio. The resulting evolution was a rapid increase of the N:P ratio
746 from 22.8 to 24.2 in the first 15 days of the autumnal bloom (1 December to 15 December), and
747 a second slow increase from 24.2 to 25 during the following month (15 December to 15
748 January).

749 During the main convective period (16 January to 7 March 2013), the contributions of individual
750 biogeochemical processes to N:P variations were low (Fig 11B). Besides, the strong deepening
751 of the mixed layer in mid-January induced a rapid decrease of surface N:P, due to vertical
752 imports of lower N:P deep waters (Fig. 11C). During the rest of the convective period, the N:P
753 ratio reached a relatively stationary phase: the positive trend of the nutrient uptake that
754 dominated the biology was balanced by the negative trend of the vertical mixing. During this
755 period, the model N:P ratio was around 23, which is close to the mean value of 22.5 (standard
756 deviation: 0.6) deduced from the observations of the February cruise. This difference between
757 the two ratios could be explained by an underestimation of the N:P ratio of the deep waters at the
758 model initialization.

759 Then, the sudden and strong consumption of nutrients at the onset of the winter/spring bloom
760 induced a pronounced increase of the N:P ratio to 26 (Fig. 11A and 11B). This increase was

761 interrupted during the secondary convective mixing of the third week of March, inducing a small
762 decrease of the N:P ratio of 0.3 (Fig. 11C).

763 The period with the highest N:P ratio corresponds to the transition between winter and spring
764 (late March - early April) when the phytoplankton growth and nutrient uptake were strong (Fig.
765 10B and 11A). In early April, phosphate excretion increased proportionally more rapidly than the
766 production of nitrate by nitrification (Fig. 10C). This induced a decrease of the N:P ratio (Fig.
767 11B and 11D), intensified by the effect of vertical physical processes.

768 From mid-April, the contribution of physical processes to the variations of N:P was very low,
769 N:P being mostly affected by the balance between excretion and uptake processes. The time lag
770 between excretion of phosphate, nitrification and uptakes of nitrate and phosphate, as well as the
771 difference in the rate of these processes, produced a biogeochemical contribution that was
772 alternately positive and negative, with a decreasing trend until the end of spring.

773 From early June to early August, the effect of vertical motions balanced the effect of horizontal
774 motions, and, likewise, the effect of uptake processes balanced the effect of production
775 processes. Overall, the variations of N:P were negligible. For the period of the MOOSE summer
776 cruise, the modeled N:P (24.2) is close to the ratio deduced from observations (25.1).

777 Our results shows that the N:P ratio was submitted to strong changes in the upper layer at the
778 beginning of phytoplankton blooms. Those rapid modeled increases of N:P ratio, reflecting a
779 phosphorus limitation for phytoplankton growth, are in agreement with the increase measured by
780 Séverin et al. [2014] in March 2011 after restratification. This is also coherent with the results of
781 *Lazzari et al.* [2016], based on 3D modelling on the whole Mediterranean sea, indicating a
782 limitation of primary production by phosphate in our study area. Two other rapid changes
783 (decrease) were also modeled during the studied period. The first modeled decrease of N:P ratio
784 in the upper layer occurring at the beginning ot the deep convection event is coherent with the
785 negative vertical gradient observed in the study region. The second modeled decrease occurred

when uptake of nitrate by phytoplankton started to decrease after the peak of the spring bloom. This should be addressed and confirmed with further observations.

4.2 Annual budgets of nitrogen and phosphorus

The annual nitrogen and phosphorus budgets of the deep convection area were calculated with the model in the upper layer (0-130 m) and in the deep layer (130 m - seafloor) (Fig. 12). The total stocks of nitrogen and phosphorus in this area exhibit a variation of -0.37% for nitrogen and -1.37% for phosphorus between September 2012 and September 2013.

The annual net vertical import of nitrate and phosphate is estimated at 1029 mmolN m^{-2} y^{-1} and 59 mmolP m^{-2} y^{-1} respectively. The nutrient vertical supply occurring over the convection period (17 January - 17 March) corresponds to 68% of the annual vertical supply. According to the comparison exercise (section 3), it may have been underestimated. The simulated vertical nutrients import is of the same order of magnitude as previous estimates for the NW Med [*Pujo-Pay and Conan*, 2003; *Severin et al.*, 2014] (Table 1). It is also of the same order of magnitude as the estimation of 1400 mmolN m^{-2} y^{-1} in the convective Atlantic subpolar region [*Williams et al.*, 2000]. The annual lateral exports of nitrate and phosphate from the surface layer of the convection zone, to the surrounding areas, are low and are estimated at 5 mmolN m^{-2} y^{-1} and 2 mmolP m^{-2} y^{-1} respectively.

Regarding the biogeochemical processes budget in the surface layer, the consumption of nitrate and ammonium makes up 39% and 61%, respectively, of the total nitrogen uptake. The annual production of nitrate by nitrification is 103% of the annual nitrate supply from deep waters and 50% of the nitrate uptake. Therefore, the new production as defined by *Dugdale and Goering* [1967] (primary production fueled by non-regenerated nutrients) could be overestimated by 100% if nitrification rates are taken into account in the calculation. Our results are coherent with

those of *Raimbault et al.* [1998], who showed a 20% to 100% overestimation of new primary production in the Pacific Ocean when nitrification was not taken into account in the calculation. They agree also with those of *Dore and Karl* [1996], who established that 47 to 142% of the nitrate assimilated by primary producers was produced by nitrification at the ALOHA oligotrophic station, and those of *Martin and Pondaven* [2006] who found that uptake of regenerated nitrate through nitrification constituted 22 to 57% of the total nitrate uptake. Our results are also close to the results of *Gentilhomme* [1992] who found that nitrification represented 23% of total nitrogen uptake (18% in this study) in the Algerian basin. From a quantitative point of view, using the Redfield ratio to facilitate comparison with previous studies, we have obtained a new production ranging between 77 and 162 gC m^{-2} y^{-1}, depending on whether nitrification is considered in the calculation. As mentioned in section 2.3 the choice of a constant depth corresponding to the base of the productive layer could lead to an overestimation of the new production. Indeed, as demonstrated by previous studies [*Martin and Pondaven*, 2006; *Kortzinger et al.*, 2008; *Palevsky et al.*, 2016], nitrate originating from the recycling of organic matter exported downward during deep mixing periods could have been reinjected in the upper layer. We estimate nitrification in the deep layer during deep convection period at 158 mmol m^{-2} (28% of the annual deep nitrification). If the whole nitrate produced by nitrification in the deep layer during convection period is reinjected in the upper layer and used by phytoplankton for its growth, then our estimate of new production is overestimated by 13 gC m^{-2} y^{-1} (using a Redfield ratio). The lower values of our estimate of new production (65-77 gC m^{-2} y^{-1}) are in the range of a previous estimate for the offshore NW Med (Table 1), a region that exhibits the highest values in the open Mediterranean Sea [*Béthoux*, 1989].

The net amount of organic matter produced in the surface layer is mostly exported towards the deep layer. The amount of produced organic matter advected horizontally toward the adjacent surface regions represents a small percentage of the net amount produced: 11% of the total organic nitrogen and 9% of the total organic phosphorus. The vertical export to the deep layer of

836 dissolved and particulate organic nitrogen and phosphorus is estimated at 724 mmolN m^{-2} y^{-1} and
837 52 mmolP m^{-2} y^{-1} respectively. These estimates are in the same order of magnitude as the
838 estimates in *Pujo-Pay and Conan* [2003] (Table 1). During the convection period (17 January to
839 17 March), the export represents 55% of the annual amount of organic nitrogen and 58% of the
840 annual amount of organic phosphorus. Two thirds of the total exported organic matter is
841 remineralized by heterotrophs and one third is advected to the surrounding deep regions. With
842 respect to the deep-water biogeochemical nitrogen cycle, the ammonium produced by
843 remineralization is mostly transformed into nitrate by nitrification. The difference in the
844 nitrification:uptake of ammonium ratio (<1 in the upper layer and >1 in the deep layer) in upper
845 and deep layer is explained by both higher ammonium uptake rates in the upper layer and lower
846 nitrification rates due to an inhibition effect by light in the upper layer. An annual import of
847 nitrate (260 mmolN m^{-2} y^{-1}) and phosphate (6 mmolP m^{-2} y^{-1}) is obtained by horizontal advection
848 in the deep layer. It is worth noting that this net horizontal supply results from two strong
849 opposite fluxes: an import of 936 mmolN m^{-2} y^{-1} for nitrate and of 39 mmolP m^{-2} y^{-1} for
850 phosphate in the intermediate waters (between 130 m and 800 m) and an export of 676 mmolN
851 m^{-2} y^{-1} for nitrate and of 33 mmolP m^{-2} y^{-1} for phosphate in the deep waters (below 800 m).

852 The model results suggest that, at the annual scale, the Deep Convection Area appears as an
853 autotrophic system (uptake rates dominate excretion rates) where deep inorganic nutrients
854 injected in the surface layer are almost entirely consumed by phytoplankton. Our estimates for
855 the period 2012-2013 suggest that, at the scale of the Mediterranean Sea, the total vertical supply
856 by physical processes in the NW deep convection region could constitute a major source of
857 nutrients in the surface layer compared to the terrestrial and atmospheric inputs [*Ribera d'Alcala*
858 *et al.*, 2003; *Krom et al.*, 2004] (Table 2).

859 Atmospheric deposition and nitrogen fixation were not taken into account in the simulation.
860 Results of previous studies suggested that they would have little influence on the annual N and P

861 budget in the NW Med deep convection region, where there is a large vertical supply of
862 nutrients. Aphotic nitrogen fixation was shown to contribute 0.5% of the total nitrogen inputs in
863 the whole Mediterranean basin [*Benavides et al.*, 2016]. Regarding the atmospheric deposition,
864 *Lazzari et al.* [2012], using coupled modeling, showed that atmospheric and terrestrial inputs led
865 to a 5% increase in the net primary production. The experiments performed by *Ridame and*
866 *Guieu* [2002] showed that, in the western Mediterranean, the inputs of Saharan dissolved
867 inorganic phosphorus had a negligible impact on the new production integrated over the
868 productive layer, at the scale of the oligotrophic period, when the contribution of atmospheric
869 deposition to the total nutrient input to the euphotic layer is largest.

870 The budget of the present study was obtained using a given coupled model and for a one-year
871 period. Multi-year simulations would allow the variability of these terms in response to the
872 interannual variability of atmospheric and ocean conditions to be evaluated. Moreover,
873 uncertainties on the various terms of this budget could be estimated from additional experiments
874 based on other coupled models.

875

Process	**Unit**	**Reference**	**Period**	**Values**	
Vertical import of inorganic nutrients	mmol m^{-2} y^{-1}			NO3	P04
		Pujo-Pay and Conan [2003]	1993	433-650	-

		Severin et al. [2014]	Feb./March 2011 convection events	760/800	36/36
		This study	2013 deep convection event	674	40
		This study	Sept. 2012-Sept. 2013	1029	59
New production	mgC m^{-2} y^{-1}				
		Severin et al. [2014]	Feb./March 2011	46/63	
		This study	Sept. 2012-Sept. 2013	65-77	
Export of organic matter	mmol m^{-2} y^{-1}				
		Pujo-Pay and Conan [2003]	1993	274-814	
		This study	Sept. 2012-Sept. 2013	724	

876 **Table 1.** Compilation of nutrient flux estimates in the northwestern Mediterranean deep sea.

877

Sources in the surface layer	**N**	**P**	**Reference**
Atmospheric inputs in the western basin	10,042-72,825	357-697	Ribera d'Alcalà et al. [2003]
Terrestrial inputs in the western basin	7,840-18,020	168-1,258	Ribera d'Alcalà et al. [2003]
Atmospheric inputs in the eastern basin	6,064-73,621	379-957	Ribera d'Alcalà et al. [2003]
	111,000	950	Krom et al. [2004]
Terrestrial inputs in the eastern basin	11,592-77,519	248-1,541	Ribera d'Alcalà et al. [2003]
	63,000	2,400	Krom et al. [2004]
Vertical physical inputs in the NW Med deep convection area	63,474	3,640	This study

878 **Table 2**. Estimates of the net inputs of nitrogen and phosphorus in the surface layer in the
879 Mediterranean Sea (in 10^6 mol y^{-1}).
880

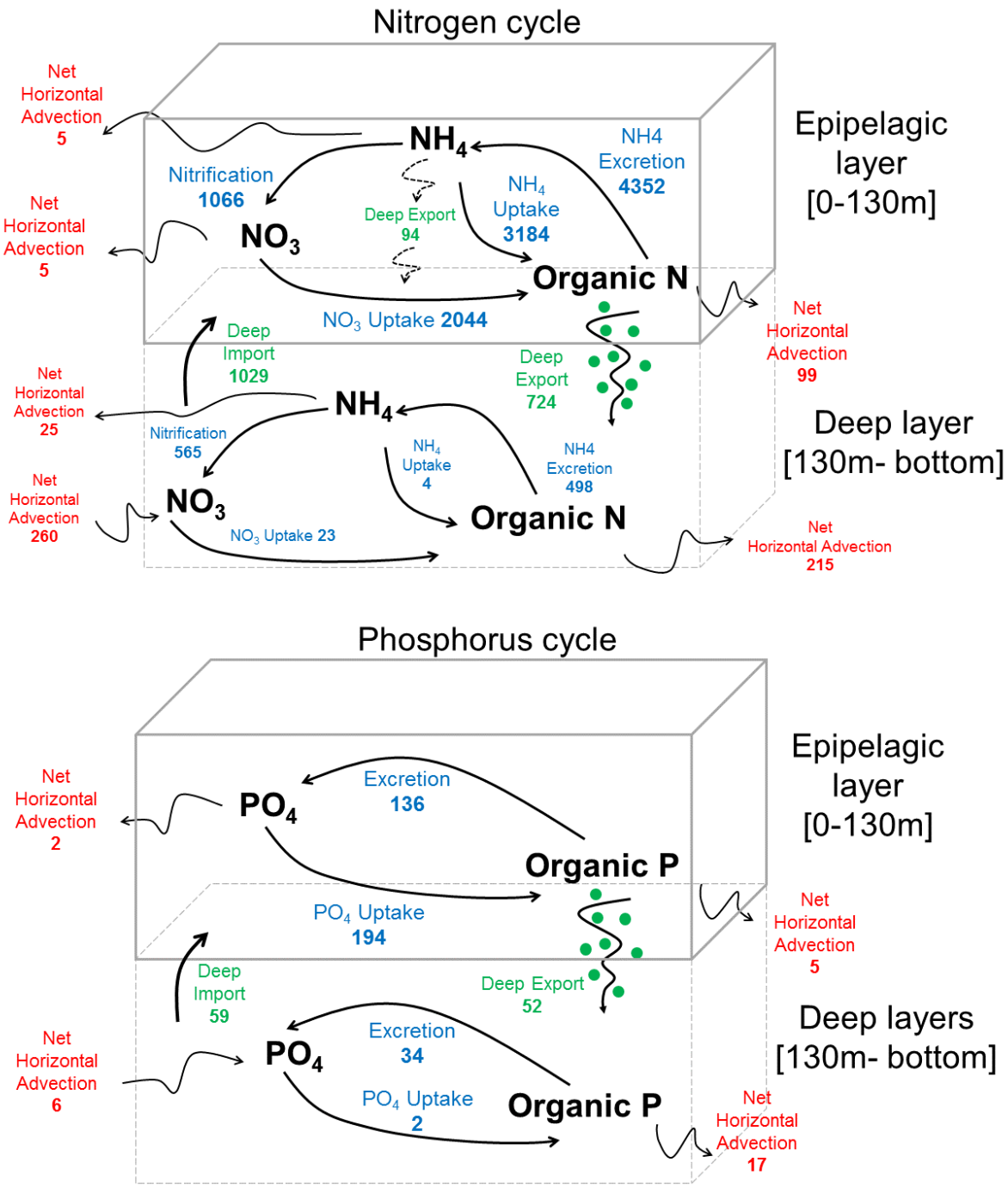
Nitrogen cycle
Net Horizontal Advection 5
NH4
NH4 Excretion 4352
Nitrification 1066
NH4 Uptake 3184
Deep Export 94
NO3
Net Horizontal Advection 5
Organic N
NO3 Uptake 2044
Epipelagic layer [0-130m]
Net Horizontal Advection 99
Deep Import 1029
Deep Export 724
Net Horizontal Advection 25
NH4
Nitrification 565
NH4 Uptake 4
NH4 Excretion 498
Deep layer [130m- bottom]
Net Horizontal Advection 260
NO3
NO3 Uptake 23
Organic N
Net Horizontal Advection 215
Phosphorus cycle
Net Horizontal Advection 2
Excretion 136
PO4
Organic P
PO4 Uptake 194
Epipelagic layer [0-130m]
Net Horizontal Advection 5
Deep Import 59
Deep Export 52
Net Horizontal Advection 6
Excretion 34
PO4
PO4 Uptake 2
Organic P
Deep layers [130m- bottom]
Net Horizontal Advection 17

881

882 **Figure 12.** Modeled annual fluxes of nitrogen (top panel) and phosphorus (bottom panel) in the
883 deep convection region (in mmol m^{-2} y^{-1}) over the period from September 2012 to September
884 2013.

885

886 **5. Conclusion and perspectives**

887 A coupled physical-biogeochemical model was compared to a high-resolution dataset of three
888 seasons of the same year (2013) and Bio-Argo float data, which document a strong convective
889 winter, a phytoplankton bloom and an oligotrophic period in the NW Med. Despite some limits
890 highlighted through the comparisons with observations, the model was shown to be able to
891 reproduce the general observed seasonal dynamics of the physical and biogeochemical events
892 correctly.

893 Our study shows that injections of nutrients during the wind intensification period triggered the
894 autumn bloom. Then, convection in winter upwelled large amounts of nutrients into the upper
895 layer. Decoupling of phytoplankton and zooplankton due to dilution as suggested by the collapse
896 of heterotrophs when the mixed layer deepened strongly (mid-January), reduced the grazing
897 pressure. When the conditions for phytoplankton development were all present (reduction of
898 vertical mixing, low grazing pressure), a bloom was triggered with a massive consumption of
899 nutrients during more than one month, resulting in a depletion of nutrients at the surface by the
900 end of April. Nutrient consumption continued to deplete nutrients at increasing depths, inducing
901 a deepening of the nutricline and DCM. This finally led to the summer oligotrophy of the water
902 column.

903 The N:P ratio changed mainly through physical or biogeochemical processes during transition
904 periods. Firstly, during the intense convection mixing, the large enrichment of surface waters in
905 deep nutrients suddenly reduced the surface N:P ratio. Secondly, during the beginning of the

bloom, the predominance of high nutrient uptake over low excretion induced a strong increase of the N:P. Thirdly, during the peak of the bloom when the nutrient stock decreased strongly, uptake decreased, and excretion was maximum. Nitrification created a decoupling in the recycling of nutrients, decreasing the ratio N:P. At the annual scale, the surface N:P ratio did not appear to be impacted by the intense vertical mixing and spring bloom induced by the deep convection.

At the annual scale and for the studied year, the dense water formation area was a sink of nitrate and phosphate in intermediate layers, and a source of organic nitrogen and phosphorus throughout the water column, for the surrounding regions (Fig. 13). The upward nutrient fluxes into the surficial NW Med deep convection area is estimated to be in the same order of magnitude as the atmospheric and terrestrial inputs of each of the western and eastern sub-basins of the Mediterranean Sea.

Further multi-year simulations from the coupled model will be used to better understand and quantify the impact of atmospheric and ocean interannual variability of the pelagic ecosystem and associated carbon, nitrogen and phosphorus cycles in this region. Previous studies suggested that deep convection could be strongly weakened [Somot et al., 2006; Adloff et al., 2015] or strengthened [Adloff et al., 2015] by the end of XXI century. We will then use the coupled model to explore and quantify how climate change and anthropogenic forcing may alter the NW Med deep convection biogeochemical cycles, in particular the nutrient vertical supply in the euphotic layer and the new production, in the near future.

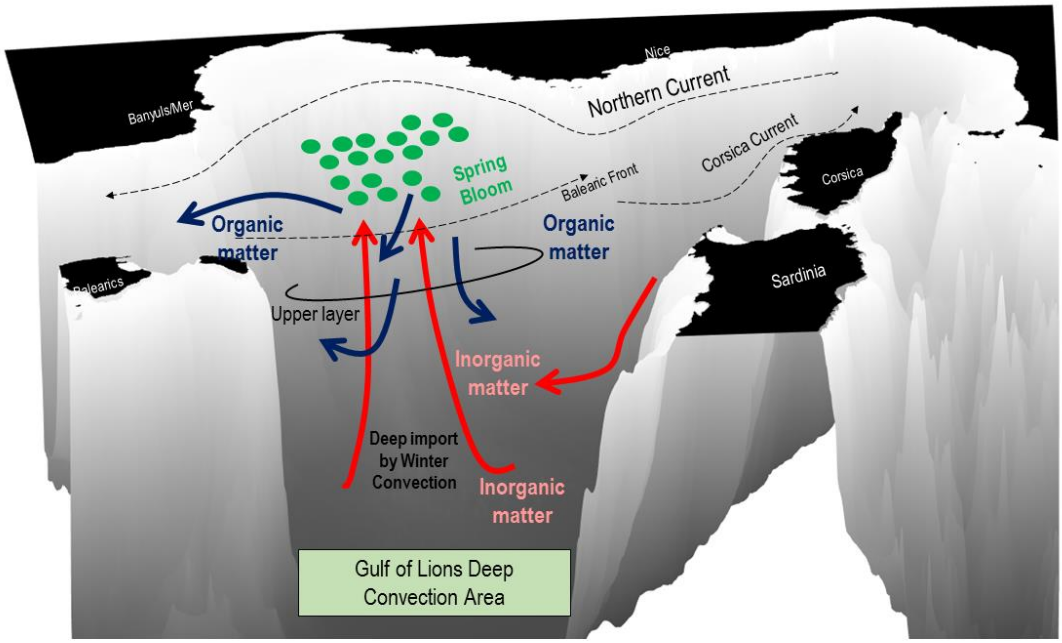

927

928 **Figure 13.** Conceptual model of the main processes driving the organic and inorganic matter
929 dynamics in the NW Mediterranean Sea over the period from September 2012 to September
930 2013.

931

932 **Additional Supporting Information**

933

Symbol	Description	Unit	Value		
			Phy_1	Phy_2	Phy_3

T_{Phy}^{REF}	Reference temperature	°C	14	14	14
τ_{mort,Phy_i}	Natural mortality rate	d^{-1}	0.09	0.03	0.05
φ_{max,Phy_i}	Maximum quantum yield	mmolC J^{-1}	2.6 10^{-4}	2.87 10^{-4}	3.85 10^{-4}
			Zoo_1	Zoo_2	Zoo_3
T_{Zoo}^{REF}	Reference temperature	°C	18	18	18
τ_{mort,Zoo_i}	Natural mortality rate	d^{-1}	0.01	0.008 d^{-1}	-
	Non-living matter remineralization rate				
$\tau_{rem,CDet}$	Detritus remineralisation rate, C	d^{-1}	0.17		
$\tau_{rem,NDet}$	Detritus remineralisation rate, N	d^{-1}	0.2		
$\tau_{rem,PDet}$	Detritus remineralisation rate, P	d^{-1}	0.18		
$\tau_{rem,ChlDet}$	Detritus remineralisation rate, Si	d^{-1}	0.4		
$\tau_{rem,SiDet}$	Detritus remineralisation rate, Chl	d^{-1}	0.02		

934

935 Table S1. List of recalibrated parameters of the biogeochemical model compared to *Ulses et al.*
936 [2016]

937

938

939

940 **Acknowledgments**

941 This study has been funded by the PERSEUS project (European Union FP7 Grant Agreement
942 287600). It is a contribution to the MerMex (Marine Ecosystem Response in the Mediterranean
943 Experiment. http://dx.doi.org/10.17600/13020010, http://dx.doi.org/10.17600/13020030,
944 http://dx.doi.org/10.17600/13450110), particularly DeWEX and MOOSE projects project of the
945 MISTRALS international program. Numerical simulations were performed using the computing
946 cluster of Laboratoire d'Aérologie and HPC resources from CALMIP (grants P1325 and P1331).
947 The biogeochemical floats have been funded by the French NAOS project (« Investissement
948 d'Avenir », ANR J11R107-F).

949 **Figures and tables captions**

950 **Figure 1.** A/ Bathymetry (m) of the coupled physical-biogeochemical model domain. The red
951 dots represent the modeled river locations. The blue area DCA (Deep Convection Area)
952 corresponds to the simulation analysis area. The yellow star corresponds to the LION station
953 where the heat flux plotted on Fig. 6 was modeled. Maps B, C and D represent the
954 biogeochemical measurement stations of the DeWEX Leg 1 (February 2013), DeWEX Leg 2
955 (April 2013) and MOOSE-GE 2013 (July 2013) cruises respectively. Stations in red on Fig. B
956 and C are located on the transect presented in Fig. 3 and Fig. 4

Figure 2. Eco3m-S biogeochemical model scheme.

Figure 3. Comparison of modeled and observed surface (A) nitrate and (B) phosphate concentrations (mmol m^{-3}) during the winter cruise. Vertical section of (C) chlorophyll (mg m^{-3}), (D) nitrate (mmol m^{-3}) and (E) phosphate (mmol m^{-3}) concentrations across the Deep Convection Area, indicated by red dots on Fig. 1B. The model is represented by background colors and observations are indicated in colored circles (DeWEX Leg1, February 2013). White lines in the vertical sections (C to E) represent the 29.05 kg m^{-3} isopycnal potential density anomaly. The maps (A and B) correspond to an average modeled concentration over the period of the cruise (1 to 21 February) while the vertical cross section represents a model average over the transect observation period (12 to 13 February). The numbers of the measurement stations along the vertical section are indicated on the x-axis of panels. C and D. Latitudes are indicated on the x-axis of panel. E

Figure 4. Same as Figure 3 but for spring cruise (DeWEX Leg 2) in April 2013. Model outputs are averaged over the period 5-24 April for panel. A and B, and over the period 8-10 April for panels C, D, and E. The numbers of the measurement stations along the vertical section are indicated on the x-axis of panels C and D. Latitudes are indicated on the x-axis of panel E.

Figure 5: Comparison of modeled (red) and observed (black) nitrate and phosphate concentration (mmol m^{-3}) profiles during MOOSE cruise in July 2013.

Figure 6. Hovemöller diagram of the nitrate concentration (mmol m^{-3}) along the float track from April to September 2013. Data are extracted from the float Lovbio17B (upper panel) and from the model (lower panel). White line represents the depth of the nitracline (position of the 1 mmol m^{-3} concentration) and the green dashed line represents the MLD.

Figure 7. Time series of modeled total heat flux (W m^{-2}) at LION (indicated on Fig. 1A) from September 2012 to September 2013. Blue bars represent the period when the MLD was higher than 1000 m (convective mixing), while the green bar represents the restratification period coinciding with the phytoplankton development maximum.

Figure 8. Time series of the depth (m) of the modeled mixed layer (in black), nitracline (in red), phosphacline (in blue) and deep chlorophyll maximum (in green) averaged over the deep convection region from September 2012 to September 2013. The background color stands for the season: yellow for autumn, blue for winter, with the dark blue representing the period when the MLD was higher than 1000 m (convective mixing), gray for spring and white for summer.

Figure 9. Time evolution of modeled nitrate (upper panel) and phosphate (lower panel) stocks (in mmol m^{-2}) in the upper layer [0-130 m] of the Deep Convection Area from September 2012 to September 2013. Stock estimates derived from observations are shown as horizontal bars overlaying the model outputs. The four seasons identified in section 4.1.2 are indicated with background colors: yellow represents autumn, blue is for winter - with the dark blue representing the period when the MLD was higher than 1000 m (deep convective mixing), gray is for spring and white is for summer.

Figure 10. Time series of physical and biogeochemical fluxes that impact the stock of the inorganic nitrogen and phosphorus in the surface layer (0-130 m) from September 2012 to September 2013. These fluxes are inferred from the model and averaged over the open Deep Convection Area. (A) Net import due to vertical advection and turbulent mixing of nitrate (red) and of phosphate (blue) into the surface layer, (B) uptake of nitrate (red) and phosphate (blue), (C) nitrification (red) and inorganic phosphorus excretion rates (blue), (D) ammonia excretion (red) and uptake (blue). Units: mmol m^{-2} d^{-1}.

Figure 11. (A) Time series of the modeled N:P ratio (molN $molP^{-1}$) averaged in the upper layer [0-130 m] of the Deep Convection Area from September 2012 to September 2013. Estimates from observations are shown as horizontal bars overlaying the model output. (B) Biogeochemical and (C) physical processes (molN $molP^{-1}$ d^{-1}) influencing the N:P dynamics and (D) their net time integrated resultant.

Figure 12. Modeled annual fluxes of nitrogen (top panel) and phosphorus (bottom panel) in the deep convection region (in mmol m^{-2} y^{-1}) over the period from September 2012 to September 2013.

Figure 13. Conceptual model of the main processes driving the organic and inorganic matter dynamics in the NW Mediterranean Sea over the period from September 2012 to September 2013.

Table 1: Compilation of nutrient flux estimates in the northwestern Mediterranean open sea.

Table 2: Estimates of the net inputs of nitrogen and phosphorus in the surface layer in the Mediterranean Sea (in 10^6 mol y^{-1}).

Table S1. List of recalibrated parameters of the biogeochemical model compared to Ulses et al. [2016]

References

- Adloff, F., Somot, S., Sevault, F., Jordà, G., et al. (2015) Mediterranean Sea Response to Climate Change in an Ensemble of Twenty First Century Scenarios. Climate Dynamics, 45,2775-2802. http://dx.doi.org/10.1007/s00382-015-2507-3
- Allen, J. I., Somerfield, P., and Gilbert, F. (2007), Quantifying uncertainty in high-resolution coupled hydrodynamic-ecosystem models, J. Marine Syst., 64, 3–14, doi:10.1016/j.jmarsys.2006.02.010, 2007.
- Anderson, T. R., and P. Pondaven (2003), Non-redfield carbon and nitrogen cycling in the Sargasso Sea: Pelagic imbalances and export flux, Deep Sea Res., Part I, 50, 573–591.
- Antoine, D., A. Morel, H.R. Gordon, V.F. Banzon, and R.H. Evans (2005), Bridging ocean color observations of the 1980s and 2000s in search of long-term trends, *J. Geophys. Res.*,

110, C06009, doi:10.1029/2004JC002620.

- Arrigo K.R. (2005), Review Marine microorganisms and global nutrient cycles. *Nature* **437**, 349-355 (15 September 2005) | doi:10.1038/nature04159.
- Auger, P., C. Ulses, C. Estournel, L. Stemmann, S. Somot, and F. Diaz (2014), Interannual control of plankton communities by deep winter mixing and prey/predator interactions in the NW Mediterranean: Results from a 30-year 3D modeling study, Prog. Oceanogr., 124, 12–27, doi:10.1016/j.pocean.2014.04.004.
- Auger, P., F. Diaz, C. Ulses, C. Estournel, J. Neveux, F. Joux, M. Pujo-Pay, and J.-J.Naudin, (2011), Functioning of the planktonic ecosystem on the Gulf of Lions shelf (NW Mediterranean) during spring and its impact on the carbon deposition: A field data and 3-D modelling combined approach, Biogeosciences, 8(11), 3231–3261, doi:10.5194/bg-8-3231-2011.
- Baklouti, M., V. Faure, L. Pawlowski, and A. Sciandra (2006), Investigation and sensitivity analysis of a mechanistic phytoplankton model implemented in a new modular numerical tool (Eco3M) dedicated to biogeochemical modelling, Prog. Oceanogr., 71(1), 34–58, doi:10.1016/j.pocean.2006.05.003.
- Banse, K., and D. C. English (1994), Seasonality of coastal zone color scanner phytoplankton pigment in the offshore oceans, J. Geophys. Res., 99(C4), 7323–7345, doi:10.1029/93JC02155.
- Behrenfeld, M.J. (2010), Abandoning Sverdrup's critical depth hypothesis on phytoplankton blooms. Ecology, 91: 977–989.
- Benavides, M., et al. (2016), Basin-wide N2 fixation in the deep waters of the Mediterranean

1052 Sea, Global Biogeochem. Cycles, 30, 952–961, doi:10.1002/ 2015GB005326.
1053 - Bentsen, M., G. Evensen, H. Drange, and A. D. Jenkins (1999), Coordinate Transformation
1054 on a Sphere Using Conformal Mapping. Monthly Weather Review, 2733-2740
1055 - Béthoux, J. P., P. Morin, C. Chaumery, O. Connan, B. Gentili, D. Ruiz-Pino (1998).
1056 Nutrients in the Mediterranean Sea, mass balance and statistical analysis of concentrations
1057 with respect to environmental change. Marine Chemistry 63 1998. 155–169
1058 - Béthoux, J. P., (1989). Oxygen consumption, new production, vertical advection and
1059 environmental evolution in the Mediterranean Sea. Deep Sea Research, 36, 5, 769-781.
1060 doi:10.1016/0198-0149(89)90150-7
1061 - Bianchi, M, C.Fosset, and P. Conan (1999), Nitrification rates in the NW Mediterranean Sea,
1062 Aquatic Microbial Ecology, 17, 267-278.
1063 - Butenschön, M., M. Zavatarelli, and M. Vichi (2012), Sensitivity of a marine coupled
1064 physical biogeochemical model to time resolution, integration scheme and time splitting
1065 method, Ocean Modell., 52–53, 36–53, doi:10.1016/j.ocemod.2012.04.008.
1066 - Conan, P. (2013), DEWEX-MERMEX 2013 LEG2 cruise, RV Le Suroît, edited by SISMER,
1067 doi:10.17600/13020030.
1068 - D'Ortenzio, F. et al. (2014), Observing mixed layer depth, nitrate and chlorophyll
1069 concentrations in the northwestern Mediterranean: A combined satellite and NO_3 profiling
1070 floats experiment, Geophys. Res. Lett., 41, 6443–6451, doi:10.1002/2014GL061020.
1071 - D'Ortenzio, F., and M. Ribera d'Alcala (2009), On the trophic regimes of the Mediterranean
1072 Sea: a satellite analysis. Biogeosciences 6, 139–148.
1073 - Dilek E., A. Yilmaz and S. Tugrul (2005), Vertical profiles of particulate organic matter and

its relationship with chlorophyll-a in the upper layer of the NE Mediterranean Sea. J. Mar. Syst. 55 (2005) 311– 326.

- Dore J. E., and D.M. Karl (1996), Nitrification in the euphotic zone as a source for nitrite, nitrate, and nitrous oxide at Station ALOHA. Limnol Oceanogr, 41,1619-1628
- Dugdale R.C., and J.J. Goering J J (1967), Uptake of new and regenerated forms of nitrogen in primary productivity. Limnol. Oceanogr, 12, 196-206.
- Durrieu de Madron, X. and Mermex Group (2011), Marine ecosystems' responses to climatic and anthropogenic forcings in the Mediterranean. Prog. Oceanogr., 91(2), 97–166. doi:10.1016/j.pocean.2011.02.003.
- Estournel, C., P. Testor, I. Taupier-Letage, M.N. Bouin, L. Coppola, P. Durand, P. Conan, A. Bosse, P.E. Brilouet, L. Beguery, S. Belamari, K. Béranger, J. Beuvier, D. Bourras, G. Canut, A. Doerenbecher, X. Durrieu de Madron, F. D'Ortenzio, P. Drobinski, V. Ducrocq, N. Fourrié, H. Giordani, L. Houpert, L. Labatut, C. Lebeaupin Brossier, M. Nuret, L. Prieur, O. Roussot, L. Seyfried, and S. Somot (2016a), HyMeX-SOP2, the field campaign dedicated to dense water formation in the north-western Mediterranean. Oceanography, *29*,4.
- Estournel, C., P. Testor , P. Damien , F. D'Ortenzio, P. Marsaleix, P. Conan, F. Kessouri, X. Durrieu de Madron, L. Coppola, J-M. Lellouche, S. Belamari, L. Mortier, C. Ulses, M-N. Bouin and L. Prieur (2016b), High resolution modeling of dense water formation in the north-western Mediterranean during winter 2012-2013: Processes and budget. J. Geophys. Res. Oceans DOI: 10.1002/2016JC011935.
- Estournel, C., V. Zervakis, P. Marsaleix, A. Papadopoulos, F. Auclair, L. Perivoliotis, and E. Tragou (2005), Dense water formation and cascading in the Gulf of Thermaikos (North

Aegean) from observations and modelling, Cont. Shelf Res., 25, 2366-2386 doi:10.1016/j.csr.2005.08.014.

- Estrada, M., M. Latasa, M. Emelianov, A. Gutiérrez-Rodríguez, B. Fernández-Castro, J. Isern-Fontanet, B. Mouriño-Carballido, J. Salat, M. Vidal (2014), Seasonal and mesoscale variability of primary production in the deep winter-mixing region of the NW Mediterranean. *Deep Sea Res. Part I Oceanogr. Res. Pap.*, 94, 45–61. doi:http://dx.doi.org/10.1016/j.dsr.2014.08.003
- Gačić, M., Civitarese, G., Miserocchi, S., Cardin, V., Crise, A., Mauri, E. (2002), The open-ocean convection in the Southern Adriatic: a controlling mechanism of the spring phytoplankton bloom. Cont. Shelf Res., 22, 1897–1908. doi:10.1016/S0278-4343(02)00050-X
- Geider R. and La Roche J. (2002), Redfield revisited: variability of C:N:P in marine microalgae and its biochemical basis, European Journal of Phycology, 37:1, 1-17, DOI: 10.1017/S0967026201003456
- Gentilhomme, V. (1992), Quantification des flux d'absorption et de regénération de l'azote minéral (nitrate, nitrite, ammonium) et organique (urée) dans la couche euphotique des océans oligotrophes. Thèse de 1'Université Aix-Marseille
- Gogou, A., A. Sanchez-Vidal, X. Durrieu de Madron, S. Stavrakakis, A. M. Calafat, M. Stabholz, S. Psarra, M. Canals, S. Heussner, I. Stavrakaki, and E. Papathanassiou (2014), Reprint of: Carbon flux to the deep in three open sites of the Southern European Seas (SES), J. Mar. Syst., 135, 170–179, doi:10.1016/j.jmarsys.2014.04.012.
- Hauser, D., H. Branger, S. Bouffies-Cloché, S. Despiau, W. Drennan, H. Dupuis, P. Durand,

X. Durrieu de Madron, C. Estournel, L. Eymard, C. Flamant, H. Graber, C. Guérin, K. Kahma, G. Lachaud, J.-M. Lefèvre, J. Pelon, H. Pettersson, B. Piguet, P. Queffeulou, D. Tailliez, J. Tournadre, and A. Weill (2003), The FETCH experiment: an overview, Journal of Geophysical Res., 108, doi:10.1029/2001JC001202

- Herrmann, M., F. Diaz, C. Estournel, P. Marsaleix, and C. Ulses (2013), Impact of atmospheric and oceanic interannual variability on the Northwestern Mediterranean Sea pelagic planktonic ecosystem and associated carbon cycle. J. Geophys. Res. Oceans, 118, 5792–5813.
- Herrmann, M., S. Somot, F. Sevault, C. Estournel, and M. Déqué (2008), Modeling the deep convection in the Northwestern Mediterranean sea using an eddy-permitting and an eddy-resolving model: Case study of winter 1986–87, J. Geophys. Res., 113, C04011, doi:10.1029/2006JC003991.
- Houpert L., P. Testor, X. Durrieu de Madron, S. Somot, F. D'Ortenzio, C. Estournel, H. Lavigne (2015), Seasonal cycle of the mixed layer, the seasonal thermocline and the upper-ocean heat storage rate in the Mediterranean Sea derived from observations. Progress in Oceanography 132 (2015) 333–352.
- Huertas, E., A. F. Ríos, J. García-Lafuente, G. Navarro, A. Makaoui, A. Sánchez-Román, S. Rodriguez-Galvez, A. Orbi, J. Ruíz, and F. F. Pérez (2012), Atlantic forcing of the Mediterranean oligotrophy. Global Biogeochem. Cycles, Vol. 26, GB2022, doi :10.1029/2011GB004167.
- Krom M. D., Herut B., Mantoura R. F. C., (2004), Nutrient budget for the Eastern Mediterranean: Implications for phosphorus limitation, Limnology and Oceanography, 5,

doi: 10.4319/lo.2004.49.5.1582.

- Körtzinger, A., U. Send, D. W. R. Wallace, J. Kartensen, and M. DeGrandpre (2008), Seasonal cycle of O_2 and pCO_2 in the central Labrador Sea: Atmospheric, biological, and physical implications, Global Biogeochem. Cycles, 22, GB1014, doi:10.1029/2007GB003029.
- Krom, M. D., Kress, N., Brenner, S., Gordon, L.I., (1991), Phosphorus limitation of primary productivity in the eastern Mediterranean Sea. Limnol. Oceanogr. 36, 424–432.
- Large, W. G. and S. G. Yeager (2004), Diurnal to decadal global forcing for ocean and sea-ice models: the data sets and flux climatologies. NCAR Technical Note NCAR/TN-460+STR, DOI: 10.5065/D6KK98Q6.
- Lavigne, H., D'Ortenzio, F., M. Ribera D'Alcala, H. Claustre, R. Sauzede and M. Gacic (2015), On the vertical distribution of the chlorophyll-a 1 concentration in the Mediterranean Sea: a basin scale and seasonal approach. Biogeoscience, 12, 5021–5039, doi:10.5194/bg-12-5021-2015
- Lavigne, H. (2013), Impact of mixed layer depth seasonal variations on the phytoplankton phenology in the Mediterranean Sea, PhD thesis, University Pierre et Marie Curie, Paris, France.
- Lazzari P., C. Solidoro,S. Salon,G. Bolzon. (2016), Spatial variability of phosphate and nitrate in the Mediterranean Sea: A modeling approach. Deep Sea Research Part I: Oceanographic Research Papers. Volume 108, February 2016, Pages 39-52. https://doi.org/10.1016/j.dsr.2015.12.006
- Lellouche, J.-M., O. Le Galloudec, M. Drévillon, C. Régnier, E. Greiner, G. Garric, N. Ferry,

C. Desportes, C.E. Testut, C. Bricaud, R. Bourdallé-Badie, B. Tranchant, M. Benkiran, Y. Drillet, A. Daudin, and C. De Nicola (2013), Evaluation of global monitoring and forecasting systems at Mercator Océan, Ocean Sci., 9, 57-81, doi:10.5194/os-9-57-2013.

- Ludwig, W., A. F. Bouwman, E. Dumont, and F. Lespinas (2010), Water and nutrient fluxes from major Mediterranean and Black Sea rivers: Past and future trends and their implications for the basin-scale budgets, Global Biogeochem. Cycles, 24, GB0A13, doi:10.1029/2009GB003594.
- Manca, M., M. Burca, A. Giorgetti, C. Coatanoan, M.J. Garcia, and A. Iona (2004), Physical and biochemical averaged vertical profiles in the Mediterranean regions: an important tool to trace the climatology of water masses and to validate incoming data from operational oceanography, J. Mar. Syst., 48, 1–4, 83-116.
- Maraldi C., J. Chanut, B. Levier, N. Ayoub, P. De Mey, G. Reffray, F. Lyard, S. Cailleau, M. Drevillon, E.A. Fanjul, M.G. Sotillo, P. Marsaleix, and the Mercator Research and Development Team (2013), NEMO on the shelf: assessment of the Iberia–Biscay–Ireland configuration. Ocean Science, 9, 745–771. http://dx.doi.org/10.5194/os-9-745-2013
- Marshall, J., and F. Schott (1999), Open-ocean convection: Observations, theory, and models, Rev. Geophys., 37(1), 1–64, doi:10.1029/98RG02739.
- Marsaleix, P., F. Auclair, J.W. Floor, M.J. Herrmann, C. Estournel, I. Pairaud, and C. Ulses (2008), Energy conservation issues in sigma-coordinate free-surface ocean models. Ocean Modell.. 20, 61-89. http://dx.doi.org/10.1016/j.ocemod.2007.07.005
- Marsaleix, P., C. Ulses, I. Pairaud, M.J. Herrmann, J.W. Floor J. W., C. Estournel, and F. Auclair (2009), Open boundary conditions for internal gravity wave modelling using

polarization relations. Ocean Modell., 29, 27-42. http://dx.doi.org/10.1016/j.ocemod.2009.02.010

- Marsaleix, P., F. Auclair, C. Estournel, C. Nguyen, and C. Ulses (2011), An accurate implementation of the compressibility terms in the equation of state in a low order pressure gradient scheme for sigma coordinate ocean models. Ocean Modell., 40, 1-13 http://dx.doi.org/10.1016/j.ocemod.2011.07.004
- Marsaleix, P., F. Auclair, T. Duhaut, C. Estournel, C. Nguyen, and C. Ulses (2012), Alternatives to the Robert-Asselin filter. Ocean Modell., 41, 53-66
- Martin, A.P.; Pondaven, P. (2006), New primary production and nitrification in the western subtropical North Atlantic: a modeling study. Global Biogeochemical Cycles, 20 (4). GB4014.10.1029/2005GB002608
- Marty, J-C., J. Chiavérini, M-D.Pizay, and B. Avril (2002), Seasonal and interannual dynamics of nutrients and phytoplankton pigments in the western Mediterranean Sea at the DYFAMED time-series station (1991–1999). Deep-Sea Res. II , 49 , 1965–1985.
- Mayot, N., D'Ortenzio, F., Ribera d'Alcalà, M., Lavigne, H., and H. Claustre (2016), The Mediterranean trophic regimes from ocean color satellites: a reappraisal. *Biogeoscience*, 13, 1901–1917, doi:10.5194/bg-13-1901-2016
- Mayot, N., D'Ortenzio, F., Taillandier, V., Prieur, L., Pasqueron de Fommervault, O., Claustre, H., Bosse, A., Testor, P and Conan, P. (2017) Physical and biogeochemical controls of the phytoplankton blooms in North Western Mediterranean Sea: a multiplatform approach over a complete annual cycle (2012-2013 DEWEX experiment), J. Geophys. Res.
- MEDOC Group (1970), Observation of formation of deep water in the Mediterranean Sea,

Nature, 227(1037), 1040.

- Mignot, A., H. Claustre, J. Uitz, A. Poteau, F. D'Ortenzio, and X. Xing (2014), Understanding the seasonal dynamics of phytoplankton biomass and the deep chlorophyll maximum in oligotrophic environments: A Bio-Argo float investigation, Global Biogeochem. Cycles, 28, doi:10.1002/2013GB004781.
- Moutin, T., P. Raimbault, H.L. Golterman, and B. Coste (1998), The input of nutrients by the Rhône river into the Mediterranean Sea: recent observations and comparison with earlier data, Hydrobiologia, 373: 237. doi:10.1023/A:1017020818701
- Nittis, K., A. Lascaratos, A. Theocharis (2003), Dense water formation in the Aegean Sea: Numerical simulations during the Eastern Mediterranean Transient. Journal of Geophysical Research. Vol.. 108, No. c9, 8120, doi:10.1029/2002JC001352, 2003
- Ovchinnikov, I. M. (1984). The formation of Intermediate Water in the Mediterranean. Oceanology 24: 168–173.
- Pasqueron de Fommervault, O., C. Migon, F. D'Ortenzio, M. Ribera d'Alcalà and L. Coppola (2015a) , Temporal variability of nutrient concentrations in the northwestern Mediterranean sea (DYFAMED time-series station), Deep Sea Res. I, 100, 1-12.
- Pasqueron de Fommervault, O., F. D'Ortenzio, A. Mangin, R. Serra, C. Migon, H. Claustre, H. Lavigne, M. Ribera d'Alcalà, L.Prieur, V. Taillandier, C. Schmechtig, A. Poteau, E. Leymarie, A. Dufour, F. Besson, G. Obolensky (2015b), Seasonal variability of nutrient concentrations in the Mediterranean Sea: Contribution of Bio-Argo floats. J. Geophys. Res. Oceans, 120, 8528–8550, doi:10.1002/2015JC011103.
- Pastor, L., C. Cathalot, B. Deflandre, E. Viollier, K. Soetaert , F. J. R. Meysman, C. Ulses, E.

Metzger, and C. Rabouille (2011), Modeling biogeochemical processes in sediments from the Rhone River prodelta area (NW Mediterranean Sea), Biogeosciences, 8, 1351-1366

- Petrenko, A., C. Dufau, and C. Estournel (2008), Barotropic eastward currents in the western Gulf of Lion, north-western Mediterranean Sea, during stratified conditions, J. Mar. Syst., 74, 406-428 doi:10.1016/j.jmarsys.2008.03.004
- Pollak, M. (1951), The sources of deep water of the Eastern Mediterranean Sea. J. Mar. Res. 10: 128–152
- Pujo-Pay, M., P. Conan, L. Oriol, V. Cornet-Barthaux, C. Falco, J.-F. Ghiglione, C. Goyet, T. Moutin, and L. Prieur (2011), Integrated survey of elemental stoichiometry (C, N, P) from the western to eastern Mediterranean Sea. Biogeosciences, 8(4), 883–899. doi:10.5194/bg-8-883-2011.
- Pujo-Pay, M. and Conan, P. (2003), Seasonal variability and export of dissolved organic nitrogen in the northwestern Mediterranean Sea. *Journal of Geophysical Research 108: doi: 10.1029/2000JC000368. issn: 0148-0227.*
- Raimbault, P., Coste, B., (1990), Very high values of nitrate:phosphate ratio (>30) in the subsurface layers of the western Mediterranean Sea. Rapp. Comm. Int. Mer. Mediterr. 32 (1), C-18.
- Raimbault, P., G. Slawyk, B. Boudjellal, C. Coatanoan, P. Conan, B. Coste, N. Garcia, T. Moutin, M. Pujo-Pay (1998), Carbon and nitrogen uptake and export in the equatorial Pacific at 150°W: evidence of an efficient regenerated production cycle. J Geophys Res 104:3341-3356.
- Redfield, A. C., B. H. Ketchum and F. A. Richards (1963), The influence of organisms on

the composition of sea-water. Contribution No 1113, Woods Hole Oceanographic Institution and Contribution No. 238, Department of Oceanography of the University of Washington.

- Ribera d'Alcalà, M., G. Civitarese, F. Conversano, and R. Lavezza (2003), Nutrient ratios and fluxes hint at overlooked processes in the Mediterranean Sea, J. Geophys. Res., 108, 8106, doi:10.1029/2002JC001650, C9.
- Ridame, C., and Guieu, C. (2002). Saharan input of phosphate to the oligotrophic water of the open western Mediterranean Sea. *Limnol. Oceanogr*. 47, 856–869. doi: 10.4319/lo.2002.47.3.0856
- Santinelli, C., V. Ibello, R. Lavezza, G. Civitarese, and A. Seritti (2012), New insights into C, N and P stoichiometry in the Mediterranean Sea: The Adriatic Sea case. Cont. Shelf Res., 44 (2012) 83–93
- Sempéré, R., B. Charrière, F. Van Wambeke, and G. Cauwet (2000), Carbon Inputs of the Rhöne River to the Mediterranean Sea: Biogeochemical Implications, Global Biogeochem. Cycles, 14, 2, 669–681.
- Severin, T., et al. (2017), Open-oceanconvection process: A driver of thewinter nutrient supply and the springphytoplankton distribution in theNorthwestern Mediterranean Sea, J.Geophys. Res. Oceans, 122, doi:10.1002/2016JC012664.
- Severin, T., P. Conan, X. Durrieu de Madron, L. Houpert, M.J. Oliver, L. Oriola, J. Caparros, J.F. Ghiglione, and M. Pujo-Pay (2014), Impact of open-ocean convection on nutrients, phytoplankton biomass and activity, Deep Sea Res. I, doi: 10.1016/j.dsr.2014.07.015
- Soetaert, K., P.M.J.
- Herman, J.J. Middelburg, C. Heip, C.L. Smith, P. Tett, and K. Wild-Allen (2001), Numerical

modelling of the shelf break ecosystem: reproducing benthic and pelagic measurements. Deep-Sea Res. II, 48, 3141 – 3177.

- Somot, S., F. Sevault, and M. Déqué, 2006: Transient climate change scenario simulation of the Mediterranean Sea for the 21st century using a high-resolution ocean circulation model. Climate Dyn., 27, 851–879
- Testor, P. (2013), DEWEX-MERMEX 2013 LEG1 cruise, RV Le Suroît, edited by SISMER, doi:10.17600/13020010.
- Testor, P., L. Coppola, and L. Mortier (2013), MOOSE-GE 2013 cruise, RV Téthys II, edited by SISMER, doi:10.17600/13450110.
- Ulses, C., C. Estournel, P. Puig , X. Durrieu de Madron, and P. Marsaleix (2008), Dense shelf water cascading in the northwestern Mediterranean during the cold winter 2005: Quantification of the export through the Gulf of Lion and the Catalan margin. Geophys. Res. Lett. 35.
- Ulses, C., P.-A. Auger, K. Soetaert, P. Marsaleix, F. Diaz, L. Coppola, M. Herrmann, F. Kessouri, and C. Estournel (2016), Budget of organic carbon in the North-Western Mediterranean Open Sea over the period 2004-2008 using 3D coupled physical biogeochemical modeling, J. Geophys. Res. , doi:10.1002/2016JC011818.
- Williams, R. G., and A. J. McLaren (2000), Estimating the convective supply of nitrate and implied variability in export production over the North Atlantic, Global Biogeochemical Cycles. Vol. 14. , NO 4, Pages 1299-1313.
- Yilmaz, A. and S. Tugrul (1998), The effect of cold- and warm-core eddies on the distribution and stoichiometry of dissolved nutrients in the northeastern Mediterranean. J.

Mar. Syst., 16, 3-4, 253–268.

Figure 1.

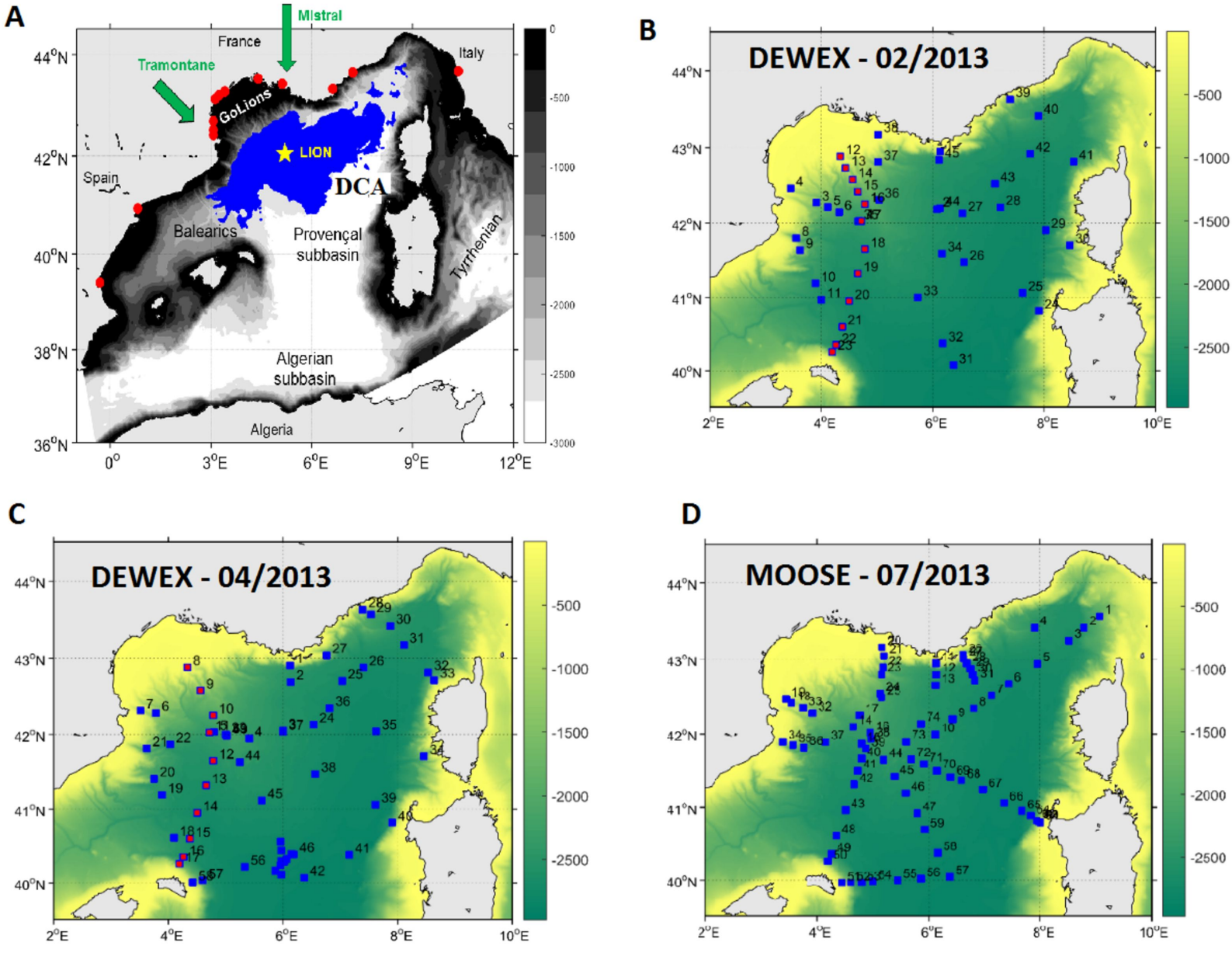
A
Mistral
Tramontane
France
Italy
GoLions
LION
DCA
Spain
Balearics
Provençal
subbasin
Tyrrhenian
Algerian
subbasin
Algeria
44°N
42°N
40°N
38°N
36°N
0°
3°E
6°E
9°E
12°E
0
-500
-1000
-1500
-2000
-2500
-3000
B
DEWEX - 02/2013
C
DEWEX - 04/2013
D
MOOSE - 07/2013
2°E
4°E
6°E
8°E
10°E
41°N
43°N

Figure 2.

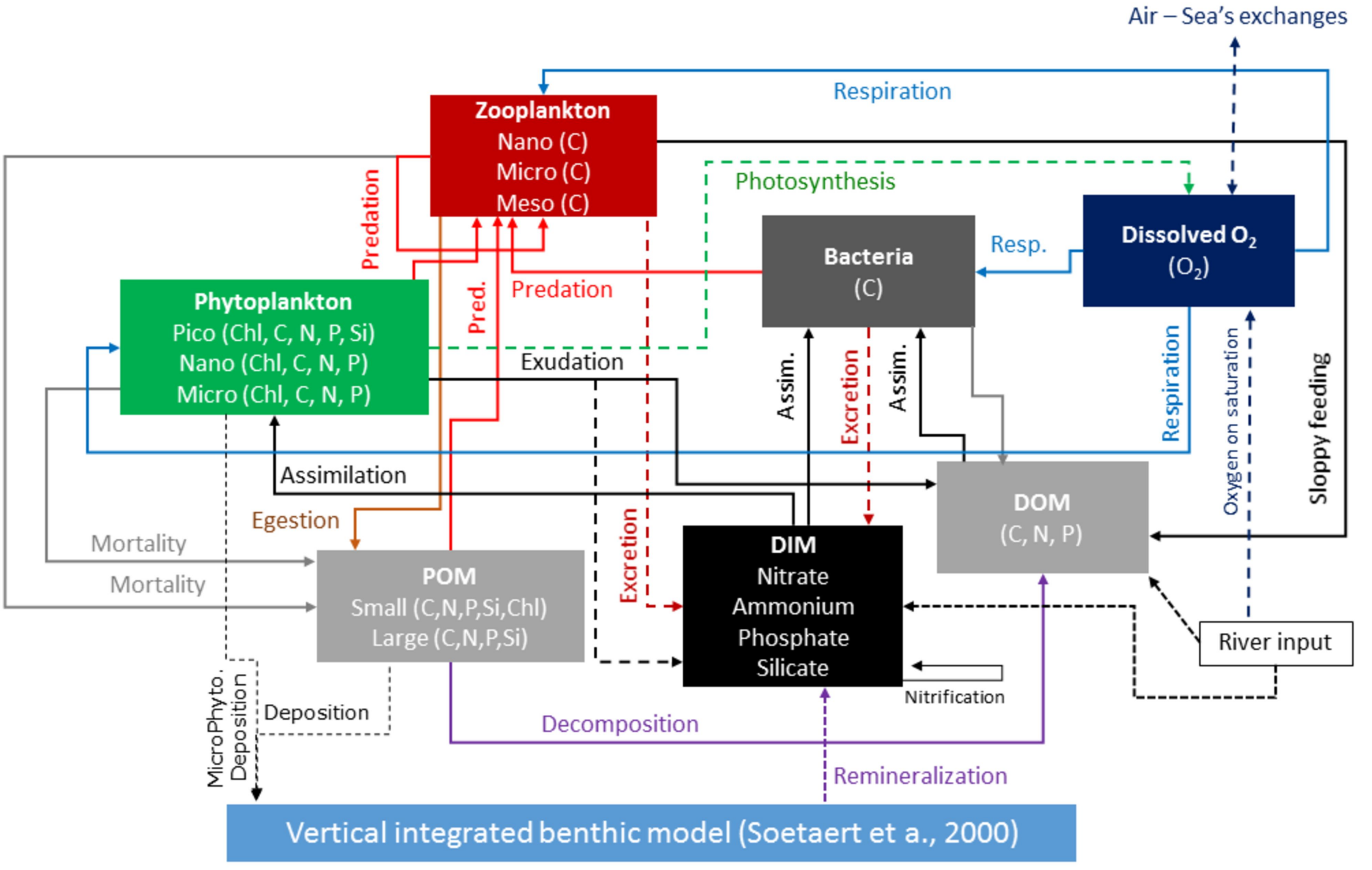
Air – Sea's exchanges
Respiration
Zooplankton
Nano (C)
Micro (C)
Meso (C)
Predation
Photosynthesis
Bacteria
(C)
Resp.
Dissolved O_2
(O_2)
Phytoplankton
Pico (Chl, C, N, P, Si)
Nano (Chl, C, N, P)
Micro (Chl, C, N, P)
Pred.
Predation
Exudation
Assim.
Excretion
Assim.
Respiration
Oxygen on saturation
Sloppy feeding
Assimilation
DOM
(C, N, P)
Egestion
Mortality
Mortality
DIM
Nitrate
Ammonium
Phosphate
Silicate
Excretion
POM
Small (C,N,P,Si,Chl)
Large (C,N,P,Si)
River input
Nitrification
MicroPhyto. Deposition
Deposition
Decomposition
Remineralization
Vertical integrated benthic model (Soetaert et a., 2000)

Figure 3.

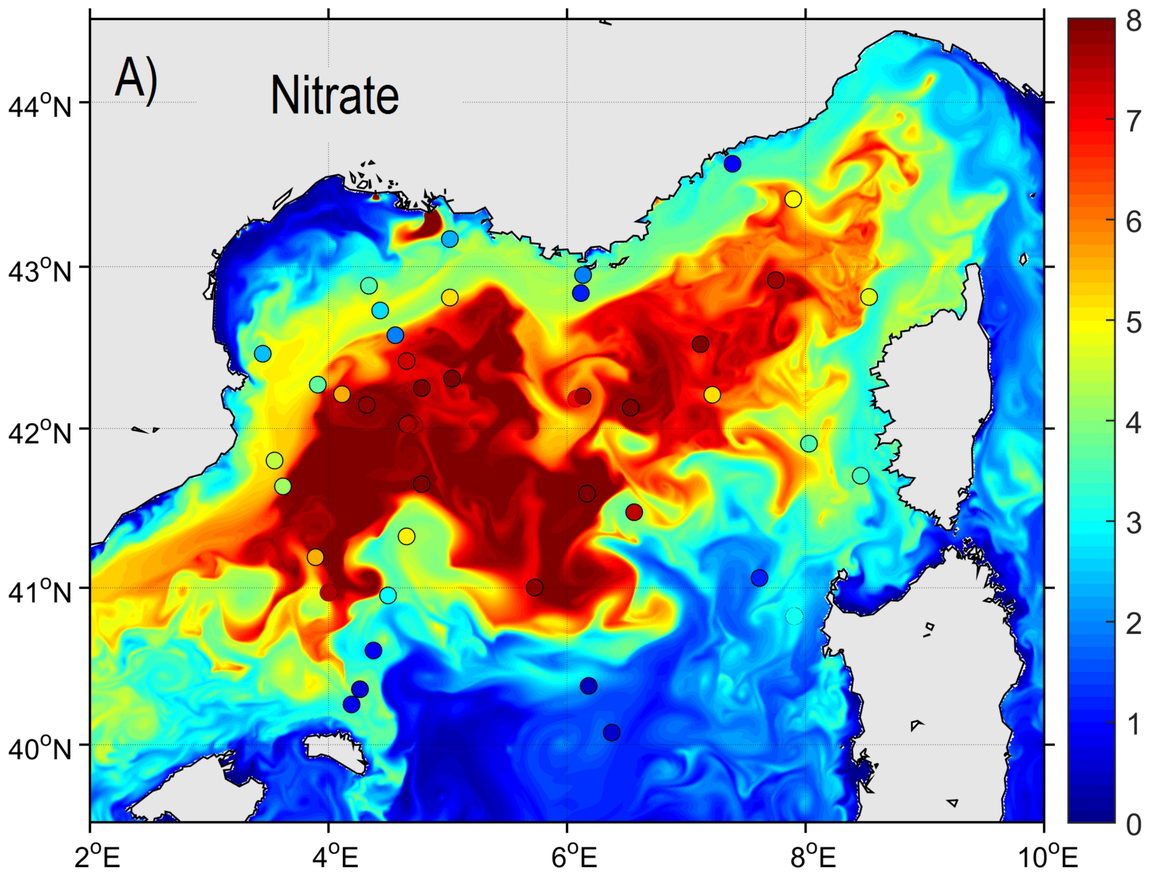
A)
Nitrate
44°N
43°N
42°N
41°N
40°N
2°E
4°E
6°E
8°E
10°E
8
7
6
5
4
3
2
1
0

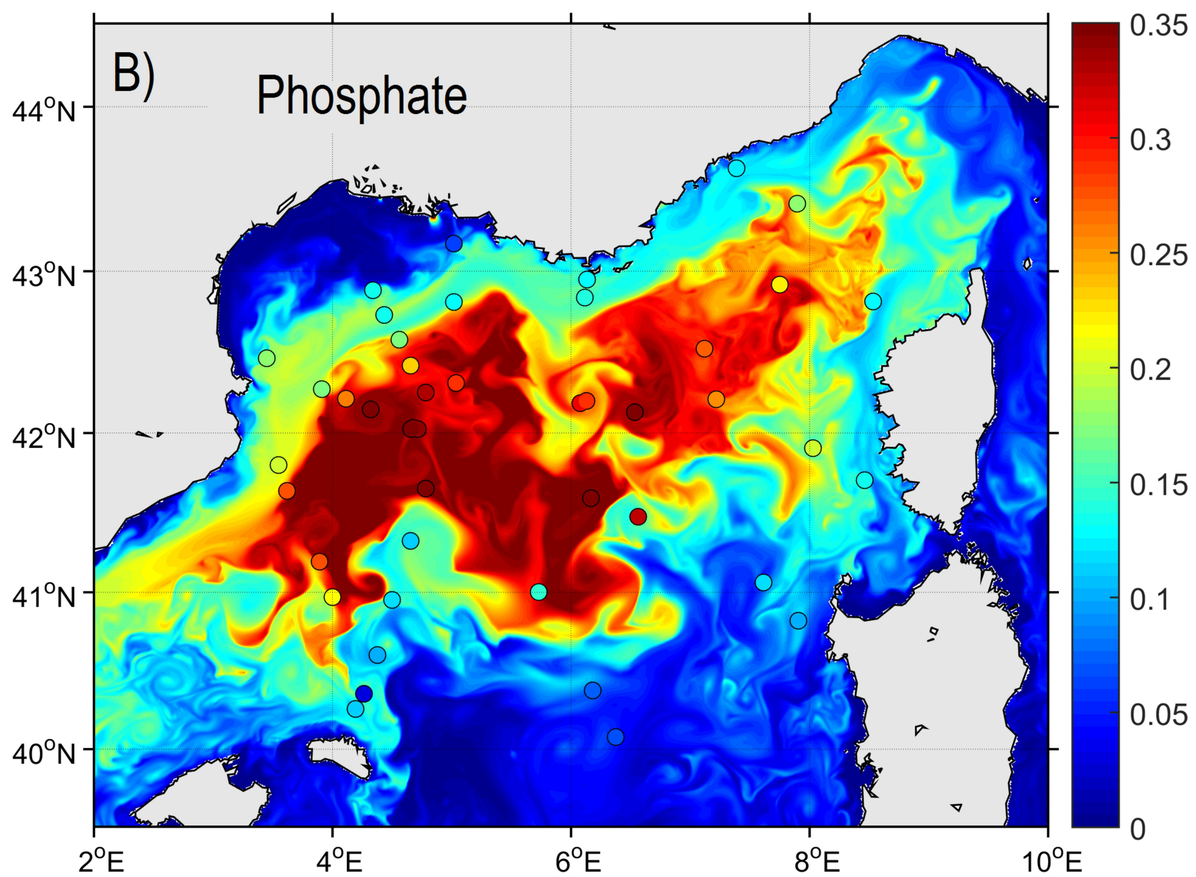
B)
Phosphate
44°N
43°N
42°N
41°N
40°N
2°E
4°E
6°E
8°E
10°E
0.35
0.3
0.25
0.2
0.15
0.1
0.05
0

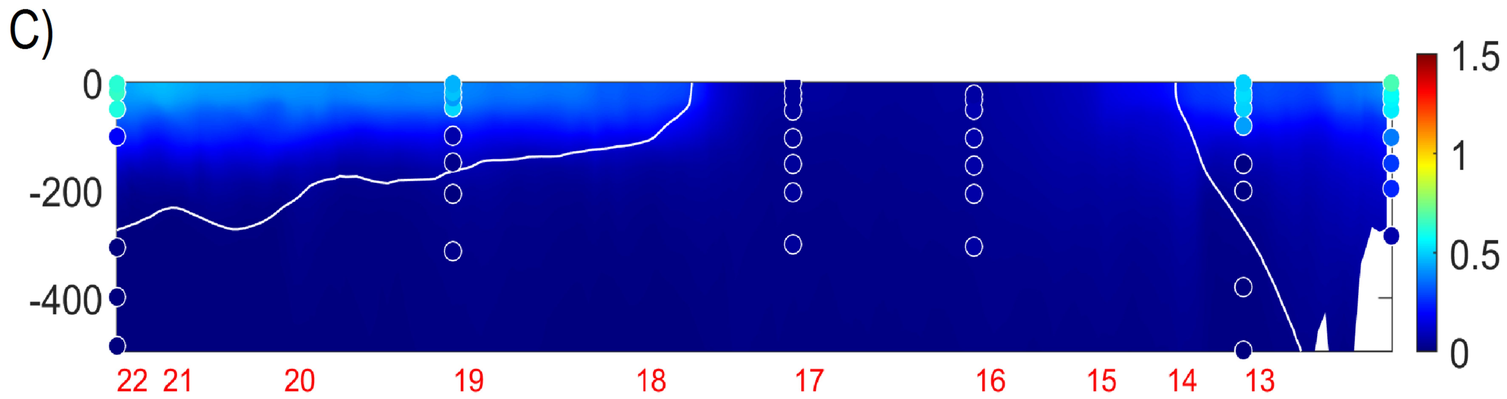
C)
Chla
0
-200
-400
22 21 20 19 18 17 16 15 14 13
1.5
1
0.5
0

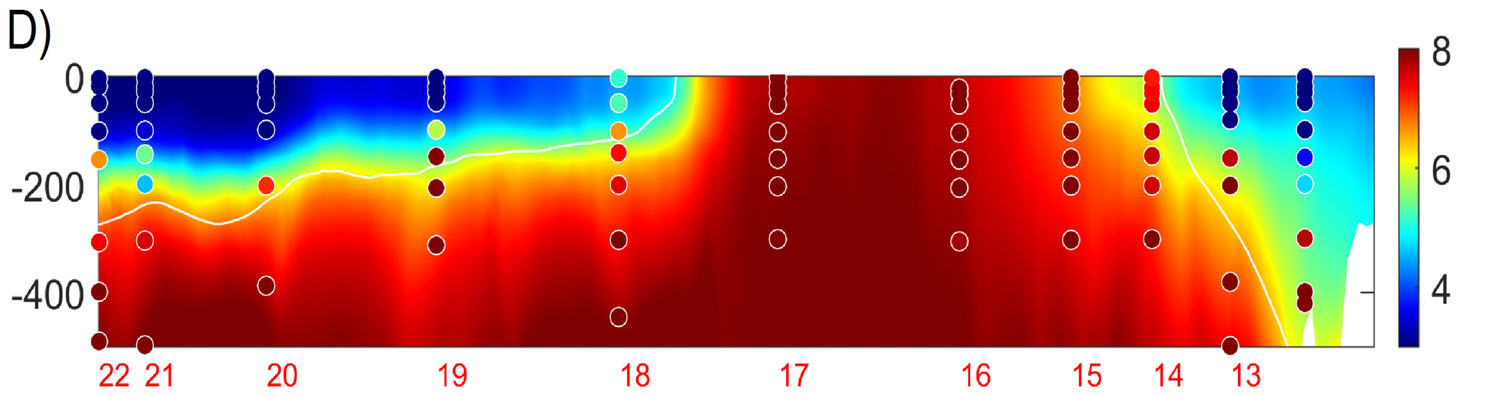
D)
Nitrate
0
-200
-400
22 21 20 19 18 17 16 15 14 13
8
6
4

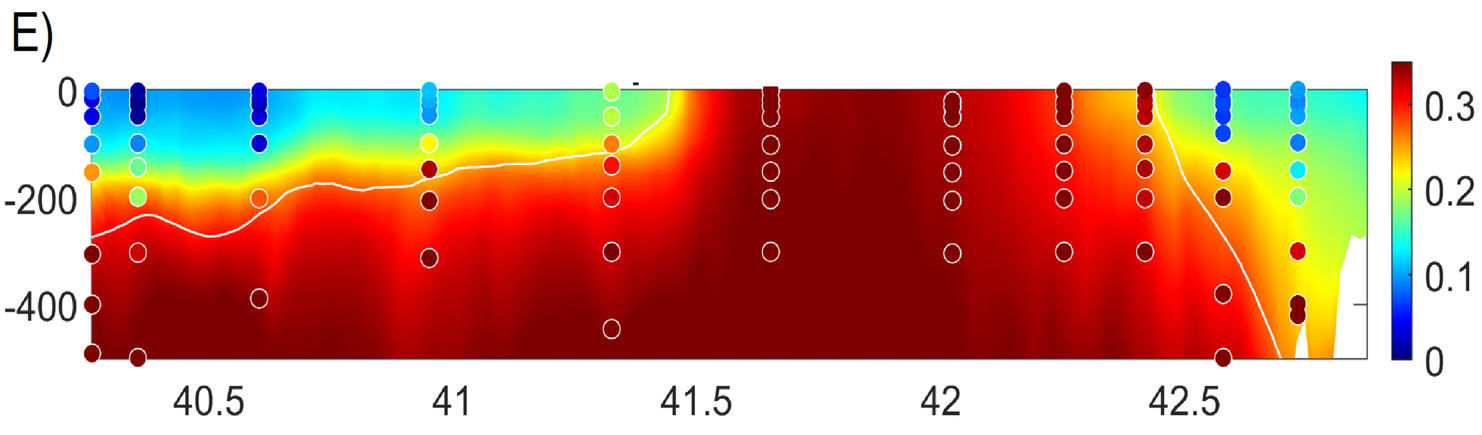
E)
Phosphate
0
-200
-400
40.5
41
41.5
42
42.5
0.3
0.2
0.1
0

Figure 4.

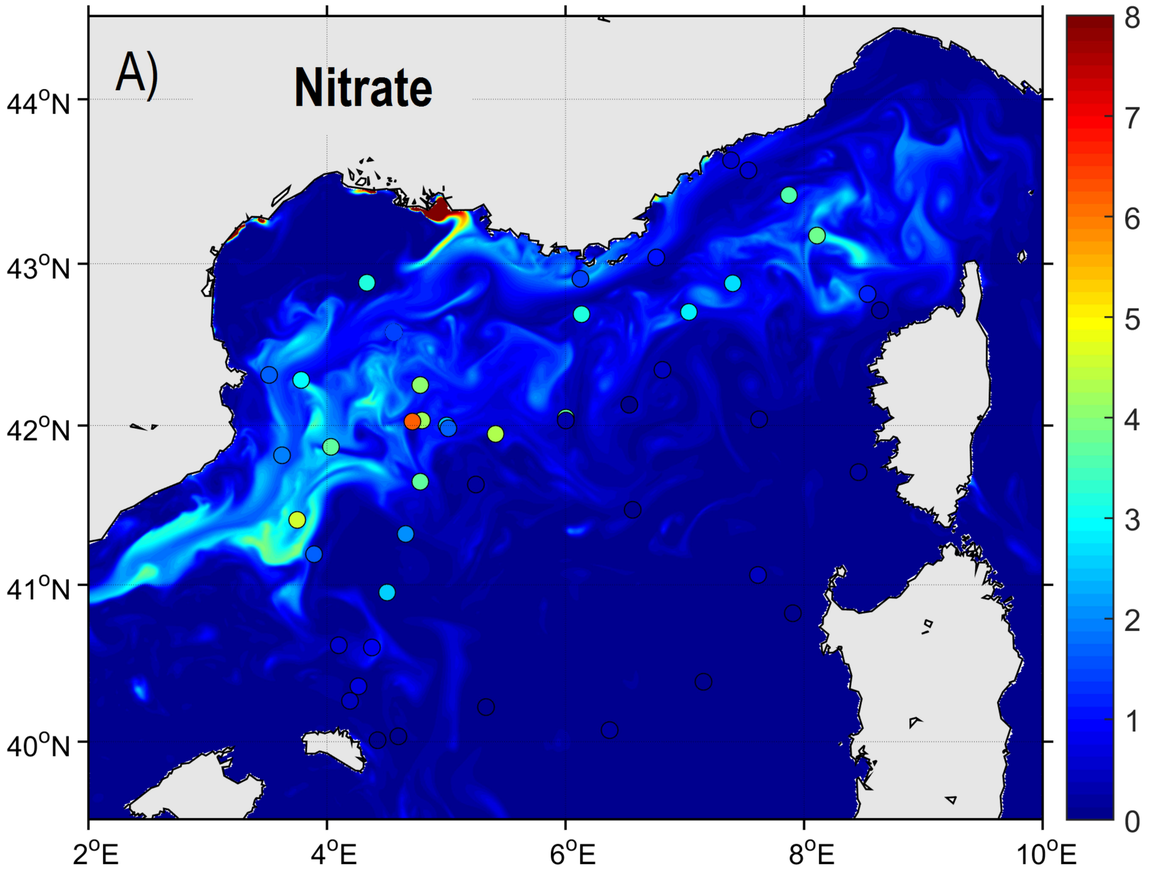
A)
Nitrate
44°N
43°N
42°N
41°N
40°N
2°E
4°E
6°E
8°E
10°E
0
1
2
3
4
5
6
7
8

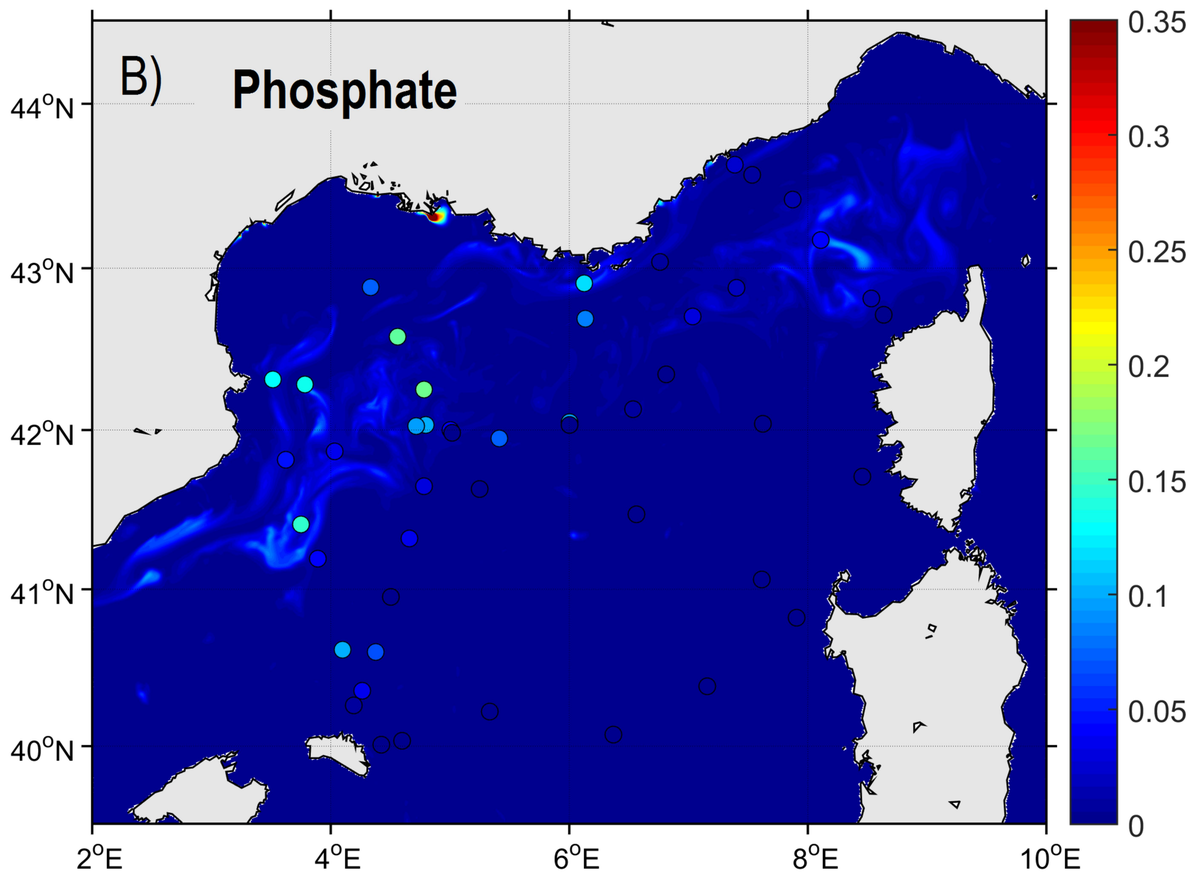
B)
Phosphate
44°N
43°N
42°N
41°N
40°N
2°E
4°E
6°E
8°E
10°E
0
0.05
0.1
0.15
0.2
0.25
0.3
0.35

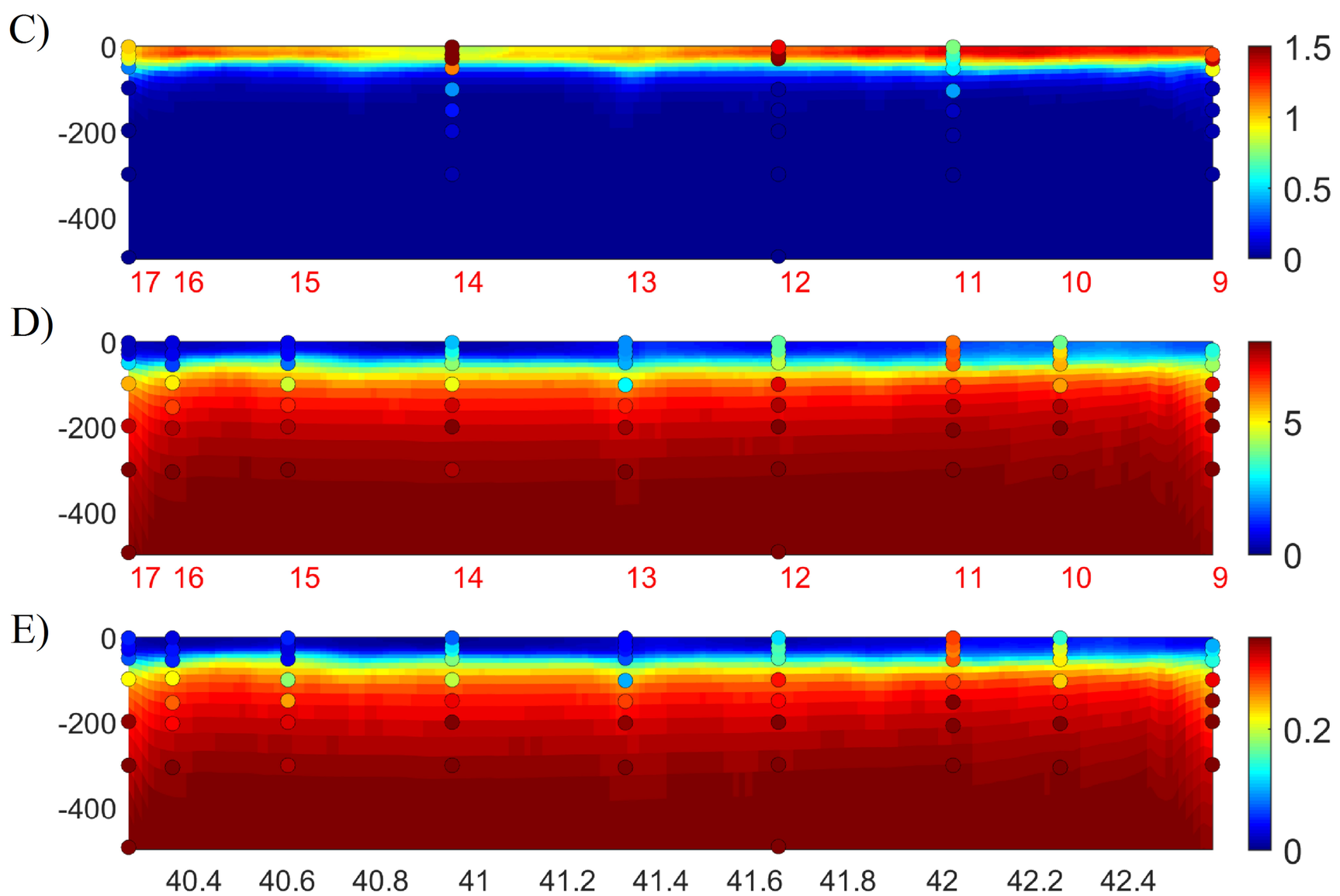
C)
Chla
D)
Nitrate
E)
Phosphate
0
-200
-400
17 16 15 14 13 12 11 10 9
40.4 40.6 40.8 41 41.2 41.4 41.6 41.8 42 42.2 42.4
0
0.5
1
1.5
0
5
0
0.2
0

Figure 5.

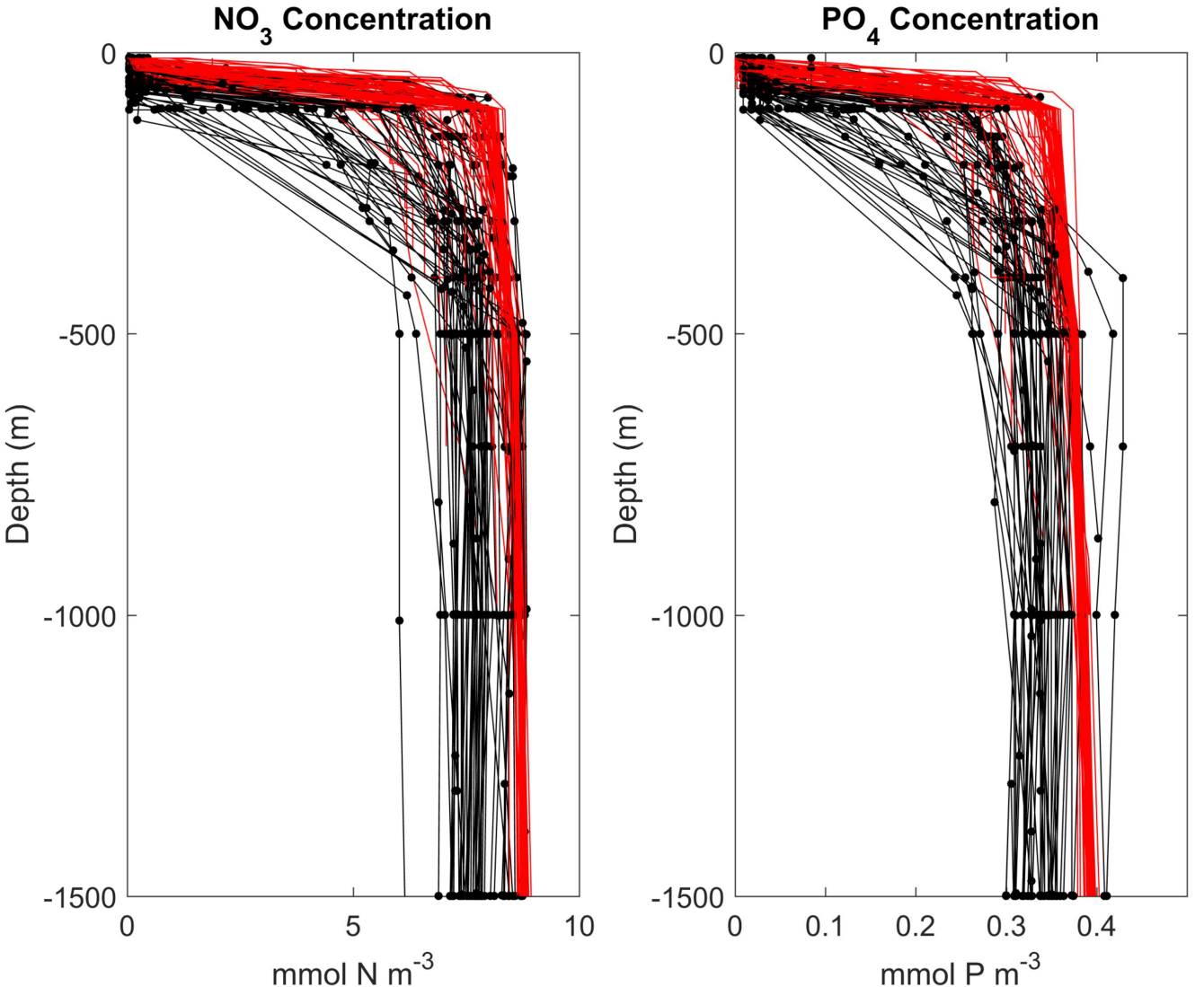
NO3 Concentration
PO4 Concentration
Depth (m)
0
-500
-1000
-1500
0
5
10
0.1
0.2
0.3
0.4
mmol N m-3
mmol P m-3

Figure 6.

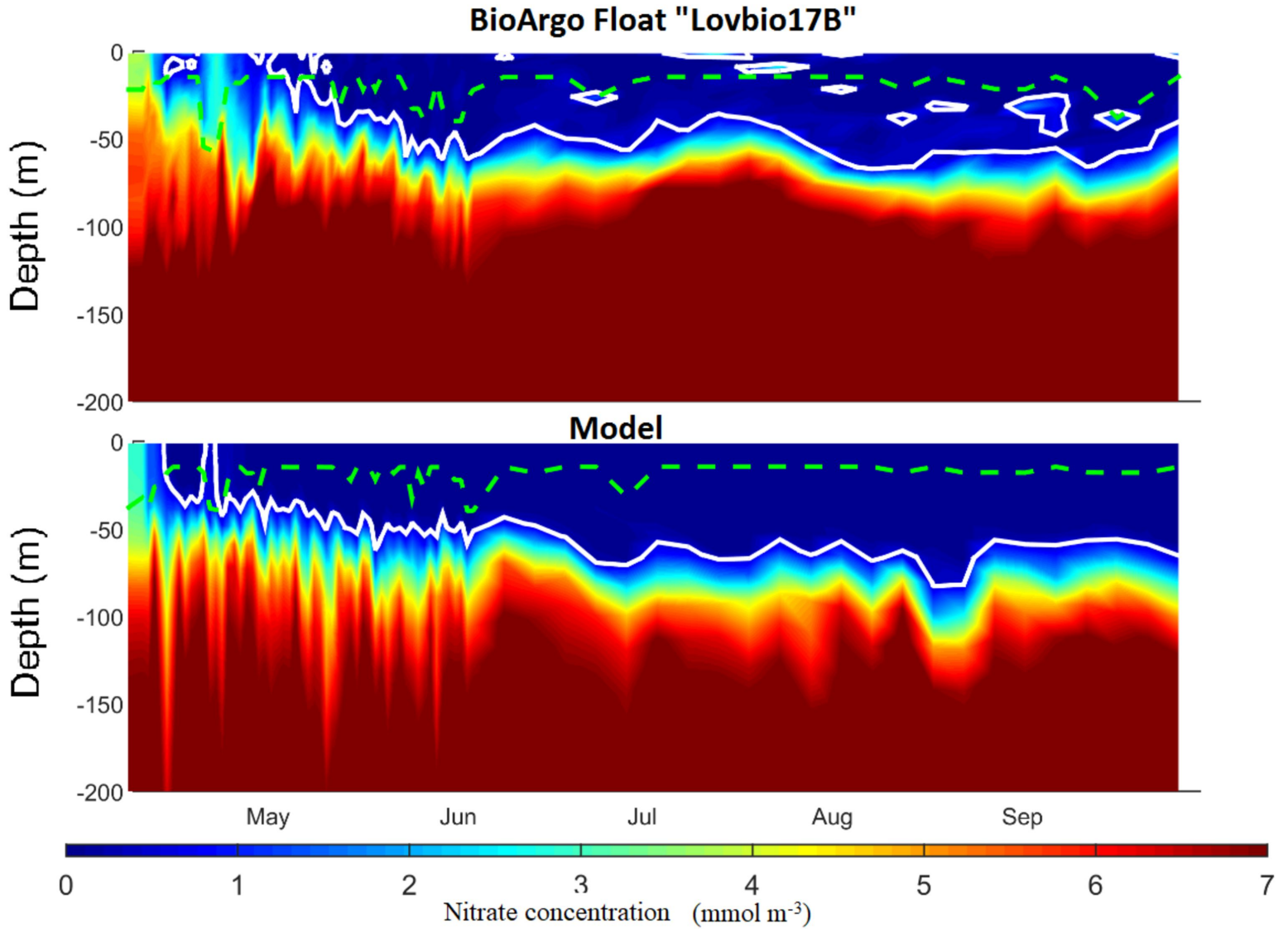
BioArgo Float "Lovbio17B"
Model
Depth (m)
0
-50
-100
-150
-200
May
Jun
Jul
Aug
Sep
0
1
2
3
4
5
6
7
Nitrate concentration (mmol m-3)

Figure 7.

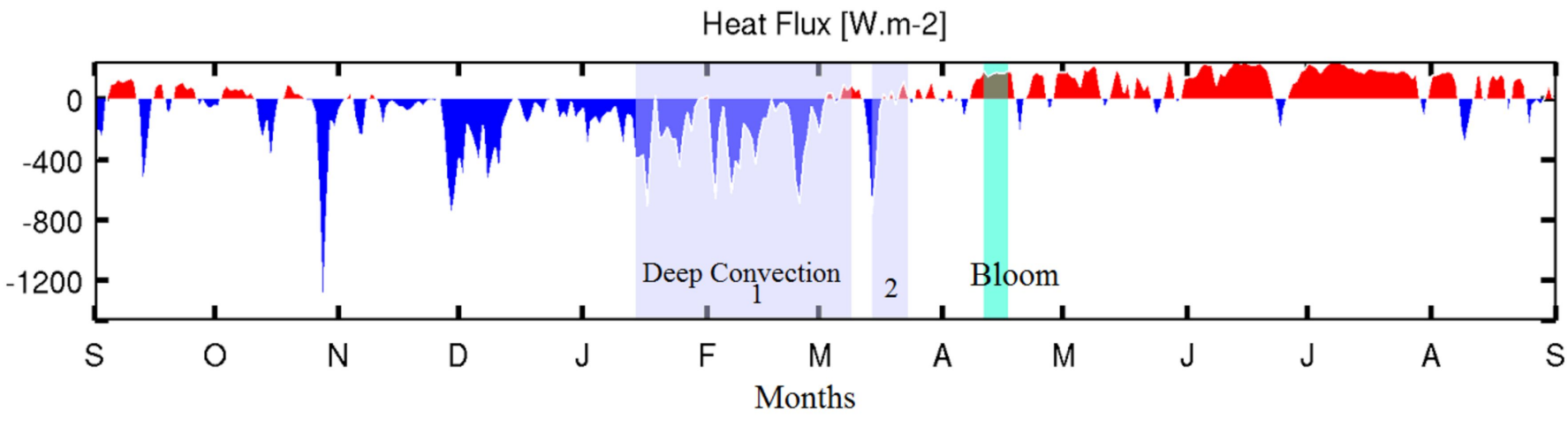
Heat Flux [W.m-2]
0
-400
-800
-1200
Deep Convection
1
2
Bloom
S
O
N
D
J
F
M
A
M
J
J
A
S
Months

Figure 8.

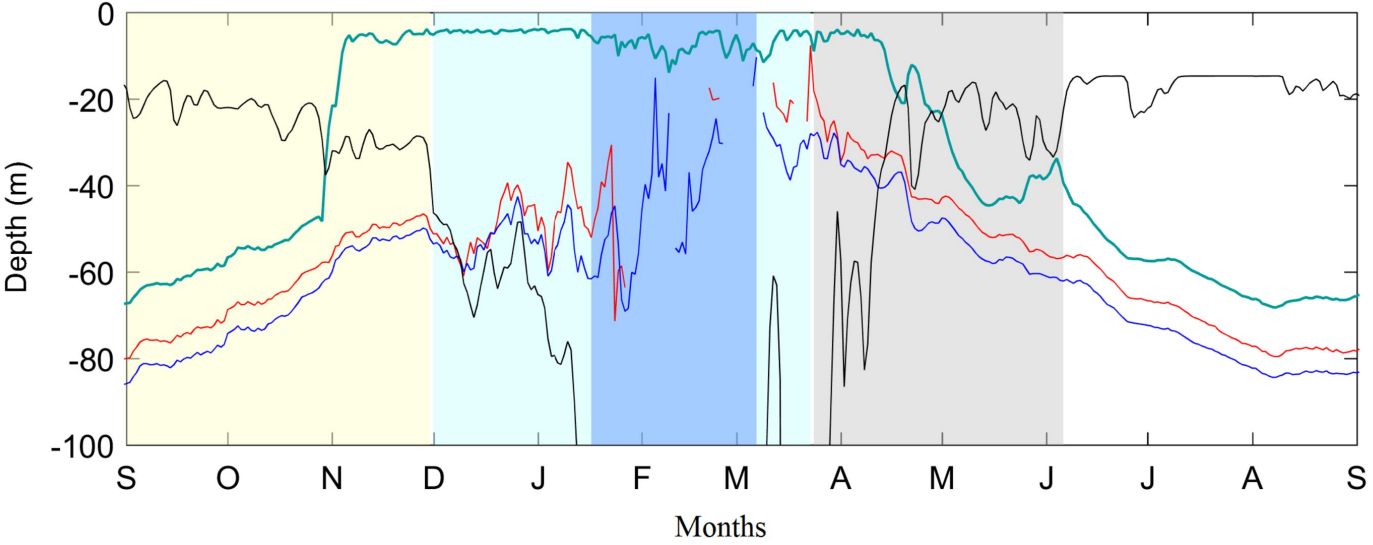
0
-20
-40
-60
-80
-100
Depth (m)
S
O
N
D
J
F
M
A
M
J
J
A
S
Months

Figure 9.

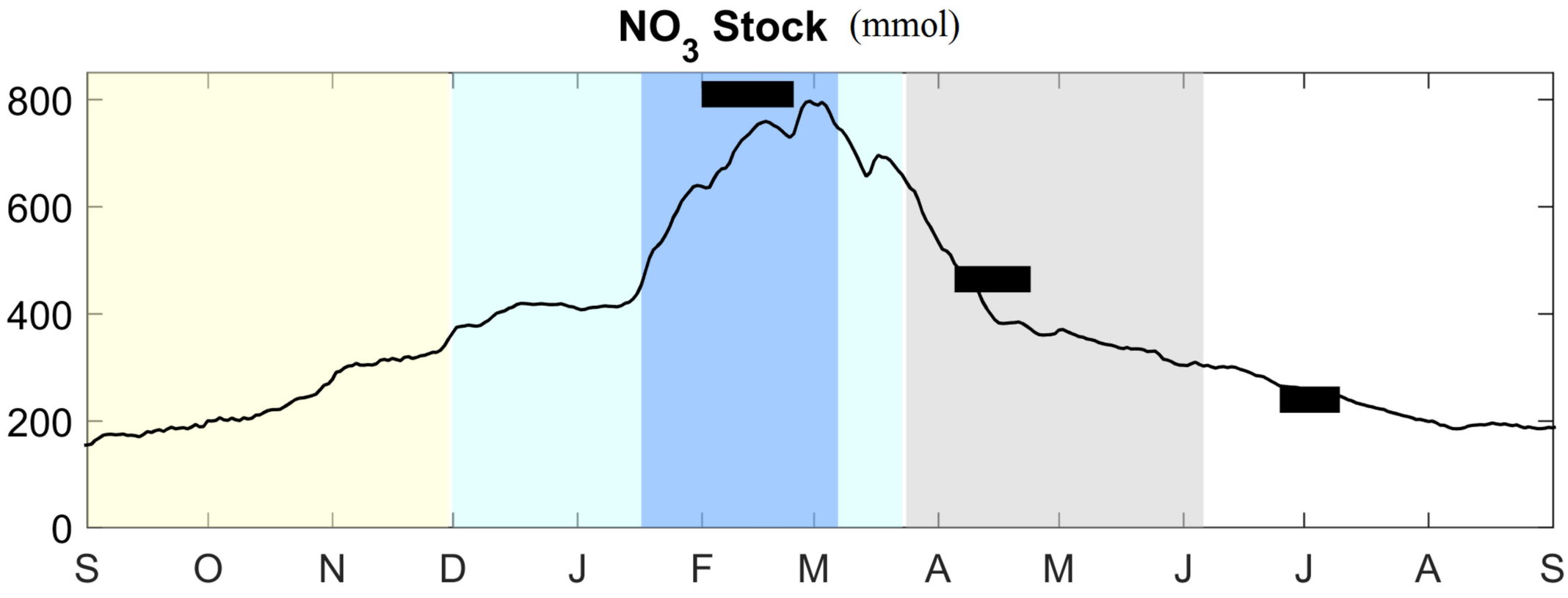
NO3 Stock (mmol)
800
600
400
200
0
S
O
N
D
J
F
M
A
M
J
J
A
S

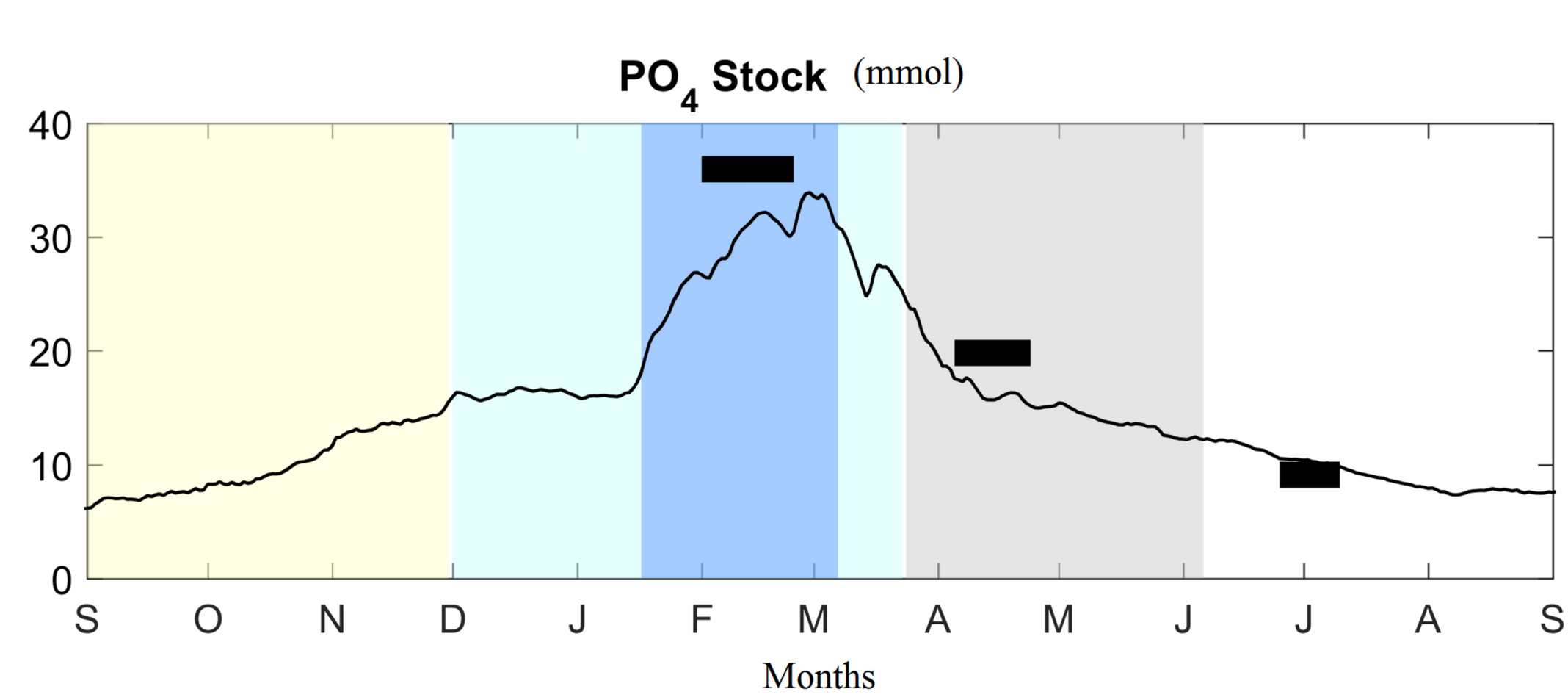
PO4 Stock (mmol)
40
30
20
10
0
S
O
N
D
J
F
M
A
M
J
J
A
S
Months

Figure 10.

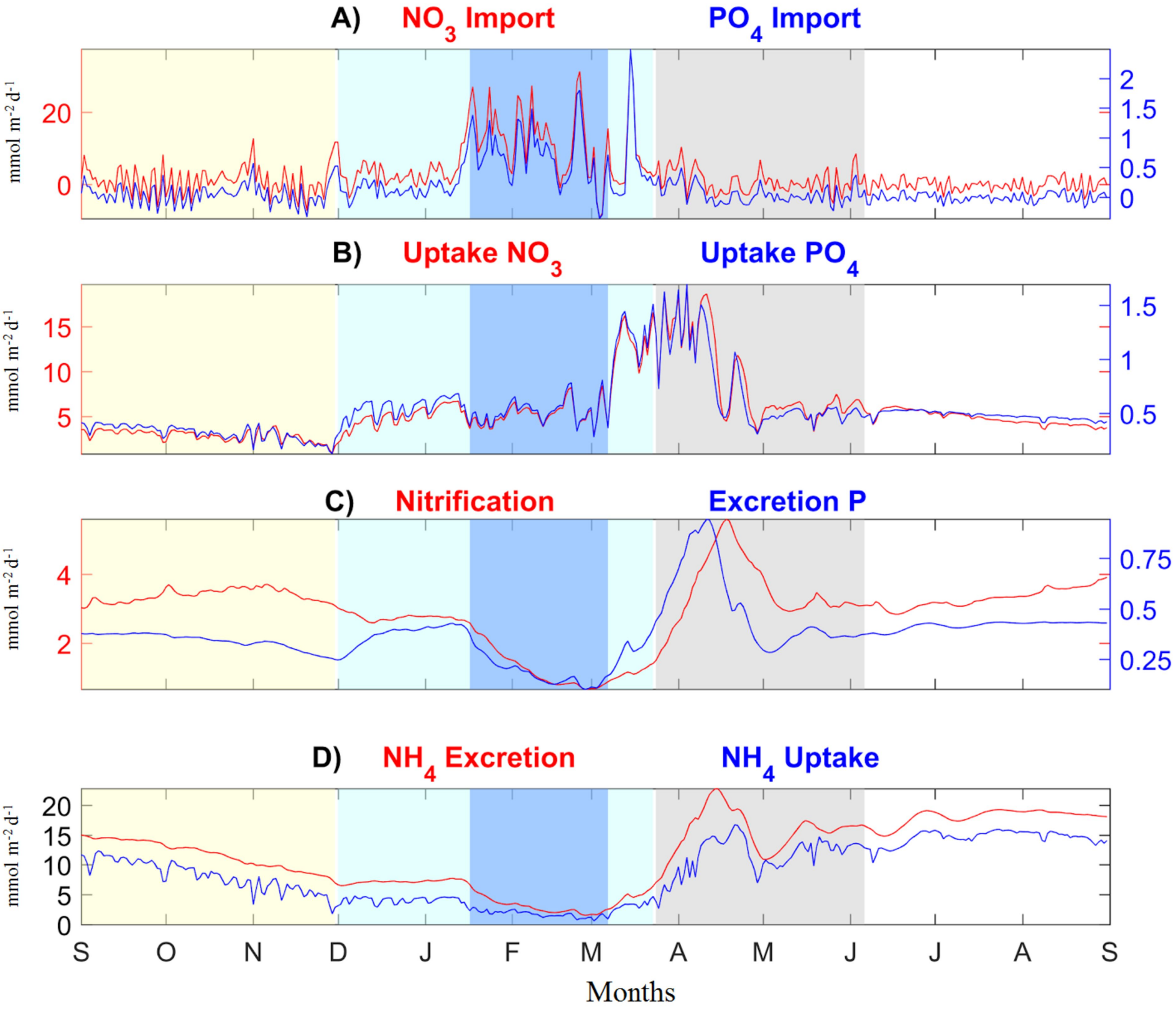
A) NO3 Import
PO4 Import
mmol m-2 d-1
20
0
2
1.5
1
0.5
0
B) Uptake NO3
Uptake PO4
mmol m-2 d-1
15
10
5
1.5
1
0.5
C) Nitrification
Excretion P
mmol m-2 d-1
4
2
0.75
0.5
0.25
D) NH4 Excretion
NH4 Uptake
mmol m-2 d-1
20
15
10
5
0
S
O
N
D
J
F
M
A
M
J
J
A
S
Months

Figure 11.

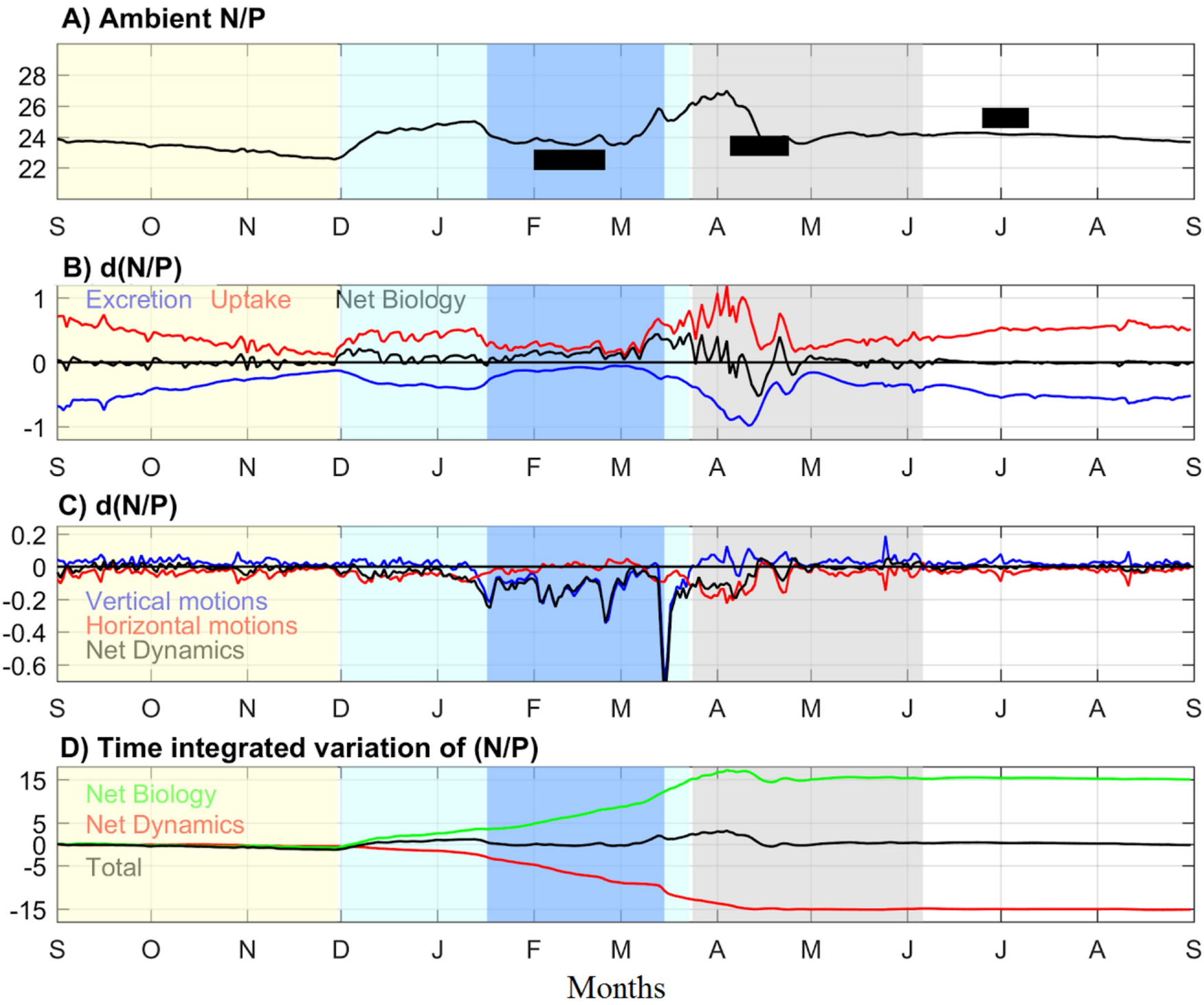
A) Ambient N/P
28
26
24
22
S O N D J F M A M J J A S
B) d(N/P)
Excretion
Uptake
Net Biology
1
0
-1
S O N D J F M A M J J A S
C) d(N/P)
0.2
0
-0.2
-0.4
-0.6
Vertical motions
Horizontal motions
Net Dynamics
S O N D J F M A M J J A S
D) Time integrated variation of (N/P)
15
5
0
-5
-15
Net Biology
Net Dynamics
Total
S O N D J F M A M J J A S
Months

Figure 12.

Nitrogen cycle

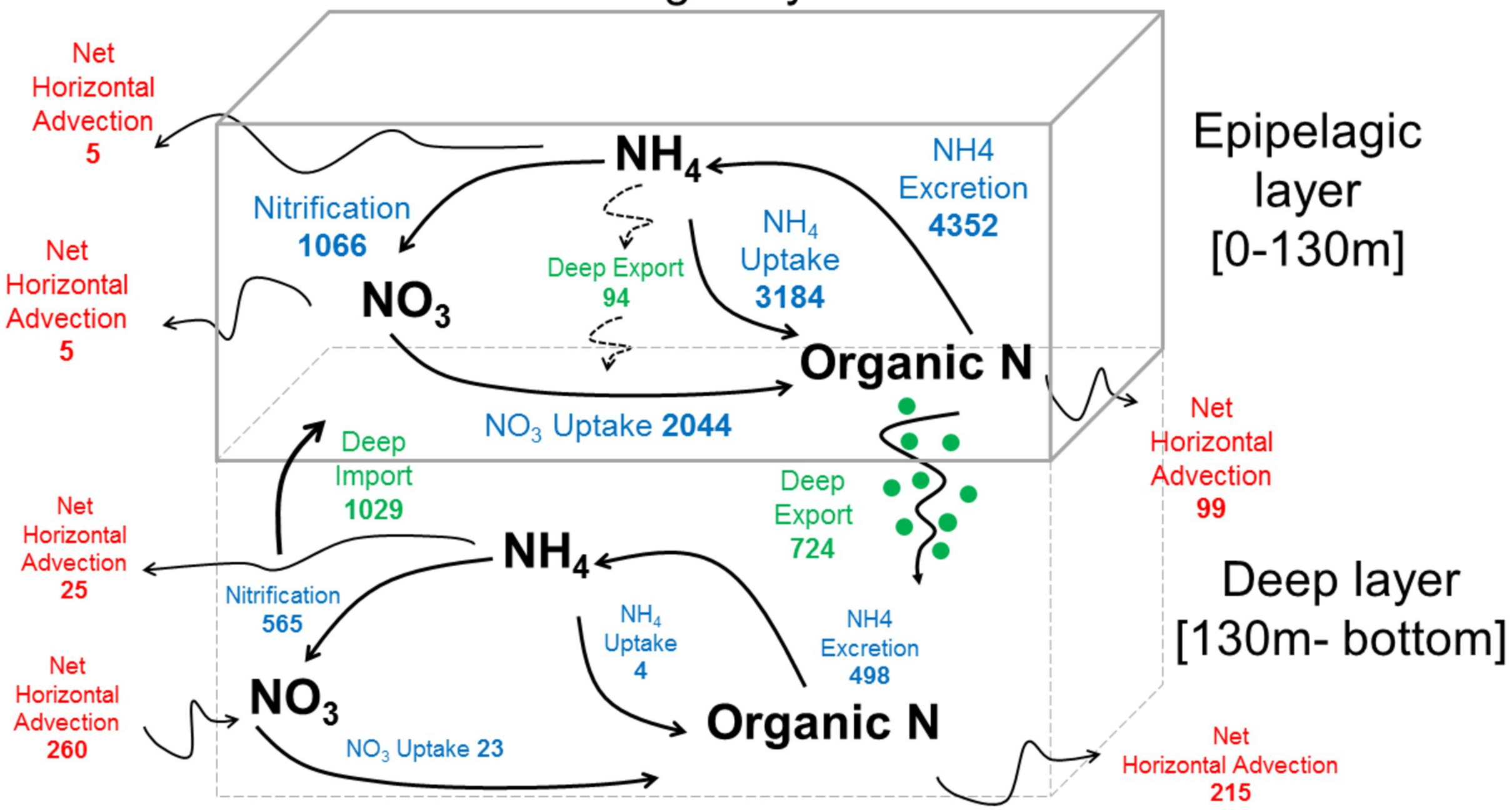

Epipelagic layer [0-130m]

Deep layer [130m- bottom]

Phosphorus cycle

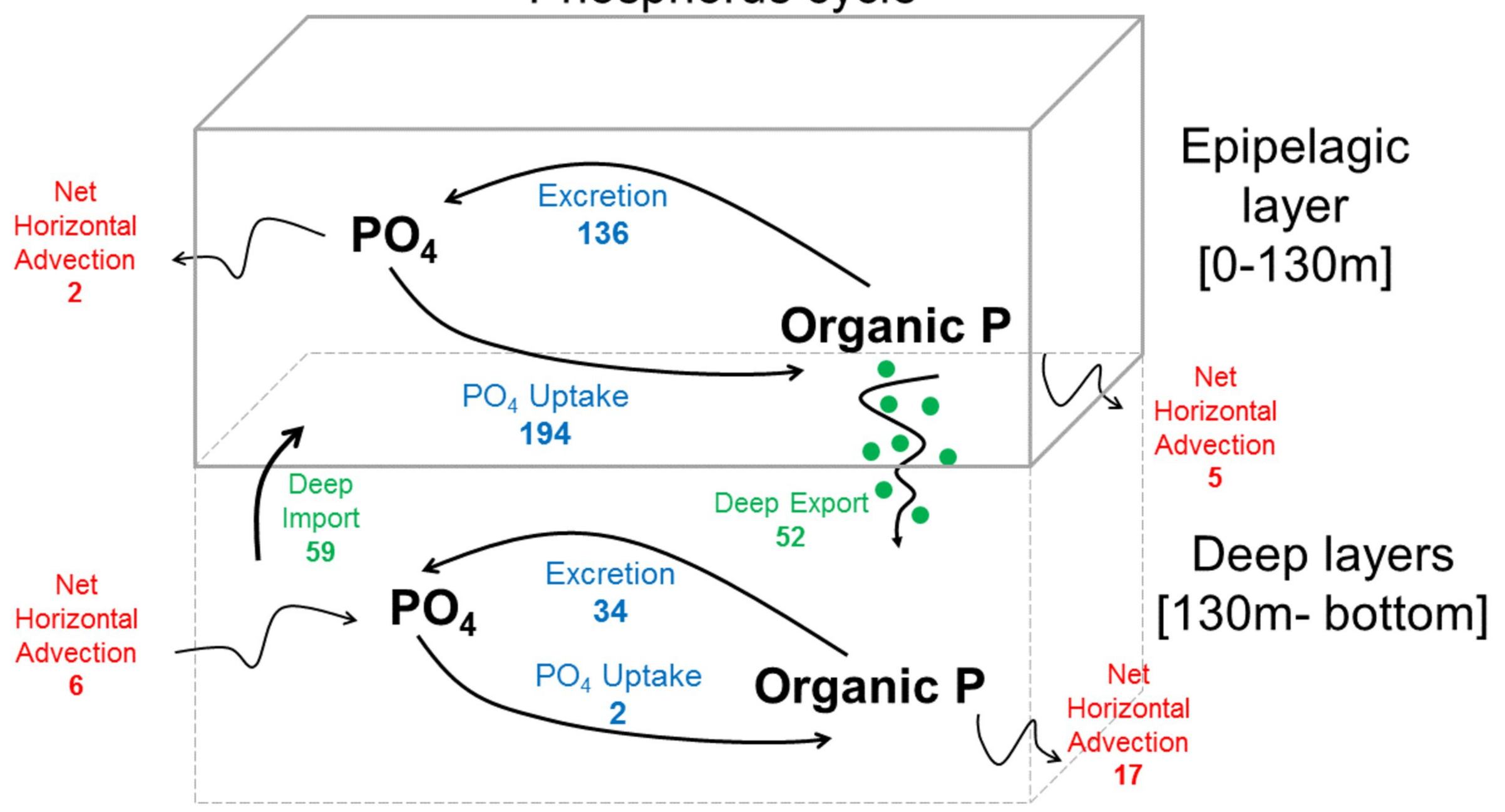

Epipelagic layer [0-130m]

Deep layers [130m- bottom]

Figure 13.

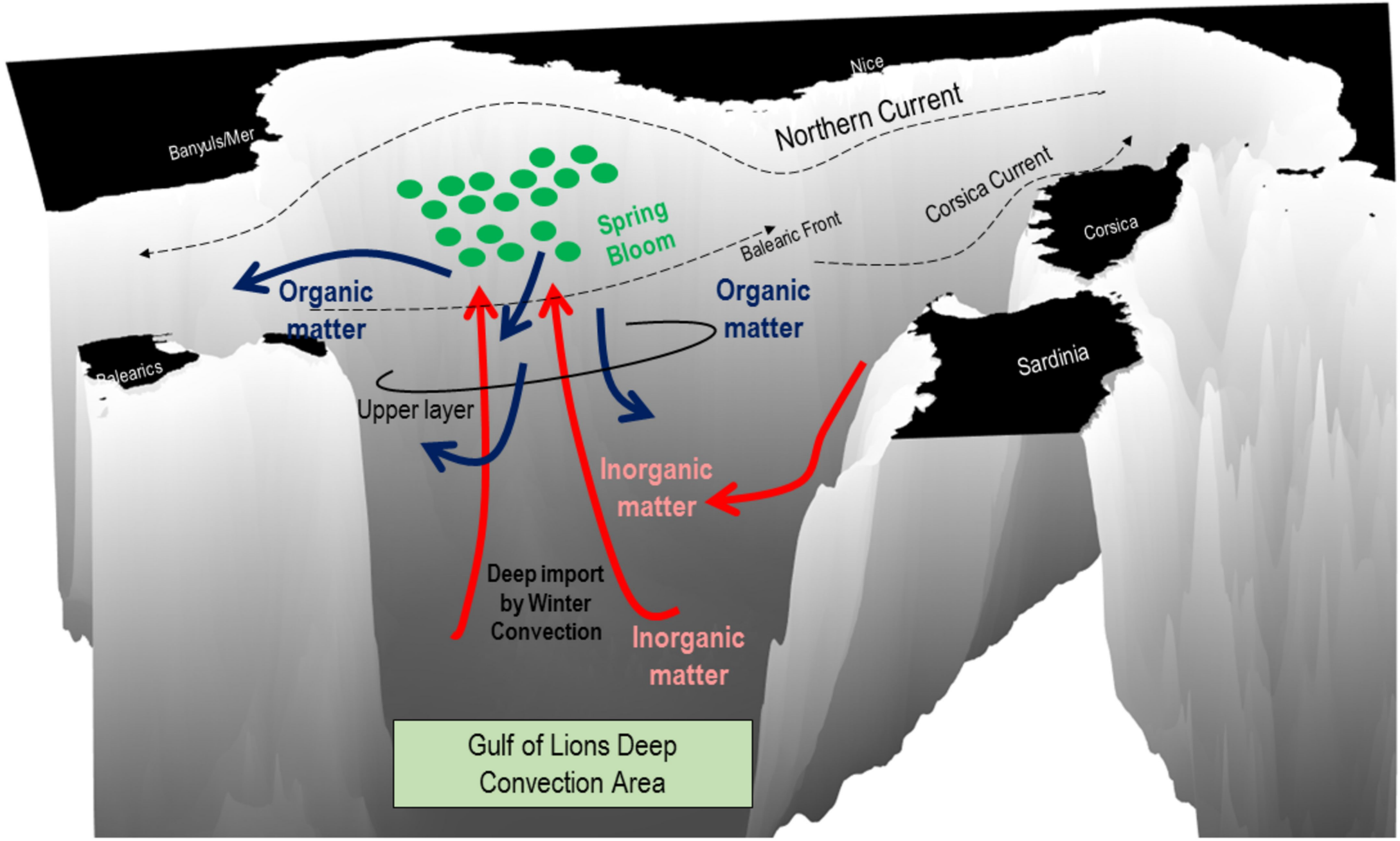
Nice
Banyuls/Mer
Northern Current
Corsica Current
Corsica
Spring Bloom
Balearic Front
Organic matter
Organic matter
Balearics
Sardinia
Upper layer
Inorganic matter
Deep import by Winter Convection
Inorganic matter
Gulf of Lions Deep Convection Area

Process	Unit	Reference	Period
Vertical import of inorganic nutrients	mmol m^{-2} y^{-1}		
		Pujo-Pay and Conan [2003]	1993
		Severin et al. [2014]	Feb./March 2011 convection events
		This study	2013 deep convection event
		This study	Sept. 2012-Sept. 2013
New production	mgC m^{-2} y^{-1}		
		Severin et al. [2014]	Feb./March 2011
		This study	Sept. 2012-Sept. 2013
Export of organic matter	mmol m^{-2} y^{-1}		
		Pujo-Pay and Conan [2003]	1993
		This study	Sept. 2012-Sept. 2013

Values	
NO3	P04
433-650	-
760/800	36/36
674	40
1029	59
46/63	
77	
274-814	
724	

Sources in the surface layer	**N**	**P**
Atmospheric inputs in the western basin	10,042-72,825	357-697
Terrestrial inputs in the western basin	7,840-18,020	168-1,258
Atmospheric inputs in the eastern basin	6,064-73,621 111,000	379-957 950
Terrestrial inputs in the eastern basin	11,592-77,519 63,000	248-1,541 2,400
Vertical physical inputs in the NW Med deep convection area	63,474	3,640

Reference
Ribera d’Alcalà et al. [2003]
Ribera d’Alcalà et al. [2003]
Ribera d’Alcalà et al. [2003]
Krom et al. [2004]
Ribera d’Alcalà et al. [2003]
Krom et al. [2004]
This study